



HAL
open science

The magmatic and magmatic-hydrothermal evolution of felsic igneous rocks as seen through Nb-Ta geochemical fractionation, with implications for the origins of rare-metal mineralizations

Christophe Ballouard, Malcolm Massuyeau, Marlina A Elburg, Sebastian Tappe, Fanus Viljoen, Jean-Tristan Brandenburg

► To cite this version:

Christophe Ballouard, Malcolm Massuyeau, Marlina A Elburg, Sebastian Tappe, Fanus Viljoen, et al.. The magmatic and magmatic-hydrothermal evolution of felsic igneous rocks as seen through Nb-Ta geochemical fractionation, with implications for the origins of rare-metal mineralizations. *Earth-Science Reviews*, 2020, 203, pp.103115. 10.1016/j.earscirev.2020.103115 . hal-04627202

HAL Id: hal-04627202

<https://cnrs.hal.science/hal-04627202>

Submitted on 27 Jun 2024

HAL is a multi-disciplinary open access archive for the deposit and dissemination of scientific research documents, whether they are published or not. The documents may come from teaching and research institutions in France or abroad, or from public or private research centers.

L'archive ouverte pluridisciplinaire **HAL**, est destinée au dépôt et à la diffusion de documents scientifiques de niveau recherche, publiés ou non, émanant des établissements d'enseignement et de recherche français ou étrangers, des laboratoires publics ou privés.

Journal Pre-proof

The magmatic and magmatic-hydrothermal evolution of felsic igneous rocks as seen through Nb-Ta geochemical fractionation, with implications for the origins of rare-metal mineralization

Ballouard Christophe, Massuyeau Malcolm, Elburg Marlina, Tappe Sebastian, Viljoen Fanus, Brandenburg Jean-Tristan



PII: S0012-8252(19)30346-0

DOI: <https://doi.org/10.1016/j.earscirev.2020.103115>

Reference: EARTH 103115

To appear in: *Earth-Science Reviews*

Received date: 29 May 2019

Revised date: 24 January 2020

Accepted date: 4 February 2020

Please cite this article as: B. Christophe, M. Malcolm, E. Marlina, et al., The magmatic and magmatic-hydrothermal evolution of felsic igneous rocks as seen through Nb-Ta geochemical fractionation, with implications for the origins of rare-metal mineralization, *Earth-Science Reviews*(2020), <https://doi.org/10.1016/j.earscirev.2020.103115>

This is a PDF file of an article that has undergone enhancements after acceptance, such as the addition of a cover page and metadata, and formatting for readability, but it is not yet the definitive version of record. This version will undergo additional copyediting, typesetting and review before it is published in its final form, but we are providing this version to give early visibility of the article. Please note that, during the production process, errors may be discovered which could affect the content, and all legal disclaimers that apply to the journal pertain.

The magmatic and magmatic-hydrothermal evolution of felsic igneous rocks as seen through Nb-Ta geochemical fractionation, with implications for the origins of rare-metal mineralization

BALLOUARD Christophe*^a, MASSUYEAU Malcolm^a, ELBURG Marlina^a, TAPPE Sebastian^a, VILJOEN Fanus^a, BRANDENBURG Jean-Tristan^b

Address:

^a Department of Geology, University of Johannesburg, P.O. Box 17003, Auckland Park 2006, South Africa

^b Sydney Brenner Institute for Molecular Bioscience, Faculty of Health Sciences, University of the Witwatersrand, Johannesburg, South Africa

*christopheballouard@outlook.com, ORCID: 0000-0001-6349-0324

Abstract

Despite Nb and Ta being considered as ‘geochemical twins’, most Ta mineral deposits are associated with muscovite bearing peraluminous granites and related pegmatites (MPG), whereas significant Nb deposits are related to peralkaline to metaluminous A1-type granites and syenites as well as nepheline syenites. Metaluminous to peraluminous A2-type granites and syenites have a lower potential for rare-metal mineralization. The Nb/Ta ratios are highly variable within each type of rare-metal-enriched felsic igneous suite and causes of the Nb-Ta geochemical fractionation remain poorly understood. Our compilation of whole-rock geochemical data indicates that Nb/Ta ratios generally anticorrelate with Ta, and at given Ta contents the Nb/Ta

ratios increase from MPG through A2-type to A1-type igneous suites. However, the Nb-Ta compositions of A1-type and silica-undersaturated felsic magmatic rocks are indistinguishable. New regression models to estimate the mineral/melt partition coefficients D_{Nb} and D_{Ta} indicate that fractional crystallization of biotite and ilmenite significantly decreases Nb/Ta, but an extreme degree of fractional crystallization is needed to explain the observed range of Nb-Ta variations in rare-metal-enriched igneous suites. Importantly, metasomatic rocks formed by the alteration of igneous suites and their country-rocks are commonly highly enriched in Ta and Nb. Their low Nb/Ta ratios suggest that magmatic-hydrothermal processes involving fluids and hydrosaline melts also play a critical role in Nb-Ta geochemical fractionation and HFSE enrichment in general. We show that the Nb-Ta compositions of the primitive end-members of rare-metal-enriched felsic igneous suites fingerprint the nature and evolution of their sources including metasomatic processes in the Earth's crust and upper mantle.

Keywords A-type and peraluminous granites; peralkaline complexes; niobium and tantalum; fractional crystallization; magmatic-hydrothermal transition; mineral/melt partition coefficients

1. Introduction

Rare-elements or rare-metals include high field strength elements (HFSE), such as Nb, Ta, W, Zr; the rare earth elements (REE) and Y; large elements, such as Cs and Sn; and also small and low-valence elements, such as Li and Be. Many of these elements represent strategic metals, which are essential in the high-tech industry and for the transition to sustainable energy sources (Linnen and Cuney, 2005; Linnen et al., 2012; Gunn, 2014). Rare-metals are mostly lithophile, and incompatible in the structure of most common rock-forming minerals. Therefore, these elements are concentrated in the upper continental crust and become enriched in silicate melts

during low-degree partial melting and fractional crystallization. Moreover, rare-metals have the capacity to form chemical complexes with, for example, F and Cl, which are typically mobile in magmatic-hydrothermal systems (e.g. Salvi et al., 2000; Veksler, 2004; Salvi and Williams-Jones, 2005; Thomas et al., 2009, 2011; Zaraisky et al., 2010; Williams-Jones et al., 2012; Veksler et al., 2012; Timofeev et al., 2015; Harlaux et al., 2017).

Among these strategic rare-metals, Ta and Nb are two geochemical “twins” characterized by the same charge ($z = 5^+$) and a similar ionic radius ($r = 0.64 \text{ \AA}$; Shannon, 1976). Therefore, they are not expected to fractionate significantly during most geological processes. Paradoxically, economic deposits of Ta and Nb are not associated with the same type of igneous rocks. Ta (\pm Li, Cs, Sn, W) deposits are generally associated with highly evolved muscovite-bearing peraluminous granites (MPG, Barbarin, 1996) including peraluminous rare element granites and Li-Cs-Ta pegmatites (Černý and Ercit, 2005; Černý et al., 2005; Linnen and Cuney, 2005; Linnen et al., 2012). In contrast, most economically significant Nb (\pm Zr, REE, Y) deposits are associated with either carbonatites or felsic, peralkaline to metaluminous, ferroan igneous rocks; the latter including A-type granites and syenites and nepheline syenites (e.g. Collins et al., 1982; Whalen et al., 1987; Eby, 1990; Bonin, 2007), and related Nb-Y-F (NYF, Černý and Ercit, 2005) pegmatites (Linnen and Cuney, 2005; Salvi and Williams-Jones, 2005; Chakhmouradian and Zaitsev, 2012).

MPG typically form by partial melting of clay-rich sediments and biotite- and muscovite-bearing igneous rocks in the continental crust in collisional to late collisional settings (e.g. Bernard-Griffiths et al., 1985; Le Fort et al., 1987; Vielzeuf and Holloway, 1988; Barbarin, 1996; Patiño-Douce, 1999; Gao et al., 2016; Shaw et al., 2016; Ballouard et al., 2018; Villaros et al., 2018), whereas carbonatites (e.g. Woolley and Church, 2005; Jones et al., 2013; Tappe et al.,

2017) and nepheline syenites (e.g. Kramm and Kogarko, 1994; Sørensen, 1997; Eby et al., 1998; Marks et al., 2003, 2004; Salvi and Williams-Jones, 2005; Estrade et al., 2014a; Marks and Markle, 2015; Möller and Williams-Jones, 2016; Elburg and Cawthorn, 2017) form generally by low-degree partial melting of the upper mantle in extensional settings. A-type granitoids, including granites, syenites and their extrusive equivalents (i.e. rhyolites and trachytes), have been divided into two types mostly based on their geodynamic setting and whole-rock Y/Nb ratios (Eby, 1990, 1992). A1-type granitoids, having the higher potential for HFSE exploration (e.g. Linnen and Cuney, 2005), are characterized by $Y/Nb < \sim 1.2$ and are commonly interpreted to originate from the differentiation and crustal contamination of mafic magmas similar to oceanic island basalts (OIB) in an intracontinental rift setting (Eby, 1990, 1992). In contrast, A2-type granitoids have $Y/Nb > \sim 1.2$ and are considered to form predominantly in late orogenic settings (Eby, 1990, 1992). These granitoids are commonly interpreted as the product of partial melting of a residual crust or calc-alkaline granitoids, and variable degrees of hybridization may have occurred with mantle-derived magmas triggering the partial melting of the deep crust (e.g. Collins et al., 1982; Clemens et al., 1986; Whalen et al., 1987; Eby, 1990, 1992; Skjerlie and Johnston, 1993, 1992; Patrice Douce, 1997; Gao et al., 2016; Finch and Tomkins, 2017). Alternatively, some studies have suggested that nepheline syenites and A-type granitoids may form by partial melting of a lower crust that was fenitized during the interaction with mantle-derived fluids enriched in alkalis and rare-metals in an extensional setting (e.g. Martin, 2006; Harris et al., 2018). Moreover, low-degree partial melting of an enriched lithospheric mantle source has also been proposed (e.g. Downes et al., 2005; Estrade et al., 2014; Dostal and Shellnutt, 2016; Elburg and Cawthorn, 2017).

The Earth's mantle (Nb/Ta ~16; Pfänder et al., 2007; Arevalo and McDonough, 2010) is characterized by higher Nb/Ta ratios than the continental crust (Nb/Ta ~11.4; Rudnick and Gao, 2003) (Fig. 1). Therefore, the relative enrichment or depletion of Nb compared to Ta in mantle- and crust-derived metallogenic systems, including the association of Nb deposits with carbonatites, nepheline syenites and A-type granitoids, but Ta deposits with MPG, can be partly explained by source differences. However, the whole-rock Nb/Ta ratio of magmatic rocks originating from these reservoirs is also highly variable with, for example, Nb/Ta values between 9 to 19 in oceanic basalts (Pfänder et al., 2007; Arevalo and McDonough, 2010) and 0.1 to 16 in crust-derived highly peraluminous granites (Ballouard et al., 2016a) (Fig. 1), including, for the latter, muscovite-bearing peraluminous granites (MPG) and cordierite-bearing peraluminous granites (CPG, Barbarin, 1996). In highly peraluminous granites, the fractional crystallization of mica with a mineral/melt partition coefficient for Nb higher than that for Ta (i.e. $D_{\text{Nb}}/D_{\text{Ta}} > 1$) can lead to a significant decrease of the Nb/Ta ratio with enrichment in Ta relative to Nb in the residual melts (e.g. Raimbault and Burnol, 1998; Stepanov et al., 2014). However, an extreme degree of fractional crystallization of an assemblage comprising feldspar and mica (over 90%) is needed to enrich the melt toward economic concentrations of Ta (Ballouard et al., 2016a). The solubility of tantalite (Ta_2O_5) is higher than that of columbite (Nb_2O_5) in peraluminous melts so that the crystallization of columbite-group minerals [CGM, $(\text{Mn, Fe})(\text{Nb, Ta})_2\text{O}_6$] will also lead to a decrease of the Nb/Ta ratio of the magma (Linnen and Keppler, 1997; Linnen and Cuney, 2005; Van Lichtervelde et al., 2018), but also rapidly deplete the residual melt in Nb-Ta. On the other hand, MPG (and LCT pegmatites) associated with rare-metal deposits, generally characterized by low Nb/Ta whole-rock values below ~5 (Ballouard et al., 2016a) (Fig. 1), commonly show evidence of important metasomatism such as albitization and greisenization. To date, the role of magmatic-hydrothermal processes in Nb-Ta geochemical fractionation and for

Ta concentration is debated (e.g. Ballouard et al., 2016a, 2016b; Stepanov et al., 2016; Van Lichtervelde et al., 2018) particularly because Ta-rich haloes were not observed in the country-rocks of rare-metal-enriched MPG and LCT pegmatites such as in the Beauvoir rare-metal granite, France (Cuney et al., 1992; Linnen and Cuney, 2005a). However, several authors have provided geochemical and textural evidences that magmatic-hydrothermal processes (i.e. magmatic brine- or hydrosaline melt-induced metasomatism or exsolution) may play a significant role in the Ta enrichment of these intrusions (e.g. Dostal and Chatterjee, 2000; Badanina et al., 2010, 2015; Thomas et al., 2011; Zhu et al., 2015; Dostal et al., 2015; Ballouard et al., 2016a, 2020; Xie et al., 2016; Wu et al., 2017, 2018; Fosso Tchente et al., 2018; Kaeter et al., 2018; Fuchsloch et al., 2019). To our knowledge, only few studies have focused on the geochemical fractionation of Nb-Ta in nepheline syenites or A-type granitoids. However, recently published whole-rock geochemical data on nepheline syenites from the Nechalacho layered suite in Canada (Möller and Williams-Jones, 2016) show highly variable Nb/Ta ratios ranging from 7 to 50 and, as in highly peraluminous granites, Nb/Ta appears to anticorrelate with both Nb and Ta contents (Fig. 1). Despite the fact that most Nb- and Ta-rich minerals from the suite, such as fergusonite and CGM, generally have a metasomatic origin (Timofeev and Williams-Jones, 2015), Möller and Williams-Jones (2016) suggested that the behavior of Nb-Ta in this intrusion principally reflects fractional crystallization of biotite and accumulation of eudialyte-group minerals (EGM). However, the experimental work of Linnen and Keppler (1997) indicates that, in contrast to peraluminous melts, Nb and Ta should have a similar solubility in peralkaline melts, so the reasons behind Nb-Ta geochemical fractionation in peralkaline suites remain unclear.

In this contribution, we focus on the behavior of Nb and Ta in MPG, nepheline syenite and A-type granitoid suites by using a compilation of natural whole-rock geochemical data and

experimental mineral/melt partition coefficients. We do not consider carbonatites here due to their different chemical and physical properties relative to silicate melts. The aim is to better understand the processes responsible for Nb-Ta geochemical fractionation in rare-metal-enriched felsic igneous rocks and to discriminate between the role of source, magmatic evolution and magmatic-hydrothermal processes. We also develop an efficient method to discriminate between A1- and A2-type granitoid suites by considering new types of geochemical diagrams. Our results suggest that Nb-Ta systematics are sensitive indicators of the origin of rare-metal-enriched felsic igneous rocks as well as their magmatic and magmatic-hydrothermal histories.

2. Background

2.1. Classification of rare-metal-enriched felsic igneous rocks

In this study, we define four main groups of rare-metal-enriched felsic igneous rocks: 1. MPG; 2. A1-type granites and syenites; 3. A2-type granites and syenites; 4. silica-undersaturated felsic igneous rocks (i.e. nepheline syenites), including for all four groups the extrusive equivalents. The principal mineralogical and geochemical characteristics of these igneous rock suites are summarized in Tables 1 and 2.

MPG are characterized by a high abundance of muscovite as well as molar A/CNK [$Al_2O_3 / (CaO + Na_2O + K_2O)$] ratios >1.1 and commonly contain biotite and minor ilmenite as mafic mineral phases (Barbarin, 1996, 1999). MPG include as their most evolved members the peraluminous, high to low P, rare element granites (Linnen and Cuney, 2005; Černý et al., 2005) and LCT pegmatites (Černý and Ercit, 2005). In contrast to most common MPG, peraluminous rare element granites and LCT pegmatites host disseminated Ta-Nb mineralization that commonly occurs as CGM and more rarely as pyrochlore-group minerals [PGM,

(Ca,Na)₂(Nb,Ta)₂O₆(O,OH,F)] or wodginite (MnSnTa₂O₈), along with Li-mica such as lepidolite (Linnen and Cuney, 2005; Černý et al., 2005).

A-type granites and syenites, here referred to as A-type granitoids, were originally defined by Loiselle and Wones (1979). They are peralkaline, metaluminous to peraluminous and have high whole-rock Fe/Mg, Ga/Al, Zr, Nb, Y, Ce, F, Cl and low Ca and Sr (e.g. Whalen et al., 1987). A-type granitoids were subdivided by Eby (1990, 1992) based on their geodynamic setting as well as their whole-rock Y/Nb values in relationship with other trace element ratios, such as Rb/Nb and Sc/Nb. The author defined A1-type granitoids that are characteristic of intracontinental rift settings and have Y/Nb values <1.2, and A2-type granitoids with Y/Nb ratios >1.2 that mainly occur in late orogenic settings. A1-type granitoids can contain variable amounts of mafic minerals such as calcic- and sodic amphibole and clinopyroxene. Although ferroan biotite is also known for A1-type granitoids, it dominates the mafic mineralogy of A2-type granitoids together with calcic amphibole. Magnetite, ilmenite and titanite are common Fe-Ti-bearing accessory phases in A-type granitoids. A1-type granitoids include the peralkaline rare element granites defined by Linnen and Cuney (2005) that host a Nb-Ta mineralization mostly consisting of PGM whereas metaluminous to slightly peraluminous rare element granites (Linnen and Cuney, 2005) are A2-type granitoids and commonly contain CGM. NYF pegmatites are also affiliated to A-type granitoids (Černý and Ercit, 2005).

Silica-undersaturated felsic igneous rocks can be spatially associated with silica-saturated A1-type granitoids in alkaline complexes and share some geochemical properties such as a significant enrichment in HFSE, F and Cl (e.g. Bailey et al., 2001; Salvi and Williams-Jones, 2005). Similarly to A1-type granitoids, nepheline syenites commonly contain sodic amphibole and pyroxene along with ferroan biotite, accessory ilmenite, magnetite and titanite. If levels of

alkalis are suitably high, then these “agpaitic” nepheline syenites can host, in addition to PGM and rare CGM, a large variety of complex REE-Nb-Zr-Ti-bearing minerals such as eudialyte-group minerals [EGM, $\text{Na}_4(\text{Ca,Ce})_2(\text{Fe}^{2+},\text{Mn,Y})\text{ZrSi}_8\text{O}_{22}(\text{OH,Cl})_2$], fergusonite [(Y,REE)NbO₄] and astrophyllite [(K,Na)₃(Fe²⁺,Mn)₇Ti₂Si₈O₂₄(O,OH)₇].

2.2. Nb-Ta compositions of the main geochemical reservoirs

Most geochemical reservoirs in the silicate Earth have a subchondritic Nb/Ta ratio (i.e. < 19.9, Münker et al., 2003) (Fig. 1), and this peculiarity is called the “missing Nb paradox” (Rudnick et al., 2000; Wade and Wood, 2001). In order to balance this apparently missing Nb, hidden reservoirs with superchondritic Nb/Ta have been proposed to exist in the Earth’s core (Wade and Wood, 2001; Cartier et al., 2014), the lower mantle as refractory eclogites derived from subducted oceanic crust (Rudnick et al., 2000), the continental lithospheric mantle in heavily metasomatized domains (Aulbach et al., 2008; Pfänder et al., 2012), or arc cumulates (i.e. arclogite, Tang et al., 2019), as well as the residual lower-middle crust (Stepanov and Hermann, 2013). Among the main igneous rock types (Fig. 1), crust-derived highly peraluminous granites show the lowest Nb/Ta values (c. 1-16), and Nb/Ta is anticorrelated with both Ta (0.5–500 ppm) and Nb (4-100 ppm) (Barouard et al., 2016a). Mid-oceanic ridge basalts (MORB, Nb/Ta ~9-19, Arevalo and McDonough, 2010), island arc volcanic rocks (IAV, Nb/Ta ~10-33, Stolz et al., 1996; König and Schuth, 2011; Münker et al., 2004), OIB (Nb/Ta ~14-18, Pfänder et al., 2007) and intraplate continental basalts (Nb/Ta ~15-19, Pfänder et al., 2012) are characterized by Nb/Ta ratios higher than those of highly peraluminous granites, with even superchondritic values for some IAV. However, IAV and MORB are depleted in Nb (IAV ~ 0.2–5 ppm; MORB ~ 0.2–20 ppm) and Ta (IAV ~ 0.01–1 ppm; MORB ~ 0.02–3 ppm) compared to OIB (Nb ~ 14–180 ppm and Ta ~ 1-10 ppm) and intraplate continental basalts (Nb ~ 25–112 ppm and Ta ~ 1-7 ppm).

Overall, the composition of oceanic basalts with mostly Nb/Ta >14 differs from the compositions of the continental crust and crust-derived granites that generally have Nb/Ta <14. The low Nb/Ta of the continental crust compared to basalts was recently suggested to reflect the delamination of arc-derived cumulates (i.e. arclogite) with Nb/Ta of 14-25 from the roots of thick and evolved magmatic arcs (Tang et al., 2019) (Fig. 1).

2.3. Magmatic behavior of Nb-Ta

The behavior of Nb and Ta in igneous processes is mainly controlled by mineral/melt partition coefficients (i.e. D_{Nb} and D_{Ta}) and literature data are summarized in Table 3. The primary hosts of Nb and Ta in common igneous rocks are Ti (\pm Fe)-bearing accessory minerals with D_{Nb} and D_{Ta} >10 such as ilmenite, rutile and titanite, as well as major rock-forming mineral groups such as the amphiboles ($0.07 < D_{\text{Nb}}$ and $D_{\text{Ta}} < 0.7$) and micas ($0.02 < D_{\text{Nb}}$ and $D_{\text{Ta}} < 4$). In contrast, K-feldspar ($0.01 < D_{\text{Nb}}$ and $D_{\text{Ta}} < 0.2$), clinopyroxene ($0.01 < D_{\text{Nb}}$ and $D_{\text{Ta}} < 0.2$) and garnet ($0.01 < D_{\text{Nb}}$ and $D_{\text{Ta}} < 0.2$) can only incorporate a limited quantity of Nb-Ta, and the incompatibility of both elements is even higher in quartz, plagioclase, orthopyroxene and olivine, which are characterized by D_{Nb} and $D_{\text{Ta}} < 0.1$. Similarly, magnetite and zircon, which have D_{Nb} and $D_{\text{Ta}} < 0.5$ and only occur in accessory proportion in common igneous rocks generally do not contribute significantly to the Nb-Ta budget. The same is true for phosphate minerals such as monazite and apatite with D_{Nb} and $D_{\text{Ta}} < 0.1$. The mineral/melt partition coefficient of Nb is higher than that of Ta for mica, with $D_{\text{Nb}}/D_{\text{Ta}} > 1$, leading to a decrease in the Nb/Ta ratio of the melt through mica fractionation (Stepanov et al., 2014). Titanite and rutile, in contrast, have $D_{\text{Nb}}/D_{\text{Ta}} < 1$ or ≤ 1 , respectively, so fractionation of these minerals will either not affect or lead to an increase of the melt Nb/Ta ratio (Tiepolo et al., 2002; Schmidt et al., 2004; Prowatke and Klemme, 2005; Xiong et al., 2011). For amphibole, the $D_{\text{Nb}}/D_{\text{Ta}}$ can be below or above unity

depending on the mineral and equilibrium melt structures and compositions (Tiepolo et al., 2000; Li et al., 2017). The previously mentioned studies observed that, in general, the D_{Nb} , D_{Ta} and $D_{\text{Nb}}/D_{\text{Ta}}$ ratio of these minerals increase with decreasing temperature and melt H_2O content, and with increasing melt polymerization such as higher SiO_2 contents (in other words, by decreasing the number of non-bridging oxygens per tetrahedron, NBO/T , of the melt).

Columbite-group minerals represent the main ore minerals of Nb-Ta and are highly soluble in granitic melts. The solubility of CGM increases with temperature, melt peralkalinity as well as with increasing concentrations of fluxing elements such as B and Li in the melt (Linnen and Keppler, 1997; Linnen, 1998; Linnen and Cuney, 2005; Bartels et al., 2010; Fiege et al., 2018). In contrast, pressure and F content of granitic melts have relatively small effects (Linnen and Keppler, 1997; Aseri et al., 2015). Melt H_2O content does not appear to affect the solubility of CGM in granitic systems containing >4 wt.% H_2O (Linnen, 2005; Bartels et al., 2010). Linnen and Keppler (1997) observed that the $D_{\text{Nb}}/D_{\text{Ta}}$ of CGM increases with the melt aluminum saturation index (i.e. melt polymerization). Therefore, crystallization of CGM, especially in peraluminous granites, will decrease the Nb/Ta ratio of the residual melt but likely deplete melt Nb-Ta concentrations. Supersaturation and disequilibrium crystallization of CGM caused by strong undercooling or other processes, may also lead to a strong geochemical fractionation between Nb and Ta in rare-metal granites and pegmatites (Van Lichtervelde et al., 2018).

2.4. Nb-Ta behavior in magmatic-hydrothermal systems

The parental magma of highly evolved granites and pegmatites is commonly highly enriched in fluxing components such as F, Cl, Li, P, B and carbonate, having the effect to reduce the viscosity and solidus of the melt, and increase H_2O solubility up to 30 wt.% (e.g. Thomas et al., 2005, 2012; Thomas and Davidson, 2012). Based on melt and fluid inclusion studies, these

authors demonstrated that, during crystallization of these intrusions in the upper crust, at least three phases can coexist, including a high viscosity, H₂O-poor, silicate-rich melt (type A), a low viscosity, H₂O (\pm carbonate)-rich, silicate-poor melt (type B), and a lower salinity aqueous (\pm carbonate-rich) fluid. This interpretation of melt inclusion analyses was challenged by London (2014) who suggested that H₂O-rich type-B inclusions may represent flux-enriched boundary layers, typically forming during the crystallization of undercooled pegmatite melts from the borders to the cores of the intrusions. However, such a process cannot explain, for example, the repartition of type A and B melt inclusions along a single solvus in a temperature versus H₂O content diagram (Thomas and Davidson, 2015). Regardless of the origins of these H₂O- and flux-rich melts (i.e. melt-melt immiscibility versus constitutional zone refining), their formation likely marks the transition from a magmatic toward a magmatic-hydrothermal system.

Experiments reproducing fluoride-silicate melt immiscibility suggest that Nb partitions preferentially into the fluoride melt compared to Ta (Veksler et al., 2012). However, Ta and Nb do not appear to preferentially partition into silicate- (type-A) or H₂O-rich (type-B) melts (Rickers et al., 2006; Thomas and Davidson, 2016). Despite the fact that Nb and Ta are relatively immobile in aqueous fluids, both elements can be mobilized at near-surface conditions and low temperature (<100°C) as polyoxometalates (Friis and Casey, 2018). Moreover, the solubility of both elements increases in F-rich aqueous solutions at elevated temperature (>100°C), and experimental studies suggest that Nb is more mobile than Ta under most conditions (Zaraisky et al., 2010; Timofeev et al., 2015, 2017). Experiments with aqueous F-rich fluids and aluminosilicate melts indicate that Nb and Ta preferentially partition into the melt (Chevychelov et al., 2005) (Table 3) and analyses of fluid inclusions hosted in quartz and topaz from the

Beauvoir rare-metal granite and its country-rock indicate that trapped magmatic-hydrothermal fluids are enriched in Nb relative to Ta (Harlaux et al., 2017).

Accordingly, in the Moose II pegmatite, Canada, fine-grained secondary muscovite is enriched in Nb relative to Ta compared to early muscovite and Nb-rich replacements are observed on CGM, suggesting an interaction with a Nb-rich and Ta-poor fluid phase (Anderson et al., 2013). A fluid metasomatic origin was also suggested for a fine-grained Ta-poor muscovite from the Tanco pegmatite, Canada (Van Lichtervelde et al., 2009). Similarly, some Nb-Ta-poor PGM and muscovite crystals from LCT pegmatites of the Orange River belt in South Africa were interpreted as late hydrothermal in origin (Ballouard et al., 2020).

On the other hand, a significant body of evidence exists for metasomatic enrichment of Ta relative to Nb in rare-metal granites and pegmatites. For example, in a LCT pegmatite from SE Ireland, Kaeter et al. (2018) demonstrated, based on detailed element mapping of coeval CGM and muscovite crystals, that the most Ta-enriched oxides formed during a late hydrothermal phase. In rare-metal MPG and LCT pegmatites from South China, numerous studies (e.g. Zhu et al., 2015; Xie et al. 2016; Wu et al. 2017, 2018) report textural evidence of replacement or overgrowth of Ta-poor CGM by Ta-rich CGM and wodginite. Wu et al. (2017, 2018) suggested that such metasomatism reflects an interaction with hydrosilicate liquids. The presence of metasomatic Ta-mineralization consisting of PGM with $Ta \gg Nb$ (i.e. microlite) or wodginite that replaced early magmatic minerals including CGM is a common feature of peraluminous rare-metal granites and LCT pegmatites such as the Beauvoir granite in France (Ohnenstetter and Piantone, 1992), the Greenbushes pegmatite in Australia (Partington et al., 1995), the Tanco Pegmatite in Canada (Van Lichtervelde et al., 2007; Linnen et al., 2012), and the Orange River pegmatite belt in South Africa (Ballouard et al., 2020). The first two examples suggested a

hydrothermal origin for the PGM mineralization, whereas the latter studies argued for flux-rich melt-dominated metasomatism. In the Orange River pegmatite belt (Ballouard et al., 2020) and the Cape Cross-Uis belt of Namibia (Fuchsloch et al., 2019), the tourmalinized, greisenized or albitized country-rocks of LCT pegmatites can reach economic concentrations of Ta up to 160 and 250 ppm, respectively, which is an important argument for significant hydrothermal transport of Ta. Finally, beryl-hosted H₂O- and CO₂-rich aqueous primary fluid inclusions with about 6500 ppm Ta were found in a LCT pegmatite from Transbaikalia, Russia (Thomas et al., 2009), and the coexistence of primary H₂O-, alkaline- and carbonate-rich melt and fluid inclusions in tantalite crystals from a LCT pegmatite from NE Brazil suggests that the transport and concentration of Ta is promoted by aqueous media (Thomas et al., 2011).

3. Whole-rock geochemical data

3.1. Geochemical characterization

We compiled whole-rock data for MPG (n = 410), A-type granitoids (n_{A1-type} = 452; n_{A2-type} = 312), silica-undersaturated felsic igneous rocks (n = 813) as well as limited extrusive equivalents (~2% for MPG, ~12 % for A1-type rocks, ~ 3% for A2-type rocks, ~14% for silica-undersaturated rocks). Metasomatic rocks (e.g. greisens, albitites, tourmalinites, skarns) related to these igneous rocks were also added to the compilation. The location, age, rock types, mineralogy, associated ore deposits, trace element analytical techniques and data sources are provided in Supplementary Material 1, and a complete whole-rock geochemical database with major and trace element, O, Sr, Nd isotope analyses along with mineralogy is provided in Supplementary Material 2. The different suites of igneous rocks were discriminated based on their mineralogy and the geochemical diagrams presented in Figure 2. In particular, A1-type and A2-type granitoids were differentiated based on the ternary Ce-Y-Nb (Supplementary Material 3)

and Rb/Nb versus Y/Nb (Fig. 2e) diagrams of Eby (1990, 1992). The distinction between A1- and A2-type granitoids was not performed on a sample-by-sample basis. Instead, we preferred to assign entire igneous suites or intrusions to either the A1- or A2-type granitoids. This explains why a few A-type granitoid samples (~5% in Fig. 2e) fall outside their respective field.

The main geochemical characteristics of compiled rare-metal-enriched igneous rocks are summarized below and in Table 2. In the total alkalis versus SiO₂ diagram (Fig. 2a), about 85% of silica-undersaturated felsic igneous rocks are classified as nepheline syenites with the remainder ranging between syenite and syenodiorite. Related extrusive rocks have a comparable composition ranging from phonolite, phonolitic tephrite to trachybasalt (Supplementary Material 3). A1-type granitoids plot in the field of granites (~10%), alkali granites (~60%) and syenites (~30%), and extrusive equivalents are mostly alkali rhyolites and trachytes. A2-type granitoids include alkali granites (~60%), granites (~20%) and syenites (~20%) with few syenodiorites, and extrusive rocks are rhyolites or alkali rhyolites. About 75 % of MPG plot in the field of alkali granites whereas the other rocks plot in the field of granites and the rare samples of extrusive rocks are rhyolites. Silica-undersaturated igneous rocks are predominantly peralkaline (~70%) and metaluminous (~30%) in composition, and the same is true for A1-type granitoids, for which peralkaline (~45%) and metaluminous (~35%) samples dominate over slightly (~15%) and highly (~5%) peraluminous samples (Fig. 2b). In contrast, A2-type granitoids are mostly metaluminous (~40%) to slightly peraluminous (~45%) with about 5% and 10% of peralkaline and highly peraluminous rocks, respectively. By definition, MPG are mostly highly peraluminous (~95%) with few slightly peraluminous granites (~5%). Around 90% and 95% of silica-undersaturated and A1-type granitoids are ferroan in composition, respectively, and A2-type granitoids tend to be magnesian (~25%) at low SiO₂ contents (Fig. 2c). MPG can be either magnesian (~45%) or

ferroan (~55%). In the agpaitic index [molar (Na+K)/Al] versus Zr + Ce + Nb + Y diagram (Whalen et al., 1987) (Fig. 2d), MPG mostly plot in the field of I and S type granites whereas A-type granitoids and silica-undersaturated igneous rocks that are enriched in alkalis and HFSE dominantly plot in the field of A-type granites. Paradoxically, the Ga/Al ratio (Whalen et al., 1987) does not differentiate between A-type granitoids and MPG (Supplementary Material 3). As demonstrated by Eby (1992), the Rb/Nb versus Y/Nb diagram is useful in discriminating A1- and A2-type granitoids (Fig. 2e). In this diagram, silica-undersaturated igneous rocks have a similar composition to A1-type granitoids, whereas MPG tend to have high Rb/Nb ratios (> ~10) with lower Y/Nb at similar Rb/Nb than other rocks and can be readily distinguished.

3.2. The Nb and Ta inventory of felsic igneous rocks

The Nb-Ta compositions of whole-rock samples compiled from literature sources in this study were originally acquired by various methods including X-ray fluorescence (XRF), instrumental neutron activation analysis (INAA), and inductively coupled plasma mass spectrometry (ICP-MS). The relative analytical bias induced by the use of “old” (i.e. XRF and INAA) and “modern” (i.e. ICP-MS) methods is assessed in Supplementary Material 4, where we show that the compositions of samples analyzed by INAA or XRF clearly overlap with those of samples analyzed by ICP-MS. Therefore, it is safe to conclude that for the purpose of this study the Nb-Ta systematics obtained by these different methods can be compared and contrasted without a significant risk of an analytical bias.

In the Nb/Ta versus Ta and Nb (Fig. 3) diagrams, super-chondritic Nb/Ta values (> 19.9) are restricted to A1-type granitoids (Ta ~0.8-300; Nb ~20-4500; Nb/Ta ~6-60) and silica-undersaturated igneous rocks (Ta ~1-150; Nb ~20-2000; Nb/Ta ~10-60); these two rock types are indistinguishable with respect to their Nb-Ta composition. On a global scale, A1-type and silica-

undersaturated rocks do not define clear evolution trends. At given Nb and Ta contents, A2-type granites and syenites (Ta ~0.5-30; Nb ~7-80; Nb/Ta ~1-20) are characterized by lower Nb/Ta values than A1-type and silica-undersaturated rocks while MPG (Ta ~0.5-500; Nb ~4-200; Nb/Ta ~0.1-10) are characterized by even lower ratios than A2-type igneous rocks. The Nb/Ta ratio tends to anticorrelate with Nb and Ta contents for MPG and A2-type suites. Lines delimiting the fields of silica-undersaturated + A1-type rocks, A2-type rocks and MPG are defined in the Nb/Ta versus Nb and Ta diagrams and discrimination between these rock types is effective at more than 90%.

3.3. Nb-Ta systematic of individual suites of felsic igneous rocks

As shown in Figure 3, whole-rock Ta and Nb contents anticorrelate with Nb/Ta ratios for MPG and, to a lesser degree, A2-type granitoids, suggesting a comparable differentiation/evolution history. In contrast, no clearly defined evolution trends appear, at a global scale, for A1-type granitoids as well as silica-undersaturated felsic igneous rocks. To better assess the behavior of Nb-Ta in rare-metal-enriched felsic igneous suites, we have selected specific magmatic suites of silica-undersaturated, A1-type and A2-type granitoids as well as MPG, showing a well-defined correlation between whole-rock Ta and Nb contents and Nb/Ta ratios. Details and references about selected suites are summarized in Supplementary Material 1 while the variation of the whole-rock Nb/Ta ratio of these suites as a function of different trace and major elements is shown in the geochemical diagrams of Figures 4 to 8 and Supplementary Material 3.

3.3.1. Silica-undersaturated felsic igneous rocks

Because of the large set of whole-rock analyses available (n=661) and well-documented petro-geochemistry, nepheline syenites of the Nechalacho layered suite in Canada (Timofeev and Williams-Jones, 2015; Möller and Williams-Jones, 2016) were selected as representative of silica-undersaturated igneous rocks. The hydrothermally altered upper part of the Nechalacho layered suite hosts one of the world's largest REE and Nb deposits. In terms of Nb-Ta bearing minerals, the peralkaline unaltered nepheline syenites from the lower part of the Nechalacho layered suite contain sodic pyroxene ± biotite as major mafic minerals, with accessory PGM and EGM. In contrast, the mostly peralkaline to metaluminous altered and mineralized upper part of the suite contains sodic pyroxene with PGM, EGM and CGM.

The lowest Nb/Ta values (6-45) and Al₂O₃ contents as well as the highest Ta (1-1000 ppm), Nb (30-6500 ppm), Zr, Y, Ce and Rb concentrations of the Nechalacho layered suite are characteristic of the altered nepheline syenites (Fig. 4 and Supplementary Material 3). In these rocks, the rare-metal content tends to increase with decreasing Nb/Ta. However, the unaltered part of the intrusion, with Nb/Ta of 10-50, has lower and less variable concentrations of rare-metals including Nb (40-500 ppm), and Ta (1-40 ppm). At relatively high TiO₂ contents between ~0.03 and 0.5 wt.%, the Nb/Ta ratio (~13-35) of unaltered nepheline syenites correlates with TiO₂ but no correlation is observed for the altered facies.

3.3.2. A1-type granitoids

The igneous suites selected for A1-type granitoids include granites from the Baerzhe pluton in NE China (Jahn et al., 2001), granites from the Boziguo'er pluton in NW China (Huang et al., 2018), granites, granitic pegmatites, syenites and trachytes from the Ambohimirahavavy complex in Madagascar (Estrade et al. 2014a, b) as well as trachytes and rhyolites from the Olkaria volcanic complex in Kenya (Macdonald et al., 1987, 2008). The peralkaline Baerzhe

pluton is associated with a supergiant REE-Nb-Be-Zr deposit and this granite commonly contains sodic pyroxene and amphibole with PGM and CGM as Nb-Ta-bearing phases. Peralkaline to metaluminous granites from the Boziguo'er pluton host a Nb deposit and contain biotite, calcic and sodic amphibole and sodic pyroxene as the major mafic minerals; accessory phases include mostly PGM and less commonly astrophyllite and Fe-Ti oxides. In the Ambohimirahavavy complex, peralkaline granites and pegmatites are associated with an economically significant Zr-Nb-REE mineralization and contain sodic pyroxene and amphibole, calcic amphibole as well as titanite, PGM and EGM. The associated metaluminous to peralkaline trachytes have sodic amphibole, calcic pyroxene and biotite as the main mafic phases with Fe-Ti oxides and rare chevkinite as accessory minerals. Biotite, sodic amphibole, calcic pyroxene as well as ilmenite, magnetite and aenigmatite can occur as phenocrysts in the peralkaline rhyolites from the Olkaria Volcanic complex and metaluminous to peralkaline trachytes contain sodic amphibole, calcic pyroxene with Fe-Ti oxides and minor chevkinite.

In all selected A1-type igneous suites, the Nb/Ta ratio anticorrelates with Ta contents but superchondritic Nb/Ta values (>1.9) are mostly restrained to the Baerzhe (Nb/Ta \sim 14-49; Ta \sim 2-20 ppm; Nb \sim 110-1560 ppm), and Boziguo'er (Nb/Ta \sim 54-14; Ta \sim 3-120 ppm; Nb \sim 90-330 ppm) plutons (Fig. 5a). In the Olkaria (Ta \sim 5-50 ppm; Nb \sim 90-590 ppm) and Ambohimirahavavy (Ta \sim 2.5-480 ppm; Nb \sim 40-3800 ppm) complexes, the Nb/Ta ratio ranges from 12 to 18 and 7 to 42, respectively. Similarly, to Ta, the Nb/Ta ratio decreases with increasing Nb, Zr, Y, Rb (\pm Ce) contents in all igneous suites except the Boziguo'er granite (Fig. 5b-e, Supplementary Material 3). With respect to TiO₂, SiO₂ and Al₂O₃ contents, the behavior of the Nb/Ta ratio is variable (Fig. 5f-h). For the Olkaria volcanic complex, the Nb/Ta values tend to decrease with increasing SiO₂ and increase with Al₂O₃, MgO, Mg# (Supplementary Material 3) and, to a lesser degree,

TiO₂. In the Baerzhe granite, Nb/Ta tends to anticorrelate with TiO₂ and correlate with SiO₂. Finally, no clear correlation exists between the Nb/Ta ratio and any element, except Ta, for the Boziguo'er granite.

3.3.3. *Transitional A-type granitoids*

Some A-type granitoid suites plot in the field of both A1-type and A2-type granitoids either in the Rb/Nb versus Y/Nb diagram, the ternary Ce-Y-Nb diagram (Eby, 1992) (Supplementary Material 3) or the Nb/Ta versus Ta and Nb diagram (Fig. 6). This is the case for the metaluminous granites and trachydacites from the Brandberg complex (Schmitt et al., 2000) as well as metaluminous to peraluminous granites and rhyolites from the Gross and Klein Spitzkoppe stocks occurring in Namibia (Frindt et al., 2004; Frindt and Haapala, 2004; Haapala et al., 2007). The Brandberg granitoids contain biotite with variable amounts of calcic amphibole and pyroxene as well as ilmenite, magnetite, titanite and chevkinite. Biotite is the main mafic mineral phase in the Spitzkoppe granitoids, whereas muscovite, magnetite, CGM, ilmenite and rare fergusonite are accessory phases.

Ta anticorrelates with the Nb/Ta ratio in both the Brandberg (Nb/Ta ~5-17; Ta ~2.5-11 ppm) and Spitzkoppe (Nb/Ta~1-47; Ta ~2-45 ppm) igneous suites (Fig. 6a). In contrast, the Nb content is relatively constant for the Brandberg granitoids (Nb~42-53 ppm) and correlates with the Nb/Ta ratio for the Spitzkoppe stocks (Nb~41-266 ppm, Fig. 6b). In both suites, the Nb/Ta values increase with the Zr (Fig. 6c), Ce (Supplementary Material 3) and TiO₂ (Fig. 6f) contents whereas the opposite is true for Rb (Fig. 6e) and SiO₂ (Fig. 6g). The Nb/Ta values correlate with MgO and, to a lesser degree, the Mg#, (Supplementary Material 3) of the Brandberg suite.

3.3.4. *A2-type granitoids*

Igneous rocks selected as representative of A2-type granitoids include metaluminous to peraluminous granites, syenites, monzonites and quartz monzonites from the Topcam pluton in Turkey (Karsli et al., 2018), granites, tuffs and ignimbrites from the Krušné hory / Erzgebirge in Central Europe (Breiter, 2012), peraluminous granites from the Lachlan Fold Belt in Australia (Collins et al., 1982) as well as metaluminous to peraluminous granites from the Qianlishan complex associated with a giant Sn-W-Mo-Bi deposit (Chen et al., 2016; Guo et al., 2015). Potential Nb-Ta-bearing phases in the Topcam granitoids include biotite, calcic amphibole and pyroxene as well as magnetite whereas magmatic rocks from the Krušné hory / Erzgebirge host biotite and, less commonly, Li-mica and PGM. Granites from the Lachlan Fold Belt contain biotite along with calcic and sodic amphibole, ilmenite and magnetite. Biotite, Li-mica as well as ilmenite, titanite and CGM were described in the Qianlishan complex.

Nb/Ta anticorrelates with Ta in the Topcam (Nb/Ta~11-18; Ta~0.5-2 ppm; Nb~8-16 ppm), Krušné hory / Erzgebirge (Nb/Ta~2-15; Ta~0.8-30 ppm; Nb~16-80 ppm) and Qianlishan (Nb/Ta~1-9; Ta~2-28 ppm; Nb~16-77 ppm) igneous rocks whereas Ta is nearly constant in the granites from the Lachlan Fold Belt (Nb/Ta~6-9; Ta~3 ppm; Nb~17-28 ppm) (Fig. 7a). In contrast, although the Nb contents of igneous rocks from Krušné hory / Erzgebirge increase with decreasing Nb/Ta values, the opposite behavior is displayed by granites from the Lachlan Fold Belt and Qianlishan complex, while no correlations appear between Nb/Ta and Nb in the Topcam pluton (Fig. 7b). In general, the Nb/Ta ratio anticorrelates with Y (Fig. 7d), Rb (Fig. 7e) and SiO₂ (Fig. 7g) whereas the opposite is true for Zr (Fig. 7c), TiO₂ (Fig. 7f), MgO and Mg# (Supplementary Material 3).

3.3.5. MPG

MPG suites include granites and some LCT pegmatites from the European Variscan belt (Armorican Massif, Beauvoir-Massif Central, Iberian Massif and Erzgebirge / Fichtelgebirge, see Supplementary Material 1 for references), granites from the South Mountain batholith (MacDonald et al., 1992; Dostal and Chatterjee, 1995) in Canada and microgranites (ongonites) from Ongon Khairkhan in Mongolia (Dostal et al., 2015). Evolved MPG from the European Variscan belt are commonly associated with Sn, W, Ta, Li or U mineralization, whereas economically significant deposits of Sn and W occur in the South Mountain batholith and at Ongon Khairkhan, respectively. In contrast to other igneous suites with rare-metal potential, MPG tend to contain a less variable Nb-Ta-bearing mineral assemblage, mostly including muscovite, biotite along with ilmenite for the primitive granites, and muscovite, Li-mica and CGM for the most evolved members, including peraluminous rare element granites and LCT pegmatites.

In MPG from the European Variscan belt ($Nb/Ta \sim 0.3-13$; $Ta \sim 0.5-190$ ppm; $Nb \sim 4-160$ ppm), South Mountain batholith ($Nb/Ta \sim 2-7$; $Ta \sim 2-13$ ppm; $Nb \sim 11-28$ ppm) and Ongon Khairkhan ($Nb/Ta \sim 0.2-3$; $Ta \sim 8-450$ ppm; $Nb \sim 70-110$ ppm), Ta generally anticorrelates with Nb/Ta while Nb can either be constant or increases with Nb/Ta (Fig. 8a-b). Rb generally anticorrelates with Nb/Ta (Fig. 8e). In contrast, Zr (Fig. 8c), Y (Fig. 8d), Ce (Supplementary Material 3), TiO_2 (Fig. 8f) and MgO (Supplementary Material 3) contents commonly increase with Nb/Ta values. Finally, the SiO_2 content of MPG displays a poorly defined negative correlation with Nb/Ta at high Nb/Ta values from 2 to 11 and shows the opposite behavior at low Nb/Ta values below ~ 2 .

3.3.6. *The Nb-Ta systematics of metasomatic rocks*

In order to assess the evolution of Nb and Ta during magmatic-hydrothermal alteration, we have compiled whole-rock data on metasomatic rocks associated with A1-type granites and MPG (Supplementary Materials 1 and 2). These rocks include endoskarns (n=4), exoskarns (n=3) and hydrothermal veinlets (n=4) associated with A1-type granitic dikes from the Ambohimirahavy complex in Madagascar (Estrade et al., 2014b; 2015), numerous greisens and some albitites associated with MPG (n=33) as well as the greisenized, albitized or tourmalinized country-rocks of LCT pegmatites from Cape Cross-Uis in Namibia (n=4; Fuchsloch et al., 2019; Fuchsloch, 2018) and the Orange River pegmatite belt in South Africa (n= 6; Ballouard et al., 2020).

Endoskarns, exoskarns and veins from the Ambohimirahavy complex contain REE fluorcarbonates, PGM, titanite and fergusonite as the main HFSE-rich hydrothermal phases. Endoskarns (Ta~158-343 ppm; Nb~1015-3461 ppm) and exoskarns (Ta~56-180 ppm; Nb~1251-5234 ppm; Nb/Ta~11-39) are enriched in Nb (and Ta) toward economic grades (Fig. 5). Endoskarns, characterized by low Nb/Ta values, from ~6 to 13, have also extremely high contents of Zr, Ce and Y and plot at the end of the evolution trends for A1-type igneous suites in the diagrams of Figure 5 and Supplementary Material 3). Exoskarns have variable Nb/Ta values from ~11 to 39 and are also significantly enriched in Zr, Ce and Y. Hydrothermal veinlets emplaced in the country-rock show Nb/Ta values from ~11 to 21 and one vein with a Nb/Ta value of 11 is significantly enriched in both Nb (417 ppm) and Ta (37 ppm, see Supplementary Material 1).

Greisens, albitites and tourmalinites are formed by the secondary muscovitization, albitization and tourmalinization, respectively, of MPG and their immediate country-rocks during magmatic-hydrothermal alteration (e.g. Schwartz and Surjono 1990; Pirajno, 2013; Launay et al.,

2019; Ballouard et al., 2020). These metasomatic rocks commonly host a rare-metal mineralization including wolframite, cassiterite, CGM, Nb-Ta rutile and PGM (Supplementary Material 1). Albitized and greisenized MPG are characterized by low Nb/Ta values from ~7 to 0.2 and mostly plot in the magmatic-hydrothermal domain defined by Ballouard et al. (2016a) (Fig. 8) with Nb/Ta < 5. These metasomatic rocks, with Ta and Nb contents ranging from 1 to 650 ppm and 2 to 140 ppm, respectively, are commonly enriched in Ta up to economic values and tend to follow the same evolutionary trends as MPG in the diagrams of Figure 8 (and Supplementary Material 3). Similarly, in the metasomatized country-rocks, Nb/Ta (0.7-5.7) anticorrelates with both Ta (3-252 ppm) and Nb (15-163 ppm) and the samples with the highest Ta content plot at the end of the evolution trends of MPG (Figs. 8a-b).

4. Mineral/melt partition coefficients

One of the main purposes of this study is to distinguish between the effects of source, mineral fractionation and magmatic-hydrothermal processes to explain the variability of Nb and Ta contents observed in felsic igneous rocks with rare-metal potential. Common hosts of Nb and Ta that potentially fractionate from the parental melts of felsic igneous systems include biotite, amphibole, ilmenite, titanite, and to a lesser extent magnetite and clinopyroxene. In order to evaluate the contributions of these minerals to the geochemical fractionation of Nb and Ta within each type of igneous rocks studied here, we compiled mineral/melt partitioning data from experimental studies and analyses performed on natural samples (Supplementary Material 5).

Information about pressure, temperature, major element melt composition, Nb and Ta contents of melts and coexisting minerals, as well as their respective partition coefficients D_{Nb} and D_{Ta} (i.e., $D_{\text{Nb}}^{\text{mineral/melt}}$ and $D_{\text{Ta}}^{\text{mineral/melt}}$, respectively) are reported in Supplementary Material

5. Pressure (P) and temperature (T) range from 0.0001 to 10 GPa and 750 to 1600°C, respectively. Most experiments performed at >2.5 GPa and >1400°C relate to clinopyroxene-melt partitioning, whereas experiments conducted at 0.0001 GPa (i.e. 1 atm) involve titanite and magnetite. The database also includes some partitioning data for biotite-melt, ilmenite-melt and magnetite-melt pairs from natural rocks (Nash and Crecraft, 1985; Acosta-Vigil et al., 2010; Fedele et al., 2015), in order to improve the representativity of these partitioning systems. In terms of melt composition, the complete database covers a large range of SiO₂ contents, from about 32 to 76 wt.%, although not every mineral/melt partitioning system covers the entire melt SiO₂ spectrum.

The partition coefficients D_{Nb} and D_{Ta} positively correlate with melt SiO₂ and/or Al₂O₃ contents for biotite, ilmenite, titanite and, to a lesser degree, amphibole, clinopyroxene and magnetite (Fig. 9). Similarly, D_{Nb} and D_{Ta} positively correlate with the A/CNK and X_{nf}/X (X_{nf} : sum of the molar fractions of network-forming cations, i.e. Si and Al; X: sum of all cations on a molar basis) melt values for most of the mineral/melt partitioning systems investigated, whereas the opposite is true for melt temperature (Supplementary Material 6). All these trends indicate that the partition coefficients of Nb and Ta increase during melt polymerization. D_{Nb} and D_{Ta} values are generally lower than 1 for clinopyroxene-melt ($D_{\text{Nb}} \sim 0.001-0.2$; $D_{\text{Ta}} \sim 0.002-0.5$), amphibole-melt ($D_{\text{Nb}} \sim 0.02-1.6$; $D_{\text{Ta}} \sim 0.02-1.6$) and magnetite-melt ($D_{\text{Nb}} \sim 0.03-0.4$; $D_{\text{Ta}} \sim 0.03-0.4$), whereas both elements are always compatible in titanite ($D_{\text{Nb}} \sim 1.3-7.3$; $D_{\text{Ta}} \sim 4.5-87$). Experimental data suggest that Nb and Ta become compatible in ilmenite ($D_{\text{Nb}} \sim 0.4-74$; $D_{\text{Ta}} \sim 0.6-47$) and biotite ($D_{\text{Nb}} \sim 0.02-9$; $D_{\text{Ta}} \sim 0.06-4$) for coexisting melts with SiO₂ contents higher than ~40-45 wt.% and ~60-65 wt.%, respectively. The $D_{\text{Nb}}/D_{\text{Ta}}$ ratio shows a variable degree of positive correlation with SiO₂ and/or Al₂O₃ (Fig. 9), X_{nf}/X and A/CNK (Supplementary Material

6) for biotite, ilmenite, amphibole, clinopyroxene and magnetite whereas the opposite is true for titanite. $D_{\text{Nb}}/D_{\text{Ta}}$ values are generally below 1 for clinopyroxene (0.03-2), titanite (0.07-0.6) and magnetite (0.03-2.7), whereas biotite (0.2-4.7) and ilmenite (0.6-1.5) incorporate more Nb than Ta in melts with a SiO_2 content higher than 50 and 55 wt.%, respectively.

In order to predict the effects of fractional crystallization on the Nb/Ta evolution of magmas, linear models were fitted to calculate the partition coefficients (transformed with \log_{10}) as a function of the melt Si and Al molar contents, i.e. the two main network-forming cations (Table 4). The calibration is based on the compiled database (Supplementary Material 5) and the method used is described in Supplementary Material 7. Multivariate regressions taking into account Al and Si are used for amphibole (D_{Nb} , $r^2 = 0.65$; D_{Ta} , $r^2 = 0.62$), clinopyroxene (D_{Nb} , $r^2 = 0.35$; D_{Ta} , $r^2 = 0.37$) and titanite (D_{Nb} , $r^2 = 0.62$; D_{Ta} , $r^2 = 0.91$). For ilmenite, we only considered Si due to the strong correlation between Al and Si ($r^2 > 0.9$) and because the determination coefficients between Si and D_{Nb} ($r^2 = 0.95$), D_{Ta} ($r^2 = 0.98$) and $D_{\text{Nb}}/D_{\text{Ta}}$ ($r^2 = 0.57$) are higher than those of Al (D_{Nb} , $r^2 = 0.80$; D_{Ta} , $r^2 = 0.87$; $D_{\text{Nb}}/D_{\text{Ta}}$, $r^2 = 0.35$, Fig. 9). Similarly, a multivariate regression using both Al and Si does not acceptably model the behavior of D_{Nb} , D_{Ta} and $D_{\text{Nb}}/D_{\text{Ta}}$ in biotite, possibly due to the poor correlation between Al and $D_{\text{Nb}}/D_{\text{Ta}}$ ($r^2 = 0.02$) compared to Si ($r^2 = 0.70$, Fig. 9). Therefore, only Si was used for the calibration of D_{Nb} ($r^2 = 0.88$) and D_{Ta} ($r^2 = 0.77$). However, no statically acceptable linear model can be fitted for magnetite based on melt Si and Al contents. The derived equations for biotite, amphibole, clinopyroxene, ilmenite and titanite are provided in Table 4 along with the number of analyses, uncertainties of regression coefficients, coefficients of determination, and the compositional range of preferred application to natural rock suites. It must be noted that these regressions may be possibly improved by taking into account the contents of melt network-modifier elements (e.g. K, Na, Ca, Mg, Fe) along with parameters

such as temperature and pressure. Moreover, the mineral compositions may also influence the geochemical fractionation of Nb and Ta as shown for amphibole by Nandedkar et al. (2016). Nevertheless, our empirical models are based on the evolution of the melt network formers (i.e., Si and Al), which are good proxies of the evolution of global melt and mineral compositions with pressure and temperature. Moreover, more complex models (e.g., thermodynamic lattice-strain modeling, Blundy and Wood, 1994) are beyond the scope of this paper and it would require a specific study dedicated to each mineral/melt system. Lastly, the use of fluid-sensitive network-modifier elements such as K, Ca, Na and estimates of temperature or pressure as well as the necessity to more precisely define the mineral compositions would strongly limit any potential application to geochemical datasets for rocks. As shown in Section 5, the equations given in Table 2 represent first-order geochemical tools that can be applied to natural felsic igneous suites to predict the impact of fractional crystallization on the behavior of Nb and Ta.

5. Discussion

5.1. Nb-Ta geochemical fractionation as a proxy for magmatic differentiation

In the compiled whole-rock datasets for rare-metal-enriched igneous suites, the Nb/Ta ratios do not positively correlate with Ta or Rb (Figs. 4 to 8). Although Rb is more fluid-sensitive than Ta, both elements generally show incompatible behavior in magmatic systems (e.g. Linnen and Cuney, 2005), and this may suggest a link between magmatic differentiation and decrease of the Nb/Ta ratio. In contrast to Rb, Nb/Ta shows a different behavior with Zr and Ce (Supplementary material 3) depending on the type of igneous suite. In transitional A-type granitoids, A2-type granitoids and MPG, the Nb/Ta ratio generally increases with Zr and Ce contents, likely reflecting the low solubility and early crystallization of specific minerals, such as zircon and monazite in metaluminous to peraluminous melts (Montel, 1993; Watson and Harrison, 1983).

However, with the exception of the Boziguo'er granites, the Nb/Ta ratio decreases with increasing Zr, Y, and Ce contents in A1-type granitoids and the Nechalacho nepheline syenites, reflecting the incompatible behavior and high solubility of these elements in peralkaline to metaluminous melts. Previous studies have shown that fractional crystallization of mica such as muscovite and biotite will result in a significant decrease in the Nb/Ta ratio of granitic melts (e.g. Stepanov et al., 2014). However, as mica is not necessarily present in A1-type igneous suites (Supplementary Material 1), a significant contribution from other minerals may be also important. Moreover, the capacity of mica to geochemically fractionate Nb and Ta was not evaluated for silica-undersaturated felsic igneous suites. In this section, we first evaluate semi-quantitatively the impact of fractional crystallization and accumulation of various minerals on theoretical magma compositions. Then, we attempt to reproduce the behavior of Nb-Ta in some rare-metal-enriched felsic igneous suites as described in Section 3.3 and shown in Figures 4 to 8.

5.1.1. Fractional crystallization and mineral accumulation modeling

In Figures 10a to 10d, we use the Rayleigh fractionation law and our regression for partitioning (Table 4) to evaluate the effects of fractional crystallization of different mineral phases on two theoretical parental melts: (1) similar to Nb-Ta-poor silica-undersaturated felsic igneous rocks ($\text{SiO}_2 = 55 \text{ wt.}\%$, $\text{Al}_2\text{O}_3 = 18 \text{ wt.}\%$; Nb = 80 ppm, Ta = 5 ppm, Nb/Ta = 16, Figs. 10a-b), and (2) similar to Nb-Ta-poor MPG ($\text{SiO}_2 = 72 \text{ wt.}\%$, $\text{Al}_2\text{O}_3 = 15 \text{ wt.}\%$; Nb = 14 ppm, Ta = 2 ppm, Nb/Ta = 7, Figs. 10c-d). For each model of crystallization, the fractionated assemblage consists of mainly feldspar, feldspathoid or quartz, for which a D_{Ta} and D_{Nb} of 0 was attributed, and a minor amount of one Nb-Ta-bearing mineral phase. The proportion of the Nb-Ta-bearing phase is either 15% for major phases such as amphibole, clinopyroxene, biotite and muscovite or 1% for accessory phases such as ilmenite, titanite and magnetite. The D_{Ta} and D_{Nb} of most

minerals are calculated using the melt SiO_2 and Al_2O_3 contents. However, no statistically robust equations could be derived for the extrapolation of magnetite D_{Nb} and D_{Ta} so we are using the average values of our compiled dataset (Supplementary Material 4) and the muscovite/melt partition coefficients are from Raimbault and Burnol (1998). Although quartz ($D_{\text{Ta}} < 0.01$) and plagioclase (D_{Nb} and $D_{\text{Ta}} < 0.1$) can only incorporate negligible amounts of Nb-Ta (Table 3), K-feldspar may reach D_{Nb} and D_{Ta} of 0.15 (e.g. White et al., 2003) in highly polymerized melts, which suggests that it could slightly affect the Nb-Ta budget of granitic melts during fractional crystallization. However, there is a dearth of K-feldspar/melt partitioning data, for both Nb and Ta, prohibiting the choice of representative values for the exercise performed in this study. Also, no mineral/melt partition coefficients for Nb and Ta are available for feldspathoids. Therefore, in these calculations, we consider the D_{Nb} and D_{Ta} of feldspar, feldspathoid and quartz to be equal to zero. This is considered a reasonable approach for our first-order modeling, and further refinements will have to await improvement of mineral/melt partitioning data.

At low-degrees of polymerization (Figs. 10a-b), biotite fractionation tends to slightly decrease the Nb/Ta ratio of the residual melt, but the Nb/Ta ratio of the melt stays relatively constant during the fractionation of amphibole, clinopyroxene and ilmenite. At a high-degree of polymerization (Figs. 10c-d), the fractionation of biotite, ilmenite, and to a lesser extent, amphibole, leads to a significant decrease of the melt Nb/Ta ratio, whereas this ratio stays constant during clinopyroxene fractionation. Similarly, magnetite fractionation does not affect the Nb/Ta ratio of the melt. In contrast, the fractionation of titanite always causes a significant increase in the melt Nb/Ta ratio, and the magnitude of the increase is even greater for melts with a high-degree of polymerization. Muscovite/melt partition coefficients suggest that fractional crystallization of this phase will decrease Nb/Ta.

Common Nb-Ta-rich mineral phases in rare-metal-mineralized felsic igneous rocks include CGM, PGM and, for peralkaline silica-undersaturated igneous suites, EGM. Unfortunately, mineral/melt partition coefficients are not available for these exotic mineral phases. In Figures 10a-d we attempt to model the effect of crystallization of these minerals using mass balance calculations and published mineral compositions (Table 5). In Figures 10a-b, the compositions of CGM, PGM and EGM correspond to the mean composition of minerals from nepheline syenites of the Nechalacho layered suite. The CGM is a columbite-Fe with $Nb/Ta = 28$ that was interpreted as magmatic in origin by Timofeev and Williams-Jones (2015), the EGM is a kentbrooksite ($Nb/Ta=13$, Johnsen et al., 2003; Möller and Williams-Jones, 2016) and the PGM is a fluorinatopyrochlore ($Nb/Ta=14$, Atencio et al., 2013; Möller and Williams-Jones, 2016). In Figure 10c-d, the CGM is a columbite-Fe ($Nb/Ta = 9$) from weakly mineralized LCT pegmatites of the Orange River belt (Ballouard et al., 2020). We predict that the crystallization of only 0.02% of PGM and CGM and 0.25% of EGM will strongly deplete the melts in Nb-Ta. However, the impact on the Nb/Ta ratio of the residual melt is variable depending on the relative Nb/Ta ratio of the fractionating mineral assemblage. If the Nb/Ta ratio of the minerals is above that of the parental melt (i.e. CGM), then crystallization of the minerals decreases the Nb/Ta of the residual melt and we predict the opposite behavior if $Nb/Ta_{\text{mineral}} < Nb/Ta_{\text{melt}}$ (i.e. PGM and EGM). Columbite and tantalite solubility experiments performed in granitic melts predict that the D_{Nb}/D_{Ta} of CGM is above unity and this value increases with melt polymerization (Linnen and Keppler, 1997) so $Nb/Ta_{\text{CGM}} > Nb/Ta_{\text{melt}}$ and, as shown in Figure 10, CGM crystallization should decrease the Nb/Ta value of the residual melt. The solubility experiment performed on PGM by McNeil et al. (2020) is not as conclusive as for CGM, but pyrochlore *sensu stricto*, the Nb-rich end-member of PGM, appears to be slightly more soluble in granitic melt than microlite (i.e. the Ta-rich end-member). Therefore, PGM crystallization should generally increase the

Nb/Ta value of the residual melt. Accordingly, the average Nb/Ta value of PGM in the Nechalacho layered suite is systematically lower than the corresponding whole-rock sample (Möller and Williams-Jones, 2016). This indicates that PGM incorporate preferentially Ta over Nb. Similarly, the mean Nb/Ta value of EGM (13) is below the mean value of whole-rock samples from the Nechalacho layered suite (14) suggesting that EGM may also preferentially incorporate Ta over Nb and therefore induce an increase of the Nb/Ta ratio of the melt upon crystallization. However, representative mineral/melt partitioning data are required to test this hypothesis. Overall, during fractional crystallization, only the presence of mica, ilmenite and, to a lesser extent, amphibole in the fractionating mineral assemblage, may cause a significant decrease of Nb/Ta in the melt with increasing Ta contents, thus reproducing the main evolutionary trends displayed by rare-metal-enriched felsic igneous suites.

Due to their low viscosity, the parental magmas of silica-undersaturated felsic intrusive rocks may be subject to gravitational crystal settling and this process of crystal accumulation may impact significantly the whole-rock Nb-Ta composition of these intrusions by inducing relative enrichments in heavy minerals (e.g. Marks and Markl, 2015). For example, cumulate layers of EGM and biotite with gravitational settling textures are common in the Nechalacho layered suite (Möller and Williams-Jones, 2016). In Figures 10e-f, we use mass balance calculations to model the evolution of the Nb and Ta contents of a relatively primitive nepheline syenite magma with 80 ppm Nb, 5 ppm Ta and a Nb/Ta ratio of 16 that underwent accumulation of minerals with a composition typical of silica-undersaturated peralkaline suites. Our model reproduces the mixing between two phases, i.e. melts and crystals, and is similar to a model of crystal assimilation. In our model, the degree of accumulation reaches up to 25% for major rock-forming mineral phases (i.e. biotite, clinopyroxene and amphibole) and 2.5% for accessory minerals (i.e. ilmenite,

titanite, EGM and PGM). Average mineral compositions are taken from the Nechalacho layered suite for biotite, clinopyroxene, EGM and PGM (Möller and Williams-Jones, 2016), the Pilanesberg complex of South Africa for clinopyroxene, titanite and amphibole (Giles, 2018), and alkaline complexes from the Ukrainian shield for ilmenite (Kryvdik, 2014) (see Table 5 for details). The accumulation of clinopyroxene ($Nb/Ta = 10$) that can only incorporate a limited amount of Nb-Ta does not have a significant effect on the Nb and Ta contents and Nb/Ta ratio of the magma. The accumulation of Nb-Ta-richer minerals with $D_{Nb}/D_{Ta} > 1$ in nepheline-syenite magmas such as biotite ($Nb/Ta = 48$) and, to a lesser extent, ilmenite ($Nb/Ta = 25$) and amphibole ($Nb/Ta = 27$), significantly increases the Nb/Ta ratio of the magma and may slightly increase the magma Nb-Ta content. In contrast, titanite ($Nb/Ta = 7$) and, probably, PGM ($Nb/Ta = 14$) and EGM ($Nb/Ta = 14$) preferentially incorporate Ta over Nb and accumulation of these exotic minerals may significantly decrease the Nb/Ta of the magma while inducing variable degrees of Nb-Ta enrichment.

5.1.2. Application to individual felsic igneous rock suites

In Figure 11, we attempt to reproduce the behavior of Nb and Ta in some silica-undersaturated felsic igneous rocks, A-type granitoids and MPG by modeling the fractional crystallization of the mineral assemblages described in the respective igneous suites (Supplementary Material 1). For simplification, the mineral/melt partition coefficients of minerals such as quartz, feldspar, feldspathoid, clinopyroxene and magnetite that cannot incorporate a significant amount of Nb-Ta (i.e. D_{Nb} and $D_{Ta} < \sim 0.2$) and influence the Nb-Ta budget of the melt during fractional crystallization are fixed to zero. The D_{Nb} and D_{Ta} of amphibole, biotite and ilmenite were estimated using the range of SiO_2 (and Al_2O_3) contents of selected igneous suites (see Figs. 4 to 8) with the equations of Table 4 and the D_{Ta} and D_{Nb} of

muscovite are from Raimbault and Burnol (1998). We would like to highlight that the composition of the parental melt and the mineral assemblages used in the crystallization models of Figure 11 are optimistic and chosen to fit the evolution trends of specific magmatic suites in the Nb/Ta versus Ta and Nb diagrams. To assess in detail their viability, these modeling would need to take into account the behavior of other elements as well as the thermodynamics of phase equilibrium but this would necessitate a dedicated study for each magmatic suite.

In unaltered nepheline syenites from the Nechalacho layered suite, the positive correlation between Nb/Ta and TiO_2 at high TiO_2 concentrations is in agreement with the crystallization of a Ti-rich phase with high Nb/Ta values such as biotite (Fig. 4f). The modeling of Figure 11a indicates that 99% of fractional crystallization of a mineral assemblage composed of 15% biotite and 85% feldspar, feldspathoid or clinopyroxene at high SiO_2 content of 65 wt.% can reproduce the behavior of Nb and Ta, but the modeling fails to reproduce the trend displayed by the suite at low SiO_2 content of 55 wt.%. Therefore, fractional crystallization alone is not sufficient to explain the Nb/Ta variation of the Nechalacho layered suite. As suggested by Möller and Williams-Jones (2016), additional Nb-Ta enrichment accompanied with a decrease of the Nb/Ta ratio might have been caused by the accumulation of Nb-Ta-rich minerals with low Nb/Ta values such as EGM that commonly occur as cumulate layers in the mineralized part of the intrusion. For example, 10% of EGM accumulation with the average composition of kentbrooksitite (Nb/Ta=13) from the Nechalacho layered suite would increase the magma Nb-Ta content by more than one order of magnitude (Fig. 11a). However, the accumulation of an EGM with lower Nb/Ta values is needed to decrease the Nb/Ta ratio of the magma below 10. Such scenario cannot be excluded as EGM reach an average Nb/Ta value of ~8 in one nepheline syenite sample (Möller and Williams-Jones, 2016) but more analyses are needed to better assess the range of Nb-

Ta composition of this mineral in the Nechalacho layered suite. Alternatively, and as further discussed in the next section, whole-rock samples with the lowest Nb/Ta and highest Nb-Ta concentrations are characteristic of the hydrothermally altered portions of the intrusion, so magmatic-hydrothermal processes might also have played a significant role in whole-rock Nb-Ta enrichment and decrease of the Nb/Ta ratio. Inversely, our mass balance calculations indicate that the superchondritic Nb/Ta values of some samples up to ~25 can be explained by the accumulation of 25% of biotite, which averages a Nb/Ta value of ~48 and commonly occurs as cumulate layers in the Nechalacho layered suite (Fig. 11a, Table 3). Additionally, a low-degree of crystallization of Nb-Ta-rich minerals with low Nb/Ta ratios such as PGM and EGM that have a mean Nb/Ta of 14 and 13, respectively, and occur as accessory mineral phases mostly all across the intrusion (Möller and Williams-Jones, 2016) may also induce significant Nb/Ta increase with Nb-Ta depletion in the residual melt. For example, 0.5% of EGM and 0.035% of PGM crystallization may increase the Nb/Ta ratio of the residual melt up to ~40 and 25, respectively, before completely depleting the melt in Ta (and Nb) (Fig. 11a).

In the Olkaria volcanic complex, the decrease of the Nb/Ta ratio with decreasing MgO, Mg# (Supplementary Material 3) and, to a lesser degree, TiO₂ (Fig. 5f) contents may reflect the fractionation of mafic phases such as ilmenite, amphibole and biotite. Similar mafic phases were described in the Ambohimirahavavy complex in Madagascar but no clear correlations are observed between MgO, Mg# and TiO₂ and Nb/Ta. In the model of Figure 11b, the behavior of Nb and Ta in both igneous suites can be reproduced by the fractional crystallization of 5% amphibole + 5% biotite + 0.04% ilmenite + ~90 % feldspar, quartz or clinopyroxene with SiO₂ and Al₂O₃ varying from 65 to 75 wt.% and 5 to 18 wt.%, respectively. The evolution trend of the

Olkaria volcanic rocks involves less than 80% of fractional crystallization whereas for the Ambohimirahavavy complex, the model indicates more than 90%.

It is worth specifying that in many A1-type granitoid suites and silica-undersaturated felsic suites, the behavior of Nb-Ta is difficult to explain by fractional crystallization only. In some cases, no correlations are observed between Nb-Ta, Ta or Nb as suggested by the data scatter observed for A1-type and silica-undersaturated samples in Figure 3. In some other cases such as in the Ambohimirahavavy complex granitoids, Boziguo'er granite and Baerzhe granite, no correlations appear between the Nb-Ta ratio and indicators of mafic phase crystallization such as TiO_2 , Mg# or MgO. This may be due to the variability of Nb-Ta-rich mineral phases that may crystallize (or accumulate) in peralkaline magma, source heterogeneities or magmatic-hydrothermal processes (see Section 5.2).

The common positive correlation between TiO_2 , MgO and Nb-Ta observed in transitional A-type granitoids from the Spitzkoppe stocks (Fig. 6f), A2-type granitoids from Krušné hory / Erzgebirge and the Qianlishan complex (Fig. 7f) as well as MPG from the European Variscan belt (Fig. 8f) is in agreement with the fractionation of mafic phases such as mica and ilmenite. The evolution of igneous rocks from the Spitzkoppe stocks (average $\text{SiO}_2 \sim 75$ wt.%), showing a decrease of the Nb-Ta ratio with a decrease of Nb and an increase of Ta can be reproduced by 99% of fractional crystallization of an assemblage composed of 10% biotite + 0.15% ilmenite + ~90% feldspar or quartz (Fig. 11c). The behavior of Nb and Ta in selected A2-type igneous rocks (Fig. 11d) and MPG (Fig. 11e) can also be easily reproduced by varying this fractionated mineral assemblage. However, an extreme degree of fractional crystallization, that even exceeds 99% for MPG, is needed to reproduce the range of variation of the Nb-Ta ratios and enrichment in Ta.

Overall, our modeling suggests that the fractional crystallization of mica, ilmenite and, to a lesser extent, amphibole may explain the anticorrelation between the Nb/Ta ratio and Ta content observed in many MPG and A-type granitoid suites but commonly involves an extreme degree of mineral fractionation above 90%. Fractional crystallization is likely to occur in magmatic bodies (Dufek and Bachmann, 2010) or during the ascent of magmas in dikes (Yamato et al., 2015), and the degree of mineral/melt segregation might be enhanced by deformation (e.g. Brown, 1994) and high concentration of fluxing components such as B, P, Li, F and H₂O which have the effect to reduce the viscosity and solidus of the magma (e.g. Černý et al., 2005; Linnen and Cuney, 2005; Thomas and Davidson, 2012). Alternatively, the extreme degree of fractional crystallization estimated based on our optimistic modeling may suggest that additional processes are requested to explain the behavior of Nb-Ta in rare-metal-enriched felsic igneous rocks. This hypothesis is supported by the absence of any obvious relation between fractional crystallization and Nb/Ta decrease in many A1-type granitoid suites (see above). Similarly, in the Nechalacho layered suite, the behavior of Nb-Ta is difficult to explain by fractional crystallization or crystal accumulation only. Alternative processes of Nb-Ta enrichment and geochemical fractionation may include the re-melting or assimilation of a previous batch or evolved igneous rocks. This was, for example, proposed to explain the particular U-enrichment of some MPG from the Variscan belt (Ballouard et al., 2018). Disequilibrium crystallization occurring due to a strong undercooling may also lead to significant geochemical fractionation between Nb and Ta (Van Lichtenvelde et al., 2018). Additionally, fluid- and melt-induced immiscibility and metasomatism may play a significant role that will be evaluated in the following section.

5.2. Nb-Ta geochemical fractionation as a marker of the magmatic-hydrothermal transition

The magmatic-hydrothermal transition in felsic igneous systems separates a system dominated by interactions between crystals and silicate melts toward a system involving complex interactions between crystals, silicate melts and immiscible aqueous media including hydrothermal fluids or hydrosaline melts (Halter and Webster, 2004). In addition to the arguments provided in Section 2.4, below we review existing whole-rock and mineral compositional evidence for Nb-Ta geochemical fractionation and mobility in magmatic-hydrothermal systems related to peralkaline and peraluminous felsic systems.

5.2.1. *Whole-rock geochemical markers*

A good whole-rock geochemical proxy of magmatic-hydrothermal evolution is represented by the lanthanide tetrad effect that corresponds to a particular type of REE patterns in curved segments that is commonly observed in highly evolved granites and associated metasomatic rocks (Fig. 12a). Such REE fractionation was also observed in minerals such as zircon (Yang et al., 2014) and CGM (Badanina et al., 2015) as well as melt inclusions (Peretyazhko and Savina, 2010). Although Duc-Tin and Keppler (2015) suggested that the tetrad effect can be explained by monazite or xenotime fractionation, this effect was observed in granites, such as the Baerzhe pluton, where evidence of monazite and xenotime fractionation is lacking and where REE behaved incompatibly (see the anticorrelation between Ce, Y and Nb/Ta in Supplementary Material 3 and Fig. 5). Moreover, most authors have argued that such REE patterns reflect selective complexation of REE by F or Cl during metasomatism or fluid and melt exsolution (e.g. Bau, 1996; Irber, 1999; Jahn et al., 2001; Veksler et al., 2005; Monecke et al., 2007; Peretyazhko and Savina, 2010). Irber (1999) quantified the degree of tetrad effect (TE_{1-3}) by determining the deviation of the first and third tetrad of REE patterns from a theoretical tetrad effect-free pattern and suggests that the tetrad effect becomes significant when $TE_{1-3} > 1.1$ (see caption of Fig. 12

for TE_{1-3} formula). In Figure 12, the Nb/Ta ratio tends to correlate negatively with TE_{1-3} for numerous magmatic suites including the A1-type Baerzhe granite, the transitional A-type Spitzkoppe granitoids as well as A2-type granitoids and MPG. Such behavior suggests a link between magmatic-hydrothermal activity and Nb-Ta geochemical fractionation.

Pervasive magmatic-hydrothermal activity in evolved felsic igneous rocks and their country-rocks is typically reflected by the partial or total replacement of primary mineral assemblages by secondary minerals such as muscovite (greisen), albite (albitite), tourmaline (tourmalinite) or calc-silicate minerals (skarn). In Figures 5 and 8, endoskarns associated with A1-type granitoids of the Ambohimirahavavy complex and greisens and albitites formed by the alteration of MPG commonly have high Nb-Ta contents, low Nb/Ta ratios, and commonly plot at the end of the evolution trends of their respective rare-metal-enriched igneous suites suggesting that magmatic-hydrothermal processes may lead to a decrease of the Nb/Ta ratio and induce significant HFSE enrichment. An important observation is that the metasomatized country-rocks of these intrusions can also reach similarly low Nb/Ta values and economic concentrations of Nb-Ta, indicating that this geochemical signature is not necessarily a reflection of prior magmatic evolution. In the Ambohimirahavavy complex, the unaltered limestone country-rocks have Nb contents between 3 and 6 ppm and Ta contents below the detection limit. In contrast, the exoskarns located at the immediate contact with A1-type granitoid dykes have Nb and Ta contents ranging from 1015 to 3461 ppm and 158 to 343 ppm, respectively, with Nb/Ta values from 11 to 39 and contain PGM and Nb-rich titanite (Estrade et al., 2015) (Supplementary Material 1). Similarly, in the Orange River pegmatite belt, the non- or weakly altered granodiorite country-rocks of LCT pegmatites ($8 < Nb/Ta < 9$) have Nb = 9-14 ppm and Ta = 1.0-1.4 ppm whereas the albitized or greisenized equivalents located at the immediate contact with pegmatites ($0.7 < Nb/Ta < 5.7$) have whole-rock

Nb and Ta concentrations from 16 to 116 ppm and 4 to 164 ppm, respectively and host Ta-Nb-rich rutile and PGM (Ballouard et al., 2020) (Supplementary Material 1). Additionally, a similar Ta enrichment up to 250 ppm was measured in metasomatized schists occurring at the contact with LCT pegmatites in the Cape Cross–Uis belt of Namibia (Fuchsloch et al., 2019). In these three cases, concerning either peralkaline or peraluminous systems, an increase by two orders of magnitude of whole-rock Ta (and Nb) concentration cannot be wholly explained by the volume decrease that commonly occurs during metasomatic processes such as albitization and greisenization (Launay et al., 2019); instead, it reflects an important hydrothermal HFSE enrichment.

5.2.2. Mineral composition markers

In Figure 13, the composition of rare-metal-rich crystals that have formed at different stages of the magmatic-hydrothermal transition in a highly peraluminous (Fig. 13a) and peralkaline granitic system (Fig. 13b) are reported in Nb/Ta versus Ta concentration diagrams. These include Nb-Ta oxide minerals from (Li)-Ta-Nb-Be mineralized LCT pegmatites from the Orange River belt (Ballouard et al., 2020) and zircon crystals from the REE-Zr-Nb mineralized A1-type Baerzhe granite (Yang et al., 2014). In LCT pegmatites from the Orange River belt, magmatic CGM are commonly replaced by PGM with a (fluor)calciomicrocline composition (Atencio et al., 2010) and the metasomatic agent was interpreted as a hydrosaline melt that was exsolved at the beginning of the magmatic-hydrothermal transition (Ballouard et al., 2020). (Fluor)calciomicrocline ($\text{Nb/Ta}_{\text{average}} = 0.1$, $\text{Ta}_2\text{O}_5_{\text{average}} = 60 \text{ wt.}\%$) is generally enriched in Ta and has lower Nb/Ta values than CGM ($\text{Nb/Ta}_{\text{average}} = 1.5$, $\text{Ta}_2\text{O}_5_{\text{average}} = 34 \text{ wt.}\%$) suggesting that the hydrosaline melt transported an important amount of Ta. Both CGM and (fluor)calciomicrocline were locally altered along the rim into a second generation of PGM with

high A-site vacancy and depleted in Ta ($\text{Nb/Ta}_{\text{average}} = 1.1$, $\text{Ta}_2\text{O}_5_{\text{average}} = 34$ wt.%). This replacement reaction was interpreted to reflect the circulation of a Ta-poor aqueous fluid exsolved at the end of the magmatic-hydrothermal transition. These data indicate that magmatic-hydrothermal alteration may cause an increase or decrease of the Nb/Ta ratio depending on the nature of the metasomatic medium. However, the oxide minerals with the highest Ta content generally have a magmatic-hydrothermal origin. Similarly, in the Baerzhe granites, prismatic and pristine magmatic zircon crystals are strongly depleted in Nb (average = 15 ppm) and Ta (average = 2 ppm) and have a high mean Nb/Ta value (11) compared to prismatic and porous metamict zircon crystals formed by the magmatic-hydrothermal alteration of magmatic zircon ($\text{Nb}_{\text{average}} = 637$ ppm, $\text{Ta}_{\text{average}} = 102$ ppm, $\text{Nb/Ta}_{\text{average}} = 6$). Although neoformed dipyramidal zircon crystals interpreted as hydrothermal in origin have similar Nb/Ta values (average = 11) as magmatic zircon, these crystals are also characterized by very high concentrations of Nb and Ta ($\text{Nb}_{\text{average}} = 1797$ ppm, $\text{Ta}_{\text{average}} = 272$ ppm). Regarding silica-undersaturated systems, in nepheline syenites from the Nechalacho layered suite, the lowest whole-rock Nb/Ta values occur in the hydrothermally altered upper part of the intrusion (Fig. 4) and despite the fact that Timofeev and Williams-Jones (2015) suggest that Nb and Ta mobility only occurs at the micron scale, most Nb- and Ta-rich minerals from the mineralized upper part, such as PGM and CGM, have a secondary origin. Interestingly, hydrothermal CGM ($\text{Ta}_2\text{O}_5_{\text{average}} = 3.8$ wt.%) from the mineralized portion of the intrusion are enriched in Ta compared to the rare magmatic CGM ($\text{Ta}_2\text{O}_5_{\text{average}} = 0.6$ wt.%, Timofeev and Williams-Jones, 2015; their Fig. 10).

Overall, we suggest that the decrease of the Nb/Ta ratio and enrichment of HFSE in rare-metal-enriched felsic igneous rocks is the result of both magmatic (i.e. fractional crystallization and disequilibrium crystallization) and magmatic-hydrothermal processes (i.e. aqueous fluid and

hydrosaline melt immiscibility and metasomatism). To date, experiments fail to reproduce the specific magmatic-hydrothermal conditions in which Ta is more mobile than Nb (see Section 2.4.). This paradox could relate to the various compositions and physical properties of H₂O-rich media, ranging from hydrosaline melts to exsolved brines, which can coexist at the end of the crystallization of highly evolved felsic igneous rocks. Such systems are likely challenging to reproduce experimentally but might be a good target for future research.

5.3. The origins of rare-metal-enriched felsic igneous suites inferred from Nb-Ta

Above, we have evaluated how magmatic and magmatic hydrothermal processes may affect the whole-rock Nb-Ta systematics of rare-metal-enriched felsic igneous suites. In this section, we use the Nb-Ta composition of the “primitive” members of these suites, characterized by low whole-rock Ta (and Nb) concentrations and high Nb/Ta values, to discuss the nature of and melting conditions in their sources.

5.3.1. *Muscovite-bearing peraluminous granites*

Muscovite-bearing peraluminous granites are typically interpreted as crustal magmas formed by the partial melting of clay-rich sediments or two mica-bearing igneous rocks in syn- to late-collisional settings (e.g. Bernard-Griffiths et al., 1985; Le Fort et al., 1987; Vielzeuf and Holloway, 1988; Barbarin, 1996; Patiño-Douce, 1999; Gao et al., 2016; Villaros et al., 2018). MPG, including primitive members with low whole-rock Ta and Nb concentrations, are characterized by low Nb/Ta ratios <10 below the average value of the bulk (11.4) and upper continental crust (13.3, Rudnick and Gao, 2003) (Fig. 3). At a global scale, this indicates that the parental melts of MPG have lower Nb/Ta ratios than their source, and that the partial melting reactions leading to the formation of MPG likely involve residual mineral phases with $D_{\text{Nb}}/D_{\text{Ta}}$

>1 at the conditions relevant to crustal melting such as biotite or ilmenite (Fig. 9). Therefore, in agreement with melting experiments (Patiño-Douce and Harris, 1998; Patiño-Douce, 1999) and thermodynamic modeling (Villaros et al., 2018), the Nb/Ta composition of primitive MPG may be explained by relatively low-temperature melting reactions of mica-bearing crustal rocks from muscovite-dehydration to incipient biotite-dehydration conditions.

5.3.2. A2-type granitoids

A2-type granitoids are commonly interpreted as having formed by either partial melting of biotite- and amphibole-bearing calc-alkaline granitoids (Skjerve and Johnston, 1992, 1993; Patiño-Douce, 1997), or by partial melting of a residual deep crust (e.g. Clemens et al., 1986; Whalen et al., 1987) with variable additions of mantle-derived melts from a source similar to island arc volcanic rocks, i.e., a lithospheric mantle that was affected by the subduction of an oceanic slab (Eby, 1990, 1992). Primitive A2-type granitoids with the lowest Ta and Nb concentrations have Nb/Ta values (1.5–2.0) that are higher than the bulk continental crust and a composition comparable to Ta- and Nb-rich IAV (Fig. 3). However, primitive A2-type granitoids are depleted in Nb and Ta compared to OIB or intraplate continental basalts. Because Nb is more compatible than Ta in biotite (Fig. 9), Stepanov and Hermann (2013) suggested that incipient melting (i.e. around muscovite-breakdown conditions) of mica-rich crustal rocks produces a biotite-rich residue with elevated Nb/Ta. The presence of residual ilmenite with $D_{\text{Nb}}/D_{\text{Ta}} > 1$ will also increase the Nb/Ta of the residue but no significant effect is expected due to the presence of residual rutile as this mineral has a $D_{\text{Nb}}/D_{\text{Ta}}$ close or slightly below unity in granitic melts (Schmidt et al., 2004). Therefore, in a late- or post-collisional setting, the high-temperature partial melting of a residual crust (i.e. a second melting event following, for example, the extraction of MPG melts) by biotite-dehydration reactions and potentially ilmenite destabilization

can form melts with relatively high Nb/Ta values possibly similar to those of A2-type granitoid suites. Accordingly, high-temperature metamorphism produces F-rich biotite (Finch and Tomkins, 2017) and the solubility of HFSE- and REE-rich mineral phases, such as zircon (Watson and Harrison, 1983), monazite (Montel, 1993) and Fe-Ti oxide minerals (e.g. Gaetani et al., 2008), increases with temperature in silicate melts. Consequently, high-temperature melting of biotite-rich residual material containing ilmenite, zircon and monazite can theoretically produce a melt enriched in F, HFSE and REE i.e. with the trace element compositional characteristic of A-type granitoids (e.g. Whalen et al., 1987).

However, the partial melting of a rock with only mica as a hydrous mineral phase produces a melt with a peraluminous composition (e.g. Gao et al., 2016) and A2-type granitoids are metaluminous to peraluminous (Fig. 2b). This suggests that some A2-type granitoids are not purely crustal melts and that they may represent the hybridization product between a felsic melt formed by the partial melting of a residual pelitic or mica-bearing igneous protolith and a mantle-derived mafic melt. As the more primitive A2-type granitoids have Nb-Ta compositions comparable to HFSE-rich IAV (Fig. 3), a likely candidate for this mafic end member would be a basaltic melt derived from the partial melting of the lithosphere. High-temperature crustal melting and hybridization may have been triggered by the emplacement of these hot mafic melts in the deep crust in a late orogenic setting. Alternatively, metaluminous to peraluminous melts with a composition similar to A2-type granitoids may be produced by the partial melting of amphibole- and biotite-bearing calc-alkaline tonalites or granodiorites typically formed in subduction setting (Skjerlie and Johnston, 1992, 1993; Patiño-Douce, 1997). However, silica-rich continental arc magmas are generally characterized by low Nb/Ta values close to the bulk continental crust (Tang et al., 2019, their Fig. 1a) so the presence of residual biotite and ilmenite (i.e. formed

during a first event of melt extraction) is likely necessary to significantly enriched the Nb/Ta ratio of these potential calc-alkaline igneous sources, and increase F content (Clemens et al., 1986; Finch and Tomkins, 2017). Overall, we suggest based on the lines of evidence described above that A2-type granitoids mostly form by the high-temperature partial melting of biotite- (and ilmenite-) rich residual crustal rocks with intermediate to felsic compositions, and variable degree of hybridization may have occurred with hot lithospheric mantle-derived melts possibly triggering melting events in the deep crust.

Present estimate of the lower continental crust composition (Nb/Ta = 8.3, Rudnick and Gao, 2003) does not support the presence of a high Nb/Ta reservoir in the deepest crust. However, the average middle crust consisting of amphibolite to lower granulite-facies rocks (i.e. with peak P-T conditions roughly around muscovite breakdown) has a high Nb/Ta ratio of 16.7 (Rudnick and Gao, 2003) that is comparable to primitive A2-type granitoids (see blue arrows in Fig. 3). This may suggest that the source of A2-type granitoids may be located in the deepest portion of the middle crust that underwent incipient partial melting but additional evidence is needed to confirm this hypothesis.

5.3.3. A1-type granitoids and silica-undersaturated felsic igneous rocks

A1-type silica-saturated and silica-undersaturated alkaline felsic igneous rocks are generally considered to form by low-degree mantle melting (e.g. Eby, 1992, 1998; Kramm and Kogarko, 1994; Sørensen, 1997), whereas the SiO₂-rich nature of A1-type granitoids is commonly interpreted, based on isotope data, to be the result of crustal contamination (e.g. Stevenson et al., 1997; Marks et al., 2003, 2004; Estrade et al., 2014a). Such rocks with rare-metal potential have been proposed to be either derived from an OIB-like source (e.g. Eby, 1992, 1998; Möller and Williams-Jones, 2016) or metasomatized lithospheric mantle (e.g. Downes et

al., 2005; Estrade et al., 2014a; Elburg and Cawthorn, 2017). Martin (2006) also suggested that partial melting of an alkali-metasomatized lower crust can lead to the formation of A-type granitoids. Despite the fact that, in contrast to nepheline syenite magmas, the parental melts of A1-type granitoids likely underwent significant crustal contamination following extraction from the mantle, the compositions of these two types of felsic igneous rocks are indistinguishable in the Nb/Ta versus Ta and Nb diagrams (Fig. 3). This is because crustal lithologies are generally depleted in Nb-Ta compared to silica-undersaturated igneous rocks and we predict that even an unrealistic amount of bulk crust assimilation (Rudnick and Gao, 2003, Nb = 8 ppm, Ta = 0.7 ppm, Nb/Ta = 11) up to 50% by a relatively Ta- and Nb-poor nepheline syenite melt (Nb = 80 ppm, Ta = 5 ppm, Nb/Ta = 16) will have no significant effect on its Nb-Ta composition (see red arrows in Figs. 10e-f). Assuming a basaltic parental melt for A1-type granitoids and nepheline syenites (e.g. Estrade et al., 2014a; Marks and Markle, 2015; Möller and Williams-Jones, 2016), we do not expect important geochemical fractionation of Nb-Ta during peridotite partial melting or basaltic melt evolutions. Indeed, the major rock-forming minerals of peridotite or basalts such as olivine, clinopyroxene, orthopyroxene, plagioclase and garnet are not able to incorporate a significant amount of Nb and Ta (Table 3) and rutile is highly soluble in basaltic melts (Gaetani et al., 2008). Similarly, amphibole and trioctahedral mica that commonly occur in metasomatized peridotites (e.g. Conceição and Green, 2004; Condamine and Médard, 2014) have a $D_{\text{Nb}}/D_{\text{Ta}}$ close to unity in low-SiO₂ basaltic melts (Fig. 9). Therefore, the Nb/Ta ratio of primitive A1-type granitoids and nepheline syenites should be comparable to their basaltic parents and ultimate mantle sources.

In Figure 3, the Nb-Ta composition of a significant proportion of Nb- and Ta-poor A1-type granitoids and nepheline syenites overlaps with modern OIB suites (Nb/Ta ~14-18) suggesting

that, at least, part of these felsic rocks may have formed by partial melting of a similar asthenospheric source. Accordingly, the similarity in terms of radiogenic isotope signature between nepheline syenites of the Kola Peninsula, Baltic shield, and modern OIB, led Kogarko et al. (2010) to suggest that the origin of these alkaline intrusions is connected to a deep-seated mantle plume. Spatial and temporal relationships between plume-related magmatism and the emplacement of alkaline complexes exist, for example, in Namibia where the Late Cretaceous Damaraland intrusive Suite hosting peralkaline granites and nepheline syenites is contemporaneous with the flood basalts of the Paraná-Etendeka large igneous Province that was linked to the Tristan plume (e.g. Schmitt et al., 2000; Trumbull et al., 2004; Miller, 2008; Owen-Smith et al., 2017). However, the Nb-Ta composition of numerous Nb- and Ta-poor A1-type granitoids and nepheline syenites also overlap with that of intraplate continental basalts from Central Europe that inherited their Nb-Ta signature by the partial melting of a metasomatized lithospheric mantle (Nb/Ta = 15-19, Pfander et al., 2012) (Fig. 3). This indicates that the Nb-Ta composition of relatively primitive nepheline syenites and A1-type granitoids does not necessarily originate from the asthenosphere. Numerous silica-undersaturated and A1-type felsic rocks display superchondritic Nb/Ta ratios of up to ~60 at relatively low Nb and Ta contents. Such superchondritic values can be reached by different processes including biotite accumulation as well as fractional crystallization of titanite and exotic mineral phases such as EGM and PGM (Figs. 10 and 11a). Eby et al. (1998) proposed that in the North Nyasa alkaline province of Malawi the superchondritic values of some nepheline syenites resulted from interaction with Nb-rich and Ta-poor hydrothermal fluids. Here we argue that in the absence of evidence for such hydrothermal overprint, such as in the Baerzhe and Boziguo'er A1-type granites (Fig. 5) as well as the transitional A-type Spitzkoppe granitoid suites (Fig. 6), the superchondritic Nb/Ta ratios of their Nb-Ta-poor end-members are likely a signature from their sources. It is possible that the

superchondritic Nb/Ta values of some samples from these intrusions (i.e. Baerzhe and Spitzkoppe granitoids) may represent an analytical artefact. However, considering the maximum analytical uncertainty of 15% on trace element concentrations specified by Jahn et al. (2001) for the Baerzhe granite, the three high Nb/Ta samples remain superchondritic (Fig. 5a). Unfortunately, this maximum analytical uncertainty was not specified for the Spitzkoppe granitoids (Frindt and Haapala, 2004; Haapala et al., 2007) but, if we take into account a maximum analytical uncertainty of 15%, the three samples with high Nb/Ta values would also remain superchondritic (Fig. 6a).

Metasomatism of the lithospheric mantle can be induced by variable agents including aqueous fluids and melts derived from the dehydration reactions or partial melting of a subducted oceanic slab as well as CO₂-rich melts such as carbonatites derived from the asthenosphere (e.g. Bebout, 2013; O'Reilly and Griffin, 2013). Aqueous fluids released at relatively low pressure during oceanic slab dehydration in the mantle wedge are generally Nb-Ta-poor and this has been used to explain the relative LILE and light REE enrichment compared to HFSE observed in most IAV (McCulloch and Gamble, 1991; Brenan et al., 1995). Consequently, lithospheric mantle metasomatized by such aqueous fluids does not represent a likely source for nepheline syenites and A1-type granitoids that are characterized by high HFSE concentration. Rutile is a common accessory phase of basaltic eclogite and its solubility in silicate melt decreases with pressure (Gaetani et al., 2008). Therefore, silicic melts formed by the partial melting of a subduction slab at high pressure in the presence of residual rutile with $D_{\text{Nb}}/D_{\text{Ta}} < 1$ can potentially reach superchondritic Nb/Ta values, and the mantle wedge metasomatized by these silicic melts is interpreted as the source of typically potassic arc volcanic rocks characterized by superchondritic values up to ~30 (Stolz et al., 1996; Gómez-Tuena et al., 2011). Nevertheless, potassic arc

volcanic rocks with high Nb/Ta values are characterized by absolute Nb and Ta contents below 20 and 1 ppm, respectively, and are not significantly enriched in Nb or Ta compared to typical IAV (Fig. 3). We, therefore, argue that a lithospheric mantle metasomatized by slab-derived silicic melts or aqueous fluids cannot represent a fertile source for A1-type granitoids or nepheline syenites. Alternatively, Pfänder et al. (2012) suggested that the high Nb/Ta ratios of intraplate alkaline basalts from Central Europe compared to OIB reflect metasomatism of the underlying continental lithospheric mantle by carbonatite melts (Fig. 3). Tappe et al. (2016) argued that primitive nephelinites from the Baltic Shield in Sweden scavenged Nb-rich pargasitic amphibole from the mantle lithosphere at <100 km depths, and these amphiboles may have been introduced to the mantle lithosphere during either carbonate or silicate melt metasomatism. Carbonatites at the Earth's surface are characterized by highly variable Nb and Ta contents (Nb ~0.1-1000 ppm; Ta ~0.1-100 ppm; Nb/Ta ~0.1-1000; Chakhmouradian, 2006), but their average Nb/Ta value (n = 203) is highly superchondritic (Nb/Ta_{average} ~124; Ta_{average} ~11 ppm; Nb_{average} ~330 ppm). However, Tappe et al. (2017) urged caution in using the trace element systematics of highly evolved melts such as carbonatites to infer their potential metasomatic impact on mantle lithosphere at >80 km depth. Interestingly, evidence of significant increase of whole-rock Nb/Ta ratios toward highly superchondritic values caused by fenitization with evolved carbonatite-related fluids exists, such as in the Lofdal intrusive suite in Namibia (Bodeving et al., 2017) (Fig. 14). In this intrusion, the Nb/Ta ratios of “unaltered” nepheline syenites are characterized by much lower Nb/Ta values (~ 18-60) than nepheline syenites fenitized at the contact with carbonatite (~ 25-230). The fenitization process is associated with a stronger increase in Nb contents relative to Ta from “unaltered” nepheline syenites (Nb ~ 110-1400 ppm, Ta ~2.5-30 ppm) toward metasomatized nepheline syenites (Nb ~ 164-4292 ppm, Ta ~2.3-43 ppm). Such metasomatic processes may also occur at greater depths within the lower crust and shallow

lithospheric mantle, where chemically overprinted lithologies provide alternative sources for silica-undersaturated and A1-type silica-saturated magmatic suites.

6. Conclusion

Silica-saturated and -undersaturated felsic igneous suites with rare-metal potential can be readily distinguished using the Nb/Ta versus Ta and Nb diagrams presented here. At given Nb and Ta contents, the Nb/Ta ratios of muscovite-bearing peraluminous granites (MPG) are lower compared to those of A-type granitoids. Generally, Nb/Ta ratios increase from A2-type to A1-type granitoid suites. The Nb-Ta compositions of A1-type granitoids are indistinguishable from those of nepheline syenites, and both igneous suites are locally characterized by superchondritic Nb/Ta (> 19.9), which is rare among magmatic rocks.

Despite a higher degree of data scatter in A1-type granitoids and nepheline syenites, the Nb/Ta ratios of rare-metal-enriched felsic igneous rocks commonly decrease with increasing Ta contents and increasing degree of differentiation. The mineral/melt partition coefficients for Nb and Ta (i.e., D_{Ta} and D_{Nb}) of biotite, amphibole, clinopyroxene, ilmenite and titanite increase with melt Si and/or Al contents (i.e. the degree of melt polymerization) so that first-order regressions can be used to estimate the D_{Nb} and D_{Ta} of these minerals as a function of the Si and Al content of a melt. Our modeling suggests that fractional crystallization of mica, ilmenite, and to a lesser degree amphibole plays a major role in the decrease of the Nb/Ta ratios. However, more than 90% of fractional crystallization is generally needed to explain the full range of Nb and Ta content variations of rare-metal-enriched igneous suites. In addition, metasomatic rocks formed by magmatic-hydrothermal alteration of igneous precursor rocks and their country-rocks, such as greisens, albitites and skarns, are also commonly enriched in both Nb and Ta. These metasomatic rocks are characterized by low Nb/Ta and they fall at the end of the evolution trends for rare-

metal-enriched felsic igneous suites. We therefore suggest that magmatic-hydrothermal processes involving hydrothermal fluids or hydrosaline melts participate in the decrease of the Nb/Ta ratio and the enrichment of HFSE leading to rare-metal deposits.

The Nb-Ta compositions of relatively primitive end-members of rare-metal-enriched felsic igneous rocks reflect the nature of their sources. MPG generally formed by a first event of partial melting of meta-sediments and mica-rich igneous rocks in the lower-middle crust during collisional to late-collisional tectonic events. A first event of incipient partial melting of mica-rich crustal rocks until muscovite-breakdown conditions will leave a residue that is enriched in biotite and ilmenite, and therefore characterized by high Nb/Ta. Subsequent high temperature partial melting of this residual crust in a late collisional setting can explain the Nb-Ta signature of A2-type granitoids. However, partial melting of a residual amphibole- and biotite-bearing source or hybridization between felsic melts that originated from a residual mica-bearing source and mafic melts derived from the lithospheric mantle is necessary to explain the metaluminous composition of some A2-type granitoids. The Nb-Ta compositions of A1-type granitoids as well as nepheline syenites overlap with OIB as well as intraplate continental basalts largely derived by partial melting of lithospheric mantle that has been metasomatized by carbonate-rich melts. This indicates that these alkali felsic igneous rocks may have formed by partial melting of the asthenosphere or an alkali-metasomatized lithosphere in rift-related intraplate tectonic settings. Rare superchondritic Nb/Ta can be explained by numerous magmatic and hydrothermal processes but, in some cases, it may also be a source signature exerted by low-volume carbonate-rich melts that percolate through the shallow continental lithospheric mantle and lower crust.

Nb-Ta geochemistry provides a powerful tool to classify rare-metal-enriched felsic igneous rocks, and to decipher their distinct origins and evolutionary paths including the processes that are critical in the formation of HFSE and REE mineral deposits.

7. Acknowledgments

The post-doctoral fellowship of C. Ballouard was funded by the University of Johannesburg, Faculty of Science and DSI-NRF CIMERA. M. Elburg, S. Tappe and F. Viljoen are supported by the National Research Foundation of South Africa (IFRR and DSI-NRF CIMERA grants). F. Viljoen acknowledges financial support from the South African Department of Science and Technology through their Research Chairs initiative (Geometallurgy), as administered by the National Research Foundation. We thank A. Stepanov and O. Müntener for comments on a previous version of the manuscript. The comments by J. Pfänder, an anonymous reviewer and editor A. Gómez-Tuena greatly improved the quality of the manuscript.

8. References

- Acosta-Vigil, A., Buick, I., Hermann, J., Cesare, B., Rubatto, D., London, D., Morgan, G.B., 2010. Mechanisms of crustal anatexis: a geochemical study of partially melted metapelitic enclaves and host dacite, SE Spain. *J. Petrol.* 51, 785–821.
- Adam, J., Green, T., 2006. Trace element partitioning between mica-and amphibole-bearing garnet lherzolite and hydrous basanitic melt: 1. Experimental results and the investigation of controls on partitioning behaviour. *Contrib. to Mineral. Petrol.* 152, 1–17.
- Adam, J., Green, T.H., 1994. The effects of pressure and temperature on the partitioning of Ti, Sr and REE between amphibole, clinopyroxene and basanitic melts. *Chem. Geol.* 117, 219–233.
- Adam, J., Green, T.H., Sie, S.H., 1993. Proton microprobe determined partitioning of Rb, Sr, Ba, Y, Zr, Nb and Ta between experimentally produced amphiboles and silicate melts with variable F content. *Chem. Geol.* 109, 29–49.
- Adam, J., Oberti, R., Cámara, F., Green, T.H., 2007. An electron microprobe, LAM-ICP-MS and single-crystal X-ray structure refinement study of the effects of pressure, melt-H₂O concentration and fO₂ on experimentally produced basaltic amphiboles. *Eur. J. Mineral.* 19, 641–655.
- Anderson, M.O., Lentz, D.R., Mcfarlane, C.R.M., Falck, H., 2013. A geological, geochemical and textural study of a LCT pegmatite: Implications for the magmatic versus metasomatic origin of Nb-Ta mineralization in the Moose II pegmatite, Northwest Territories, Canada. *J. Geosci. (Czech Republic)* 58, 299–320. <https://doi.org/10.3190/jgeosci.149>

- Arevalo, R., McDonough, W.F., 2010. Chemical variations and regional diversity observed in MORB. *Chem. Geol.* 271, 70–85. <https://doi.org/10.1016/j.chemgeo.2009.12.013>
- Aseri, A.A., Linnen, R.L., Che, X.D., Thibault, Y., Holtz, F., 2015. Effects of fluorine on the solubilities of Nb, Ta, Zr and Hf minerals in highly fluxed water-saturated haplogranitic melts. *Ore Geol. Rev.* 64, 736–746. <https://doi.org/10.1016/j.oregeorev.2014.02.014>
- Atencio, D., Andrade, M.B., Christy, A.G., Gieré, R., Kartashov, P.M., 2010. The pyrochlore supergroup of minerals: nomenclature. *Can. Mineral.* 48, 673–698.
- Aulbach, S., O'Reilly, S.Y., Griffin, W.L., Pearson, N.J., 2008. Subcontinental lithospheric mantle origin of high niobium/tantalum ratios in eclogites. *Nat. Geosci.* 1, 468.
- Badanina, E. V., Sitnikova, M.A., Gordienko, V. V., Melcher, F., Gäbler, H.E., Lodziak, J., Syritso, L.F., 2015. Mineral chemistry of columbite-tantalite from spodumene pegmatites of Kolmozero, Kola Peninsula (Russia). *Ore Geol. Rev.* 64, 720–735. <https://doi.org/10.1016/j.oregeorev.2014.05.009>
- Badanina, E. V., Syritso, L.F., Volkova, E. V., Thomas, R., Trumbull, R.B., 2010. Composition of Li-F granite melt and its evolution during the formation of the ore-bearing Orlovka massif in Eastern Transbaikalia. *Petrology* 18, 131–157. <https://doi.org/10.1134/S0869591110020037>
- Bailey, J.C., Rose-Hansen, J., Soerensen, H., Gwozdz, R., 2001. Geochemical overview of the Ilímaussaq alkaline complex, South Greenland. *Geol. Greenl. Surv. Bull.* 190, 35–53.
- Ballouard, C., Elburg, M.A., Tappe, S., Reinke, C., Ueckermann, V., Doggart, S., 2020. Magmatic-hydrothermal evolution of rare metal pegmatites from the Mesoproterozoic Orange River pegmatite belt (Namaqualand, South Africa). *Ore Geol. Rev.* <https://doi.org/10.1016/j.oregeorev.2019.103252>
- Ballouard, C., Poujol, M., Zeh, A., 2018. Multiple crust reworking in the French Armorican Variscan belt: implication for the genesis of uranium-fertile leucogranites. *Int. J. Earth Sci.* 107, 2317–2336.
- Ballouard, C., Branquet, Y., Tartèse, R., Poujol, M., Boulvais, P., Vigneresse, J.-L., 2016b. Nb-Ta fractionation in peraluminous granites: A marker of the magmatic-hydrothermal transition: Reply. *Geology* 44, e395. <https://doi.org/10.1130/G38169Y.1>
- Ballouard, C., Poujol, M., Boulvais, P., Branquet, Y., Tartèse, R., Vigneresse, J.L., 2016a. Nb-Ta fractionation in peraluminous granites: A marker of the magmatic-hydrothermal transition. *Geology* 44, 231–234. <https://doi.org/10.1130/G37475.1>
- Barbarin, B., 1999. A review on the relationships between granitoid types, their origins and their geodynamic environments. *Lithos* 46, 603–626. [https://doi.org/10.1016/S0024-4937\(98\)00085-1](https://doi.org/10.1016/S0024-4937(98)00085-1)
- Barbarin, B., 1996. Genesis of the two main types of peraluminous granitoids. *Geology* 24, 295–298. [https://doi.org/10.1130/0011-7613\(1996\)024<295:GOTTMT>2.3.CO;2](https://doi.org/10.1130/0011-7613(1996)024<295:GOTTMT>2.3.CO;2)
- Bartels, A., Holtz, F., Linnen, R.L., 2010. Solubility of manganotantalite and manganocolumbite in pegmatitic melts. *Am. Mineral.* 95, 537–544.
- Bau, M., 1996. Controls on the fractionation of isovalent trace elements in magmatic and aqueous systems: evidence from Y/Ho, Zr/Hf, and lanthanide tetrad effect. *Contrib. to Mineral. Petrol.* 123, 323–333. <https://doi.org/10.1007/s004100050159>
- Bebout, G.E., 2013. Metasomatism in Subduction Zones of Subducted Oceanic Slabs, Mantle Wedges, and the Slab-Mantle Interface, in: *Metasomatism and the Chemical Transformation of Rock*. Springer Berlin Heidelberg, pp. 289–349.
- Bennett, S.L., Blundy, J., Elliott, T., 2004. The effect of sodium and titanium on crystal-melt partitioning of trace elements. *Geochim. Cosmochim. Acta* 68, 2335–2347.
- Blundy, J.D., Robinson, J.A.C., Wood, B.J., 1998. Heavy REE are compatible in clinopyroxene on the spinel lherzolite solidus. *Earth Planet. Sci. Lett.* 160, 493–504.

- Bodeving, S., Williams-Jones, A.E., Swinden, S., 2017. Carbonate--silicate melt immiscibility, REE mineralising fluids, and the evolution of the Lofdal Intrusive Suite, Namibia. *Lithos* 268, 383–398.
- Bonin, B., 2007. A-type granites and related rocks: evolution of a concept, problems and prospects. *Lithos* 97, 1–29.
- Breiter, K., 2012. Nearly contemporaneous evolution of the A- and S-type fractionated granites in the Krušné hory/Erzgebirg Mts., Central Europe. *Lithos* 151, 105–121. <https://doi.org/10.1016/j.lithos.2011.09.022>
- Brenan, J.M., Shaw, H.F., Ryerson, F.J., Phinney, D.L., 1995. Experimental determination of trace-element partitioning between pargasite and a synthetic hydrous andesitic melt. *Earth Planet. Sci. Lett.* 135, 1–11.
- Brown, M., 1994. The generation, segregation, ascent and emplacement of granite magma: the migmatite-to-crustally-derived granite connection in thickened orogens. *Earth-Science Rev.* 36, 83–130.
- Cartier, C., Hammouda, T., Boyet, M., Bouhifd, M.A., Devidal, J.-L., 2014. Redox control of the fractionation of niobium and tantalum during planetary accretion and core formation. *Nat. Geosci.* 7, 573.
- Černý, P., Ercit, T.S., 2005. The classification of granitic pegmatites revisited. *Can. Mineral.* 43, 2005–2026. <https://doi.org/10.2113/gscanmin.43.6.2005>
- Černý, P., Masau, M., Goad, B.E., Ferreira, K., 2005. The Greer Lake leucogranite, Manitoba, and the origin of lepidolite-subtype granitic pegmatites. *Lithos* 80, 305–321. <https://doi.org/10.1016/j.lithos.2003.11.003>
- Chakhmouradian, A.R., 2006. High-field-strength elements in carbonatitic rocks: geochemistry, crystal chemistry and significance for constraining the sources of carbonatites. *Chem. Geol.* 235, 138–160.
- Chakhmouradian, A.R., Zaitsev, A.N., 2012. Rare Earth Mineralization in Igneous Rocks: Sources and Processes. *Elements* 8, 347–353. <https://doi.org/10.2113/gselements.8.3.347>
- Chen, Y., Li, H., Sun, W., Ireland, T., Tian, X., Liu, Y., Yang, W., Chen, C., Xu, D., 2016. Generation of Late Mesozoic Qianlishan A2-type granite in Nanling Range, South China: implications for Shizhuyuan W-Sn mineralization and tectonic evolution. *Lithos* 266, 435–452.
- Chevychelov, V.Y., Zaraisky, G.P., Borisovskii, S.E., Borkov, D.A., 2005. Effect of melt composition and temperature on the partitioning of Ta, Nb, Sn, and F between granitic (alkaline) melt and fluorine-bearing aqueous fluid: fractionation of Ta and Nb and conditions of ore formation in rare-metal granites. *Petrol. c/c Petrol.* 13, 305.
- Clemens, J.D., Holloway, J.R., White, A.J.R., 1986. Origin of an A-type granite; experimental constraints. *Am. Mineral.* 71, 317–324.
- Collins, W.J., Beams, S.D., White, A.J.R., Chappell, B.W., 1982. Nature and origin of A-type granites with particular reference to southeastern Australia. *Contrib. to Mineral. Petrol.* 80, 189–200.
- Corgne, A., Armstrong, L.S., Keshav, S., Fei, Y., McDonough, W.F., Minarik, W.G., Moreno, K., 2012. Trace element partitioning between majoritic garnet and silicate melt at 10–17 GPa: Implications for deep mantle processes. *Lithos* 148, 128–141.
- Cox, K.G., Bell, J.D., Pankhurst, R.J., 1979. *The interpretation of igneous rocks*. Springer Science & Business Media.
- Cuney, M., Marignac, C., Weisbrod, A., 1992. The Beauvoir topaz-lepidolite albite granite (Massif Central, France); the disseminated magmatic Sn-Li-Ta-Nb-Be mineralization. *Econ. Geol.* 87, 1766–1794.
- Dalpé, C., Baker, D.R., 2000. Experimental investigation of large-ion-lithophile-element-, high-field-strength-element-and rare-earth-element-partitioning between calcic amphibole and basaltic melt: the effects of pressure and oxygen fugacity. *Contrib. to Mineral. Petrol.* 140, 233–250.
- Dostal, J., Chatterjee, A.K., 2000. Contrasting behaviour of Nb/Ta and Zr/Hf ratios in a peraluminous granitic pluton (Nova Scotia, Canada). *Chem. Geol.* 163, 207–218. [https://doi.org/10.1016/S0009-2541\(99\)00113-8](https://doi.org/10.1016/S0009-2541(99)00113-8)
- Dostal, J., Chatterjee, A.K., 1995. Origin of topaz-bearing and related peraluminous granites of the Late Devonian

- Davis Lake pluton, Nova Scotia, Canada: crystal versus fluid fractionation. *Chem. Geol.* 123, 67–88. [https://doi.org/10.1016/0009-2541\(95\)00047-P](https://doi.org/10.1016/0009-2541(95)00047-P)
- Dostal, J., Kontak, D.J., Gerel, O., Gregory Shellnutt, J., Fayek, M., 2015. Cretaceous ongonites (topaz-bearing albite-rich microleucogranites) from Ongon Khaikhan, Central Mongolia: Products of extreme magmatic fractionation and pervasive metasomatic fluid: rock interaction. *Lithos* 236–237, 173–189. <https://doi.org/10.1016/j.lithos.2015.08.003>
- Dostal, J., Shellnutt, J.G., 2016. Origin of peralkaline granites of the Jurassic Bokan Mountain complex (southeastern Alaska) hosting rare metal mineralization. *Int. Geol. Rev.* 58, 1–13.
- Downes, H., Balaganskaya, E., Beard, A., Liferovich, R., Demaiffe, D., 2005. Petrogenetic processes in the ultramafic, alkaline and carbonatitic magmatism in the Kola Alkaline Province: A review. *Lithos* 85, 48–75. <https://doi.org/10.1016/j.lithos.2005.03.020>
- Duc-Tin, Q., Keppler, H., 2015. Monazite and xenotime solubility in granitic melts and the origin of the lanthanide tetrad effect. *Contrib. to Mineral. Petrol.* 169, 8.
- Dufek, J., Bachmann, O., 2010. Quantum magmatism: Magmatic composition gaps generated by melt-crystal dynamics. *Geology* 38, 687–690. <https://doi.org/10.1130/G30831.1>
- Dygert, N., Liang, Y., Hess, P., 2013. The importance of melt TiO₂ in affecting major and trace element partitioning between Fe-Ti oxides and lunar picritic glass melts. *Geochim. Cosmochim. Acta* 106, 134–151.
- Eby, G.N., 1992. Chemical subdivision of the A-type granitoids: Petrogenetic and tectonic implications. *Geology* 20, 641–644. [https://doi.org/10.1130/0091-7613\(1992\)020<0641:CSGAT>2.3.CO;2](https://doi.org/10.1130/0091-7613(1992)020<0641:CSGAT>2.3.CO;2)
- Eby, G.N., 1990. The A-type granitoids: a review of their occurrence and chemical characteristics and speculations on their petrogenesis. *Lithos* 26, 115–134.
- Eby, G.N., Woolley, A.R., Platt, V.D.G., 1998. Geochemistry and petrogenesis of nepheline syenites: Kasungu-Chipala, Ilomba, and Ulindi nepheline syenite intrusions, North Nyasa Alkaline Province, Malawi. *J. Petrol.* 39, 1405–1424. <https://doi.org/10.1093/петroi/39.8.1405>
- Elburg, M.A., Cawthorn, R.G., 2017. Source and evolution of the alkaline Pilanesberg Complex, South Africa. *Chem. Geol.* 455, 148–165.
- Elkins, L.J., Gaetani, G.A., Sims, K.W.W., 2008. Partitioning of U and Th during garnet pyroxenite partial melting: Constraints on the source of alkaline ocean island basalts. *Earth Planet. Sci. Lett.* 265, 270–286.
- Estrade, G., Béziat, D., Salvi, S., Tiepolo, M., Paquette, J.-L., Rakotovo, S., 2014a. Unusual evolution of silica-under-and-oversaturated alkaline rocks in the Cenozoic Ambohimirahavavy Complex (Madagascar): Mineralogical and geochemical evidence. *Lithos* 206, 361–383.
- Estrade, G., Salvi, S., Béziat, D., Rakotovo, S., Rakotondrazafy, R., 2014b. REE and HFSE mineralization in peralkaline granites of the Ambohimirahavavy alkaline complex, Ampasindava peninsula, Madagascar. *J. African Earth Sci.* 94, 141–155.
- Estrade, G., Salvi, S., Béziat, D., Williams-Jones, A.E., 2015. The origin of skarn-hosted rare-metal mineralization in the Ambohimirahavavy alkaline complex, Madagascar. *Econ. Geol.* 110, 1485–1513. <https://doi.org/10.2113/econgeo.110.6.1485>
- Fedele, L., Lustrino, M., Melluso, L., Morra, V., Zanetti, A., Vannucci, R., 2015. Trace-element partitioning between plagioclase, alkali feldspar, Ti-magnetite, biotite, apatite, and evolved potassic liquids from Campi Flegrei (Southern Italy). *Am. Mineral.* 100, 233–249.
- Fiege, A., Simon, A., Linsler, S.A., Bartels, A., Linnen, R.L., 2018. Experimental constraints on the effect of phosphorous and boron on Nb and Ta ore formation. *Ore Geol. Rev.* 94, 383–395.
- Finch, E.G., Tomkins, A.G., 2017. Fluorine and chlorine behaviour during progressive dehydration melting: Consequences for granite geochemistry and metallogeny. *J. Metamorph. Geol.* 35, 739–757.

- Förster, H.-J., Tischendorf, G., Trumbull, R.B., Gottesmann, B., 1999. Late-Collisional Granites in the Variscan Erzgebirge, Germany. *J. Petrol.* 40, 1613–1645. <https://doi.org/10.1093/petroj/40.11.1613>
- Frei, D., Liebscher, A., Franz, G., Wunder, B., Klemme, S., Blundy, J., 2009. Trace element partitioning between orthopyroxene and anhydrous silicate melt on the lherzolite solidus from 1.1 to 3.2 GPa and 1,230 to 1,535°C in the model system Na₂O-CaO-MgO-Al₂O₃-SiO₂. *Contrib. to Mineral. Petrol.* 157, 473.
- Fosso Tchunte, P., Tchameni, R., André-Mayer, A.-S., Dakoure, H., Turlin, F., Poujol, M., Nomo, E., Saha Fouotsa, A., Rouer, O., 2018. Evidence for Nb-Ta Occurrences in the Syn-Tectonic Pan-African Mayo Salah Leucogranite (Northern Cameroon): Constraints from Nb-Ta Oxide Mineralogy, Geochemistry and U-Pb LA-ICP-MS Geochronology on Columbite and Monazite. *Minerals* 8, 188.
- Friis, H., Casey, W.H., 2018. Niobium Is Highly Mobile As a Polyoxometalate Ion During Natural Weathering. *Can. Mineral.* 56, 905–912.
- Frindt, S., Haapala, I., Pakkanen, L., 2004. Anorogenic Gross Spitzkoppe granite stock in central western Namibia: Part I. Petrology and geochemistry. *Am. Mineral.* 89, 841–856.
- Frindt, S., Haapala, I., 2004. Anorogenic Gross Spitzkoppe granite stock in central western Namibia: Part II. Structures and textures indicating crystallization from undercooled melt. *Am. Mineral.* 89, 857–866.
- Frost, B.R., Frost, C.D., 2008. A Geochemical Classification for Feldspathic Igneous Rocks 49, 1955–1969. <https://doi.org/10.1093/petrology/egn054>
- Frost, B.R., Barnes, C.G., Collins, W.J., Arculus, R.J., Ellis, D.J., Frost, C.D., 2001. A geochemical classification for granitic rocks. *J. Petrol.* 42, 2033–2048. <https://doi.org/10.1093/petrology/42.11.2033>
- Fuchsloch, W.C., 2018. Pegmatites of the Cape Cross-Uis pegmatite belt, Namibia: structural, mineralogical, geochemical and mineral chemical characterisation with implications for petrogenesis and mineralisation. (Thesis, University of the Witwatersrand) (257 pp.). <http://wiredspace.wits.ac.za/handle/10539/27136>
- Fuchsloch, W.C., Nex, P.A.M., Kinnaird, J.A., 2019. The geochemical evolution of Nb-Ta-Sn oxides from pegmatites of the Cape Cross-Uis pegmatite belt, Namibia. *Mineral. Mag.* 83, 161–179.
- Fulmer, E.C., Nebel, O., van Westrenen, W., 2010. High-precision high field strength element partitioning between garnet, amphibole and alkaline melt from Akanui, New Zealand. *Geochim. Cosmochim. Acta* 74, 2741–2759.
- Gaetani, G.A., Asimow, P.D., Stolper, E.M., 2008. A model for rutile saturation in silicate melts with applications to eclogite partial melting in subduction zones and mantle plumes. *Earth Planet. Sci. Lett.* 272, 720–729.
- Gao, P., Zheng, Y.-F., Zhao, Z. F., 2016. Experimental melts from crustal rocks: a lithochemical constraint on granite petrogenesis. *Lithos* 216, 133–157.
- Giles, K.N.R., 2018. Distribution of trace elements among coexisting minerals in agpaitic nepheline syenites in the Pilanesberg Complex, South Africa. (Thesis, University of Oslo) (131 pp.). <http://urn.nb.no/URN:NBN:no-67455>
- Gómez-Tuena, A., Mori, L., Goldstein, S.L., Pérez-Arvizu, O., 2011. Magmatic diversity of western Mexico as a function of metamorphic transformations in the subducted oceanic plate. *Geochim. Cosmochim. Acta* 75, 213–241.
- Green, T.H., Blundy, J.D., Adam, J., Yaxley, G.M., 2000. SIMS determination of trace element partition coefficients between garnet, clinopyroxene and hydrous basaltic liquids at 2-7.5 GPa and 1080-1200 C. *Lithos* 53, 165–187.
- Green, T.H., Sie, S.H., Ryan, C.G., Cousens, D.R., 1989. Proton microprobe-determined partitioning of Nb, Ta, Zr, Sr and Y between garnet, clinopyroxene and basaltic magma at high pressure and temperature. *Chem. Geol.* 74, 201–216.
- Gunn, G., 2014. Critical metals handbook. John Wiley & Sons. (425 pp.)
- Guo, C.L., Wang, R.C., Yuan, S. Da, Wu, S.H., Yin, B., 2015. Geochronological and geochemical constraints on the

- petrogenesis and geodynamic setting of the Qianlishan granitic pluton, Southeast China. *Mineral. Petrol.* 109, 253–282. <https://doi.org/10.1007/s00710-014-0355-1>
- Haapala, I., Frindt, S., Kandara, J., 2007. Cretaceous Gross Spitzkoppe and Klein Spitzkoppe stocks in Namibia: Topaz-bearing A-type granites related to continental rifting and mantle plume 97, 174–192. <https://doi.org/10.1016/j.lithos.2006.12.002>
- Halter, W.E., Webster, J.D., 2004. The magmatic to hydrothermal transition and its bearing on ore-forming systems. *Chem. Geol.* 210, 1–6. <https://doi.org/10.1016/j.chemgeo.2004.06.001>
- Harlaux, M., Mercadier, J., Bonzi, W.M.-E., Kremer, V., Marignac, C., Cuney, M., 2017. Geochemical signature of magmatic-hydrothermal fluids exsolved from the Beauvoir Rare-Metal Granite (Massif Central, France): insights from LA-ICPMS analysis of primary fluid inclusions. *Geofluids* 2017.
- Harris, C., Dreyer, T., le Roux, P., 2018. Petrogenesis of peralkaline granite dykes of the Straumsvola complex, western Dronning Maud Land, Antarctica. *Contrib. to Mineral. Petrol.* 177, 8.
- Hilyard, M., Nielsen, R.L., Beard, J.S., Patin-Douce, A., Blencoe, J., 2000. Experimental determination of the partitioning behavior of rare earth and high field strength elements between perargasitic amphibole and natural silicate melts. *Geochim. Cosmochim. Acta* 64, 1103–1120.
- Huang, H., Wang, T., Zhang, Z., Li, C., Qin, Q., 2018. Highly differentiated fluorine-rich, alkaline granitic magma linked to rare metal mineralization: A case study from the Duzigao'er rare metal granitic pluton in South Tianshan Terrane, Xinjiang, NW China. *Ore Geol. Rev.* 96, 146–153.
- Irber, W., 1999. The lanthanide tetrad effect and its correlation with K/Rb, Eu/Eu*, Sr/Eu, Y/Ho, and Zr/Hf of evolving peraluminous granite suites. *Geochim. Cosmochim. Acta* 63, 489–508.
- Irvine, T.N.J., Baragar, W., 1971. A guide to the chemical classification of the common volcanic rocks. *Can. J. Earth Sci.* 8, 523–548.
- Jahn, B., Wu, F., Capdevila, R., Martineau, F., Zhao, Z., Wang, Y., 2001. Highly evolved juvenile granites with tetrad REE patterns: the Woduhe and Baerzhan granites from the Great Xing'an Mountains in NE China. *Lithos* 59, 171–198. [https://doi.org/10.1016/S0024-4937\(01\)00066-4](https://doi.org/10.1016/S0024-4937(01)00066-4)
- Jones, A.P., Genge, M., Carmody, J., 2013. Carbonate Melts and Carbonatites 75, 289–322. <https://doi.org/10.2138/rmg.2013.75.10>
- Johnsen, O., Ferraris, G., Gault, R.A., Grace, J.D., Kampf, A.R., Pekov, I. V., 2003. The nomenclature of eudialyte-group minerals. *Can. Mineral.* 41, 785–794.
- Kaeter, D., Barros, R., Menuge, J.F., Chew, D.M., 2018. The magmatic–hydrothermal transition in rare-element pegmatites from southeast Ireland: LA-ICP-MS chemical mapping of muscovite and columbite–tantalite. *Geochim. Cosmochim. Acta* 240, 98–130. <https://doi.org/10.1016/j.gca.2018.08.024>
- Karsli, O., Aydin, F., Uysal, I., Dokuz, A., Kumral, M., Kandemir, R., Budakoglu, M., Ketenci, M., 2018. Latest Cretaceous “A2-type” granites in the Sakarya Zone, NE Turkey: Partial melting of mafic lower crust in response to roll-back of Neo-Tethyan oceanic lithosphere. *Lithos* 302, 312–328.
- Klemme, S., Blundy, J.D., Wood, B.J., 2002. Experimental constraints on major and trace element partitioning during partial melting of eclogite. *Geochim. Cosmochim. Acta* 66, 3109–3123.
- Kogarko, L.N., Lahaye, Y., Brey, G.P., 2010. Plume-related mantle source of super-large rare metal deposits from the Lovozero and Khibina massifs on the Kola Peninsula, Eastern part of Baltic Shield: Sr, Nd and Hf isotope systematics. *Mineral. Petrol.* 98, 197–208. <https://doi.org/10.1007/s00710-009-0066-1>
- Klimm, K., Blundy, J.D., Green, T.H., 2008. Trace element partitioning and accessory phase saturation during H₂O-saturated melting of basalt with implications for subduction zone chemical fluxes. *J. Petrol.* 49, 523–553.
- König, S., Schuth, S., 2011. Deep melting of old subducted oceanic crust recorded by superchondritic Nb/Ta in modern island arc lavas. *Earth Planet. Sci. Lett.* 301, 265–274. <https://doi.org/10.1016/j.epsl.2010.11.007>

- Kramm, U., Kogarko, L.N., 1994. Nd and Sr isotope signatures of the Khibina and Lovozero agpaite centres, Kola Alkaline Province, Russia. *Lithos* 32, 225–242.
- Kryvdik, S.G., 2014. Geochemical features of ilmenites from the alkaline complexes of the Ukrainian Shield: LA-ICP MS data. *Geochemistry Int.* 52, 287–295.
- Launay, G., Sizaret, S., Guillou-Frottier, L., Fauguerolles, C., Champallier, R., Gloaguen, E., 2019. Dynamic permeability related to greisenization reactions in Sn-W ore deposits: Quantitative petrophysical and experimental evidence. *Geofluids* 2019, 16–20. <https://doi.org/10.1155/2019/5976545>
- Li, L., Xiong, X.L., Liu, X.C., 2017. Nb/Ta fractionation by amphibole in hydrous basaltic systems: implications for arc magma evolution and continental crust formation. *J. Petrol.* 58, 3–28.
- Linnen, R.L., 2005. The effect of water on accessory phase solubility in subaluminous and peralkaline granitic melts. *Lithos* 80, 267–280.
- Linnen, R.L., 1998. The solubility of Nb-Ta-Zr-Hf-W in granitic melts with Li and Li+ F; constraints for mineralization in rare metal granites and pegmatites. *Econ. Geol.* 93, 1015–1025.
- Linnen, R.L., Cuney, M., 2005. Granite-related rare-element deposits and experimental constraints on Ta-Nb-W-Sn-Zr-Hf mineralization, in Linnen RL and Samson IM, eds., rare-element geochemistry and mineral deposits., in: Geological Association of Canada, GAC, Short Course. pp. 45–67.
- Linnen, R.L., Keppler, H., 1997. Columbite solubility in granitic melts: consequences for the enrichment and fractionation of Nb and Ta in the Earth's crust. *Contrib. to Mineral. Petrol.* 128, 213–227. <https://doi.org/10.1007/s004100050304>
- Linnen, R.L., Van Lichtervelde, M., Černý, P., 2012. Granitic Pegmatites as Sources of Strategic Metals. *Elements* 8, 275–280. <https://doi.org/10.2113/gselements.8.2.275>
- Loiselle, M.C., Wones, D.R., 1979. Characteristics and origin of anorogenic granites, in: Geological Society of America Abstracts with Programs. p. 468.
- London, D., 2014. A petrologic assessment of internal zonation in granitic pegmatites. *Lithos* 184–187, 74–104. <https://doi.org/10.1016/j.lithos.2013.10.015>
- MacDonald, M.A., Horne, R.J., Corey, N. C., Ham, L.J., 1992. An overview of recent bedrock mapping and follow-up petrological studies of the South Mountain Batholith, southwestern Nova Scotia, Canada. *Atl. Geol.* 28.
- Macdonald, R., Belkin, H.E., Fitten, J.J., Rogers, N.W., Nejbart, K., Tindle, A.G., Marshall, A.S., 2008. The roles of fractional crystallization, magma mixing, crystal mush remobilization and volatile-melt interactions in the genesis of a young basal-peralkaline rhyolite suite, the Greater Olkaria Volcanic Complex, Kenya Rift Valley. *J. Petrol.* 49, 1515–1547.
- Macdonald, R., Davies, G.R., Bliss, C.M., Leat, P.T., Bailey, D.K., Smith, R.L., 1987. Geochemistry of high-silica peralkaline rhyolites, Naivasha, Kenya Rift Valley. *J. Petrol.* 28, 979–1008.
- Mallmann, G., O'Neill, H.S.C., 2009. The crystal/melt partitioning of V during mantle melting as a function of oxygen fugacity compared with some other elements (Al, P, Ca, Sc, Ti, Cr, Fe, Ga, Y, Zr and Nb). *J. Petrol.* 50, 1765–1794.
- Marks, M.A.W., Markl, G., 2015. The Ilímaussaq alkaline complex, South Greenland, in: Layered Intrusions. Springer, pp. 649–691.
- Marks, M., Vennemann, T., Siebel, W., Markl, G., 2004. Nd-, O-, and H-isotopic evidence for complex, closed-system fluid evolution of the peralkaline Ilímaussaq intrusion, South Greenland. *Geochim. Cosmochim. Acta* 68, 3379–3395.
- Marks, M., Vennemann, T., Siebel, W., Markl, G., 2003. Quantification of Magmatic and Hydrothermal Processes in a Peralkaline Syenite ± Alkali Granite Complex Based on Textures, Phase Equilibria, and Stable and Radiogenic Isotopes. *J. Petrol.* 44, 1247–1280.

- Martin, R.F., 2006. A-type granites of crustal origin ultimately result from open-system fenitization-type reactions in an extensional environment. *Lithos* 91, 125–136.
- McDade, P., Blundy, J.D., Wood, B.J., 2003a. Trace element partitioning between mantle wedge peridotite and hydrous MgO-rich melt. *Am. Mineral.* 88, 1825–1831.
- McDade, P., Blundy, J.D., Wood, B.J., 2003b. Trace element partitioning on the Tinaquillo Lherzolite solidus at 1.5 GPa. *Phys. Earth Planet. Inter.* 139, 129–147.
- McNeil, A.G., Linnen, R.L., Flemming, R.L., 2020. Solubility of wodginite, titanowodginite, microlite, pyrochlore, columbite-(Mn) and tantalite-(Mn) in flux-rich haplogranitic melts between 700°–850 °C and 200 MPa. *Lithos.* <https://doi.org/10.1016/j.lithos.2019.105239>
- Miller, R.M., 2008. The geology of Namibia. Ministry of Mines and Energy, Geological Survey.
- Möller, V., Williams-Jones, A.E., 2016. Petrogenesis of the Nechalacho Layered Suite, Canada: magmatic evolution of a REE--Nb-rich nepheline syenite intrusion. *J. Petrol.* 57, 229–276.
- Monecke, T., Dulski, P., Kempe, U., 2007. Origin of convex tetrads in rare earth element patterns of hydrothermally altered siliceous igneous rocks from the Zinnwald Sn–W deposit, Germany. *Geochim. Cosmochim. Acta* 71, 335–353. <https://doi.org/10.1016/j.gca.2006.09.010>
- Montel, J.-M., 1993. A model for monazite/melt equilibrium and application to the generation of granitic magmas. *Chem. Geol.* 110, 127–146.
- Münker, C., Pfänder, J.A., Weyer, S., Büchl, A., Kleine, T., Mezger, K., 2003. Evolution of planetary cores and the earth-moon system from Nb/Ta systematics. *Science* 301, 84–87.
- Münker, C., Wörner, G., Yogodzinski, G., Churikova, T., 2004. Behaviour of high field strength elements in subduction zones: constraints from Kamchatka–Aleutian arc lavas. *Earth Planet. Sci. Lett.* 224, 275–293. <https://doi.org/10.1016/j.epsl.2004.05.030>
- Nandedkar, R.H., Hürlimann, N., Ulmer, P., Müntener, O., 2016. Amphibole-melt trace element partitioning of fractionating calc-alkaline magmas in the lower crust: an experimental study. *Contrib. to Mineral. Petrol.* 171, 71.
- Nash, W.P., Crecraft, H.R., 1985. Partition coefficients for trace elements in silicic magmas. *Geochim. Cosmochim. Acta* 49, 2309–2322. [https://doi.org/10.1016/0016-7037\(85\)90231-5](https://doi.org/10.1016/0016-7037(85)90231-5)
- Nielsen, R.L., Beard, J.S., 2000. Magnetite-melt HFSE partitioning. *Chem. Geol.* 164, 21–34.
- Ohnenstetter, D., Piantone, P., 1991. Pyrochlore-group minerals in the Beauvoir peraluminous leucogranite, Massif Central, France. *Can. Mineral.* 30, 771–784.
- O'Reilly, S.Y., Griffin, W.L., 2013. Mantle metasomatism, in: *Metasomatism and the Chemical Transformation of Rock*. Springer, pp. 471–533.
- Owen-Smith, T.M., Ashwal, L.D., Sudo, M., Trumbull, R.B., 2017. Age and petrogenesis of the Doros Complex, Namibia, and implications for early plume-derived melts in the Paraná-Etendeka LIP. *J. Petrol.* 58, 423–442.
- Palme, H., O'Neill, H., 2014. Cosmochemical Estimates of Mantle Composition, in: *Treatise on Geochemistry*, 2nd Edition. Elsevier.
- Partington, G.A., McNaughton, N.J., Williams, I.S., 1995. A review of the geology, mineralization, and geochronology of the Greenbushes pegmatite, Western Australia. *Econ. Geol.* 90, 616–635. <https://doi.org/10.2113/gsecongeo.90.3.616>
- Patiño-Douce, A.E., 1999. What do experiments tell us about the relative contributions of crust and mantle to the origin of granitic magmas? *Geol. Soc. London, Spec. Publ.* 168, 55–75. <https://doi.org/10.1144/GSL.SP.1999.168.01.05>
- Patiño-Douce, A.E., 1997. Generation of metaluminous A-type granites by low-pressure melting of calc-alkaline

- granitoids. *Geology* 25, 743–746. [https://doi.org/10.1130/0091-7613\(1997\)025<0743:GOMATG>2.3.CO;2](https://doi.org/10.1130/0091-7613(1997)025<0743:GOMATG>2.3.CO;2)
- Pearce, J.A., Harris, N.B.W., Tindle, A.G., 1984. Trace element distribution diagrams for the tectonic interpretation of granitic rocks. *J. Petrol.* 25, 956–983. <https://doi.org/10.1093/petrology/25.4.956>
- Pertermann, M., Hirschmann, M.M., Hametner, K., Günther, D., Schmidt, M.W., 2004. Experimental determination of trace element partitioning between garnet and silica-rich liquid during anhydrous partial melting of MORB-like eclogite. *Geochemistry, Geophys. Geosystems* 5.
- Peretyazhko, I.S., Savina, E.A., 2010. Tetrad effects in the rare earth element patterns of granitoid rocks as an indicator of fluoride-silicate liquid immiscibility in magmatic systems. *Petrology* 18, 514–543. <https://doi.org/10.1134/S086959111005005X>
- Pfänder, J.A., Jung, S., Münker, C., Stracke, A., Mezger, K., 2012. A possible high Nb/Ta reservoir in the continental lithospheric mantle and consequences on the global Nb budget—Evidence from continental basalts from Central Germany. *Geochim. Cosmochim. Acta* 77, 232–251.
- Pfänder, J.A., Münker, C., Stracke, A., Mezger, K., 2007. Nb/Ta and Zr/Hf in ocean island basalts — Implications for crust–mantle differentiation and the fate of Niobium. *Eart. Planet. Sci. Lett.* 254, 158–172. <https://doi.org/10.1016/j.epsl.2006.11.027>
- Pirajno, F., 2013. Effects of Metasomatism on Mineral Systems and Their Host Rocks: Alkali Metasomatism, Skarns, Greisens, Tourmalinites, Rodingites, Black-Wall Alteration and Listvenites, in: *Metasomatism and the Chemical Transformation of Rock*. Springer Berlin Heidelberg, pp. 203–251.
- Prowatke, S., Klemme, S., 2005. Effect of melt composition on the partitioning of trace elements between titanite and silicate melt. *Geochim. Cosmochim. Acta* 69, 695–709.
- Qian, Q., Hermann, J., 2013. Partial melting of lower crust at 10–15 kbar: constraints on adakite and TTG formation. *Contrib. to Mineral. Petrol.* 165, 1195–1224.
- Raimbault, L., Burnol, L., 1998. The Richemont rhyolite dyke, Massif Central, France; a subvolcanic equivalent of rare-metal granites. *Can. Mineral.* 36, 265–272.
- Rudnick, R.L., Barth, M., Horn, I., McDonough, W.F., 2000. Rutile-bearing refractory eclogites: missing link between continents and depleted mantle. *Science* (80-.). 287, 278–281.
- Rudnick, R.L., Gao, S., 2003. Composition of the Continental Crust. *Treatise on Geochemistry* 3, 659. <https://doi.org/10.1016/B0-08-04371-6/03016-4>
- Salters, V.J.M., Longhi, J.E., Blundy, M., 2002. Near mantle solidus trace element partitioning at pressures up to 3.4 GPa. *Geochemistry, Geophys. Geosystems* 3, 1–23.
- Salvi, S., Williams-Jones, A.E., 2005. Alkaline granite-syenite deposits, in: Linnen, R.L., Samson, I.L. (Eds.), *Geological Association of Canada Short Course Notes*. pp. 315–341.
- Salvi, S., Fontan, F., Monchoux, P., Williams-Jones, A.E., Moine, B., 2000. Hydrothermal mobilization of high field strength elements in Alkaline Igneous Systems: Evidence from the Tamazeght complex (Morocco). *Econ. Geol.* 95, 559–575. <https://doi.org/10.2113/gsecongeo.95.3.559>
- Schmidt, M.W., Dardon, A., Chazot, G., Vannucci, R., 2004. The dependence of Nb and Ta rutile-melt partitioning on melt composition and Nb/Ta fractionation during subduction processes. *Earth Planet. Sci. Lett.* 226, 415–432.
- Schmitt, A.K., Emmermann, R., Trumbull, R.B., Bühn, B., Henjes-Kunst, F., 2000. Petrogenesis and $^{40}\text{Ar}/^{39}\text{Ar}$ geochronology of the Brandberg Complex, Namibia: evidence for a major mantle contribution in metaluminous and peralkaline granites. *J. Petrol.* 41, 1207–1239.
- Schwartz, M.O., Surjono, 1990. Greisenization and albitization at the Tikus tin-tungsten deposit, Belitung, Indonesia. *Econ. Geol.* 85, 691–713. <https://doi.org/10.2113/gsecongeo.85.4.691>
- Shannon, R.D., 1976. Revised effective ionic radii and systematic studies of interatomic distances in halides and

- chalcogenides. *Acta Crystallogr. Sect. A* 32, 751–767. <https://doi.org/10.1107/S0567739476001551>
- Sievwright, R.H., Wilkinson, J.J., O'Neill, H.S.C., Berry, A.J., 2017. Thermodynamic controls on element partitioning between titanomagnetite and andesitic-dacitic silicate melts. *Contrib. to Mineral. Petrol.* 172, 62.
- Skjerlie, K.P., Johnston, A.D., 1993. Fluid-absent melting behavior of an F-rich tonalitic gneiss at mid-crustal pressures: implications for the generation of anorogenic granites. *J. Petrol.* 34, 785–815.
- Skjerlie, K.P., Johnston, A.D., 1992. Vapor-absent melting at 10 kbar of a biotite- and amphibole-bearing tonalitic gneiss: implications for the generation of A-type granites. *Geology* 20, 263–266.
- Skulski, T., Minarik, W., Watson, E.B., 1994. High-pressure experimental trace-element partitioning between clinopyroxene and basaltic melts. *Chem. Geol.* 117, 127–147.
- Sørensen, H., 1997. The agpaitic rocks—an overview. *Mineral. Mag.* 61, 485–498.
- Spandler, C., Hammerli, J., Yaxley, G.M., 2017. An experimental study of trace element distribution during partial melting of mantle heterogeneities. *Chem. Geol.* 462, 74–87.
- Stepanov, A., Mavrogenes, J.A., Meffre, S., Davidson, P., 2014. The key role of clinica during igneous concentration of tantalum. *Contrib. to Mineral. Petrol.* 167, 1–8. <https://doi.org/10.1007/s00410-014-1009-3>
- Stepanov, A.S., Hermann, J., 2013. Fractionation of Nb and Ta by biotite and phengite: Implications for the “missing Nb paradox.” *Geology* 41, 303–306. <https://doi.org/10.1130/G33781.1>
- Stepanov, A.S., Meffre, S., Mavrogenes, J., Steadman, J., 2016. Nb-Ta fractionation in peraluminous granites: A marker of the magmatic-hydrothermal transition. COMMENT. *Geology* 44, e394–e394. <https://doi.org/10.1130/G38086C.1>
- Stevenson, R., Upton, B.G.J., Steenfelt, A., 1997. Crust-mantle interaction in the evolution of the Ilímaussaq Complex, South Greenland: Nd isotopic studies. *Lithos* 40, 189–202.
- Stolz, A.J., Jochum, K.P., Spettel, B., Hofmann, A.W., 1996. Fluid- and melt-related enrichment in the subarc mantle: evidence from Nb/Ta variations in island arc basalts. *Geology* 24, 587–590.
- Sweeney, R.J., Prozesky, V., Przybyłowicz, W., 1995. Selected trace and minor element partitioning between peridotite minerals and carbonatite melts at 18–46 kb pressure. *Geochim. Cosmochim. Acta* 59, 3671–3683.
- Tang, M., Lee, C.-T.A., Chen, K., Erdman, M., Costin, G., Jiang, H., 2019. Nb/Ta systematics in arc magma differentiation and the role of arc gneisses in continent formation. *Nat. Commun.* 10, 235.
- Tappe, S., Romer, R.L., Stracke, A., Steenfelt, A., Smart, K.A., Muehlenbachs, K., Torsvik, T.H., 2017. Sources and mobility of carbonate melts beneath cratons, with implications for deep carbon cycling, metasomatism and rift initiation. *Earth Planet. Sci. Lett.* 466, 152–167.
- Tappe, S., Smart, K.A., Stracke, A., Romer, R.L., Prelević, D., van den Bogaard, P., 2016. Melt evolution beneath a rifted craton edge: $^{40}\text{Ar}/^{39}\text{Ar}$ geochronology and Sr-Nd-Hf-Pb isotope systematics of primitive alkaline basalts and lamprophyres from the SW Baltic Shield. *Geochim. Cosmochim. Acta* 173, 1–36.
- Thomas, R., Davidson, P., 2015. Comment on “A petrologic assessment of internal zonation in granitic pegmatites” by David London (2014). *Lithos* 212–215, 462–468. <https://doi.org/10.1016/j.lithos.2014.08.028>
- Thomas, R., Davidson, P., 2012. Water in granite and pegmatite-forming melts. *Ore Geol. Rev.* 46, 32–46. <https://doi.org/10.1016/j.oregeorev.2012.02.006>
- Thomas, R., Davidson, P., Beurlen, H., 2012. The competing models for the origin and internal evolution of granitic pegmatites in the light of melt and fluid inclusion research. *Mineral. Petrol.* 106, 55–73. <https://doi.org/10.1007/s00710-012-0212-z>
- Thomas, R., Davidson, P., Beurlen, H., 2011. Tantalite-(Mn) from the Borborema Pegmatite Province, northeastern Brazil: conditions of formation and melt- and fluid-inclusion constraints on experimental studies. *Miner. Depos.* 749–759. <https://doi.org/10.1007/s00126-011-0344-9>

- Thomas, R., Davidson, P., Badanina, E., 2009. A melt and fluid inclusion assemblage in beryl from pegmatite in the Orlovka amazonite granite, East Transbaikalia, Russia: implications for pegmatite-forming melt systems. *Mineral. Petrol.* 96, 129–140. <https://doi.org/10.1007/s00710-009-0053-6>
- Thomas, R., Förster, H.-J., Rickers, K., Webster, J.D., 2005. Formation of extremely F-rich hydrous melt fractions and hydrothermal fluids during differentiation of highly evolved tin-granite magmas: a melt/fluid-inclusion study. *Contrib. to Mineral. Petrol.* 148, 582–601.
- Tiepolo, M., Oberti, R., Vannucci, R., 2002. Trace-element incorporation in titanite: constraints from experimentally determined solid/liquid partition coefficients. *Chem. Geol.* 191, 105–119.
- Tiepolo, M., Vannucci, R., Oberti, R., Foley, S., Bottazzi, P., Zanetti, A., 2000. Nb and Ta incorporation and fractionation in titanian pargasite and kaersutite: crystal-chemical constraints and implications for natural systems. *Earth Planet. Sci. Lett.* 176, 185–201.
- Tiepolo, M., Zanetti, A., Oberti, R., Brumm, R., Foley, S., Vannucci, R., 2003. Trace-element partitioning between synthetic potassic-rich richterites and silicate melts, and contrasts with the partitioning behaviour of pargasites and kaersutites. *Eur. J. Mineral.* 15, 329–340.
- Timofeev, A., Migdisov, A.A., Williams-Jones, A.E., 2017. An experimental study of the solubility and speciation of tantalum in fluoride-bearing aqueous solutions at elevated temperature. *Geochim. Cosmochim. Acta* 197, 294–304.
- Timofeev, A., Migdisov, A.A., Williams-Jones, A.E., 2015. An experimental study of the solubility and speciation of niobium in fluoride-bearing aqueous solutions at elevated temperature. *Geochim. Cosmochim. Acta*. <https://doi.org/10.1016/j.gca.2015.02.015>
- Timofeev, A., Williams-Jones, A.E., 2015. The origin of niobium and tantalum mineralization in the Nechalacho REE Deposit, NWT, Canada. *Econ. Geol.* 110, 179–1735.
- Trumbull, R.B., Harris, C., Frindt, S., Wigand, M., 2004. Oxygen and neodymium isotope evidence for source diversity in Cretaceous anorogenic granites from Namibia and implications for A-type granite genesis. *Lithos* 73, 21–40.
- Van Lichtervelde, M., Grégoire, M., Linnen, R.L., Béziat, D., Salvi, S., 2008. Trace element geochemistry by laser ablation ICP-MS of micas associated with Ta mineralization in the Tanco pegmatite, Manitoba, Canada. *Contrib. to Mineral. Petrol.* 155, 891–896. <https://doi.org/10.1007/s00410-007-0271-z>
- Van Lichtervelde, M., Holtz, F., Melcher, F., 2018. The effect of disequilibrium crystallization on Nb-Ta fractionation in pegmatites: Constraints from crystallization experiments of tantalite-tapiolite. *Am. Mineral. J. Earth Planet. Mater.* 103, 1407–1416.
- Van Lichtervelde, M., Salvi, S., Béziat, D., Linnen, R.L., 2007. Textural features and chemical evolution in tantalum oxides: Magmatic versus hydrothermal origins for Ta mineralization in the Tanco Lower pegmatite, Manitoba, Canada. *Econ. Geol.* 102, 257–276. <https://doi.org/10.2113/gsecongeo.102.2.257>
- Van Westrenen, W., Blundy, J., Wood, B., 1999. Crystal-chemical controls on trace element partitioning between garnet and anhydrous silicate melt. *Am. Mineral.* 84, 838–847.
- Veksler, I. V., 2004. Liquid immiscibility and its role at the magmatic–hydrothermal transition: a summary of experimental studies. *Chem. Geol.* 210, 7–31. <https://doi.org/10.1016/j.chemgeo.2004.06.002>
- Veksler, I. V., Dorfman, A.M., Dulski, P., Kamenetsky, V.S., Danyushevsky, L. V., Jeffries, T., Dingwell, D.B., 2012. Partitioning of elements between silicate melt and immiscible fluoride, chloride, carbonate, phosphate and sulfate melts, with implications to the origin of natrocarbonatite 79, 20–40. <https://doi.org/10.1016/j.gca.2011.11.035>
- Veksler, I. V., Dorfman, A.M., Kamenetsky, M., Dulski, P., Dingwell, D.B., 2005. Partitioning of lanthanides and Y between immiscible silicate and fluoride melts, fluorite and cryolite and the origin of the lanthanide tetrad effect in igneous rocks. *Geochim. Cosmochim. Acta* 69, 2847–2860. <https://doi.org/10.1016/j.gca.2004.08.007>

- Vielzeuf, D., Holloway, J.R., 1988. Experimental determination of the fluid-absent melting relations in the pelitic system. *Contrib. to Mineral. Petrol.* 98, 257–276. <https://doi.org/10.1007/BF00375178>
- Villaros, A., Laurent, O., Couzinié, S., Moyen, J.F., Mintrone, M., 2018. Plutons and domes: the consequences of anatectic magma extraction—example from the southeastern French Massif Central. *Int. J. Earth Sci.* 107, 2819–2842. <https://doi.org/10.1007/s00531-018-1630-x>
- Wade, J., Wood, B.J., 2001. The Earth's 'missing' niobium may be in the core. *Nature* 409, 75–78. <https://doi.org/10.1038/35051064>
- Watson, E.B., Harrison, T.M., 1983. Zircon saturation revisited: temperature and composition effects in a variety of crustal magma types. *Earth Planet. Sci. Lett.* 64, 295–304. [https://doi.org/10.1016/0012-821X\(83\)90211-X](https://doi.org/10.1016/0012-821X(83)90211-X)
- Whalen, J.B., Currie, K.L., Chappell, B.W., 1987. A-type granites: geochemical characteristics, discrimination and petrogenesis. *Contrib. to Mineral. Petrol.* 95, 407–419. <https://doi.org/10.1007/BF00402202>
- White, J.C., Holt, G.S., Parker, D.F., Ren, M., 2003. Trace-element partitioning between alkali feldspar and peralkalic quartz trachyte to rhyolite magma. Part I: Systematics of trace-element partitioning. *Am. Mineral.* 88, 316–329.
- Williams-Jones, A.E., Migdisov, A.A., Samson, I.M., 2012. Hydrothermal mobilisation of the rare earth elements—a tale of “ceria” and “yttria.” *Elements* 8, 355–360.
- Wilson, B.M., 1989. *Igneous petrogenesis a global tectonic approach*. Springer Science & Business Media.
- Wood, B.J., Trigila, R., 2001. Experimental determination of aluminous clinopyroxene–melt partition coefficients for potassic liquids, with application to the evolution of the Roman province potassic magmas. *Chem. Geol.* 172, 213–223.
- Woolley, A.R., Church, A.A., 2005. Extensive carbonatites: A brief review 85, 1–14. <https://doi.org/10.1016/j.lithos.2005.03.018>
- Wu, M., Samson, I.M., Zhang, D., 2018. Textural Features and Chemical Evolution in Ta-Nb Oxides: Implications for Deuteric Rare-Metal Mineralization in the Yichun Granite-Marginal pegmatite, Southeastern China. *Econ. Geol.* 113, 937–960. <https://doi.org/10.532/econgeo.2018.4577>
- Wu, M., Samson, I.M., Zhang, D., 2017. Textural and chemical constraints on the formation of disseminated granite-hosted W-Ta-Nb mineralization at the Dajishan Deposit, Nanling Range, Southeastern China. *Econ. Geol.* 112, 855–887.
- Xie, L., Wang, R.-C., Che, Y.-D., Huang, F.-F., Erdmann, S., Zhang, W.-L., 2016. Tracking magmatic and hydrothermal Nb–Ta–W–Sn fractionation using mineral textures and composition: A case study from the late Cretaceous Jiepailing area district in the Nanling Range in South China. *Ore Geol. Rev.* 78, 300–321. <https://doi.org/10.1016/j.oregeorev.2016.04.003>
- Xiong, X., Keppler, H., Audétat, A., Ni, H., Sun, W., Li, Y., 2011. Partitioning of Nb and Ta between rutile and felsic melt and the fractionation of Nb/Ta during partial melting of hydrous metabasalt. *Geochim. Cosmochim. Acta* 75, 1673–1692.
- Xiong, X.L., Adam, J., Green, T.H., 2005. Rutile stability and rutile/melt HFSE partitioning during partial melting of hydrous basalt: implications for TTG genesis. *Chem. Geol.* 218, 339–359.
- Yamato, P., Duretz, T., May, D.A., Tartèse, R., 2015. Quantifying magma segregation in dykes. *Tectonophysics* 660, 132–147. <https://doi.org/10.1016/j.tecto.2015.08.030>
- Yang, W., Niu, H., Shan, Q., Sun, W., 2014. Geochemistry of magmatic and hydrothermal zircon from the highly evolved Baerzhe alkaline granite: implications for Zr – REE – Nb mineralization. *Miner. Depos.* 49, 451–470. <https://doi.org/10.1007/s00126-013-0504-1>
- Zaraisky, G.P., Korzhinskaya, V., Kotova, N., 2010. Experimental studies of Ta₂O₅ and columbite–tantalite solubility in fluoride solutions from 300 to 550°C and 50 to 100 MPa. *Mineral. Petrol.* 99, 287–300.

<https://doi.org/10.1007/s00710-010-0112-z>

Zhu, Z.-Y., Wang, R.-C., Che, X.-D., Zhu, J.-C., Wei, X.-L., Huang, X., 2015. Magmatic–hydrothermal rare-element mineralization in the Songshugang granite (northeastern Jiangxi, China): Insights from an electron-microprobe study of Nb–Ta–Zr minerals. *Ore Geol. Rev.* 65, Part 4, 749–760. <https://doi.org/10.1016/j.oregeorev.2014.07.021>

Journal Pre-proof

Captions

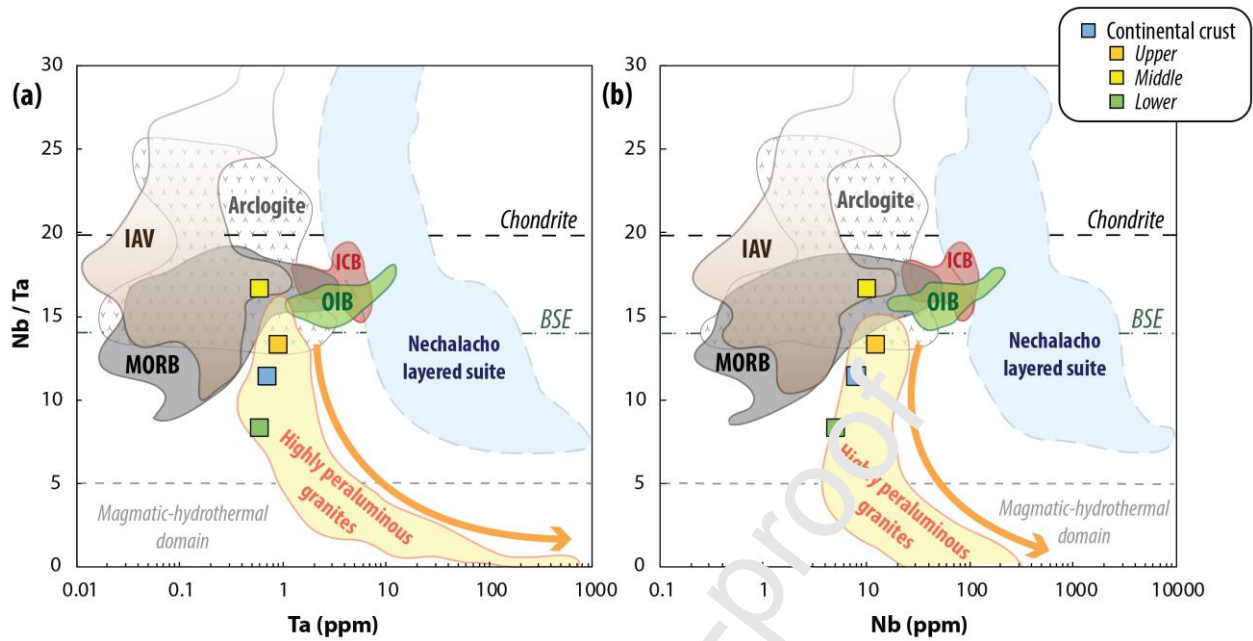


Fig. 1. Nb/Ta versus **a** Ta and **b** Nb diagrams reporting the average composition of Earth's main geochemical reservoirs (chondrite and bulk silicate Earth [BSE]: Münker et al., 2003; continental crust: Rudnick and Gao, 2003) as well as the whole-rock compositional fields of oceanic island basalts (OIB: Pfänder et al., 2007), island arc volcanic rocks (IAV: Stolz et al., 1996; Münker et al., 2004; König and Schuth, 2011), mid-ocean ridge basalts (MORB: Arevalo and McDonough, 2010), intraplate continental basalts from Central Germany (ICB: Pfänder et al., 2012), highly peraluminous granites (Ballouard et al., 2016a), the peralkaline Nechalacho layered suite, Canada (Möller and Williams-Jones, 2016) and evolved deep arc cumulates (arclogite, Mg#<0.6) from central Arizona, USA (Tang et al., 2019). The orange arrow represents the typical differentiation trend of highly peraluminous granites characterized by molar A/CNK [$\text{Al}_2\text{O}_3 / (\text{CaO} + \text{Na}_2\text{O} + \text{K}_2\text{O})$] ratios > 1.1. The grey dashed line at Nb/Ta = 5 delimits the magmatic-hydrothermal domain defined by Ballouard et al. (2016a).

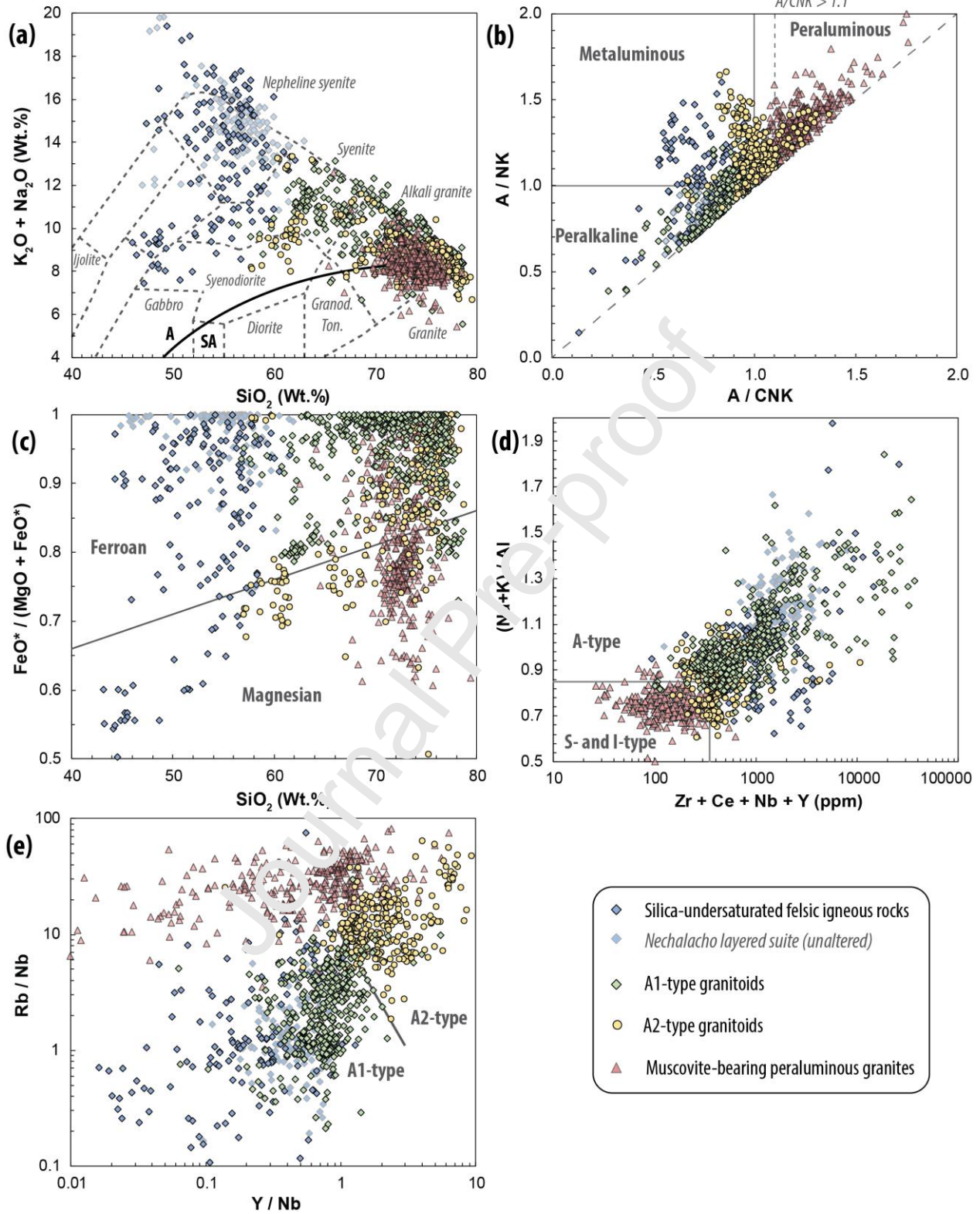


Fig. 2. Geochemical composition of compiled MPG, A1-type and A2-type, and silica-undersaturated felsic igneous rocks. **a** Total alkalis ($\text{Na}_2\text{O} + \text{K}_2\text{O}$) versus SiO_2 diagram with rock type fields from Cox et al. (1979) and Wilson (1989). Granod.: granodiorite; Ton.: tonalite. The fields of alkaline (A) and subalkaline (SA) series are from Irvine and Baragar (1971). **b** A/NK [$\text{Al}_2\text{O}_3 / (\text{Na}_2\text{O} + \text{K}_2\text{O})$] versus A/CNK [$\text{Al}_2\text{O}_3 / (\text{CaO} + \text{Na}_2\text{O} + \text{K}_2\text{O})$] diagram (molar proportions). **c** $\text{FeO}^* / (\text{MgO} + \text{FeO}^*)$ versus SiO_2 diagram (Frost and Frost, 2008). **d** Molar $(\text{Na} + \text{K})/\text{Al}$ (agpaitic index) versus $\text{Zr} + \text{Ce} + \text{Nb} + \text{Y}$ diagram with the fields of A-type as well as I- and S-type granites indicated (Whalen et al., 1987). **e** Rb/Nb versus Y/Nb diagram with the field of A1- and A2-type granites indicated (Eby, 1992). Unaltered nepheline syenites from the Nechalacho layered suite (Möller and Williams-Jones, 2016) are shown separately to compensate the effect of oversampling ($n = 132$).

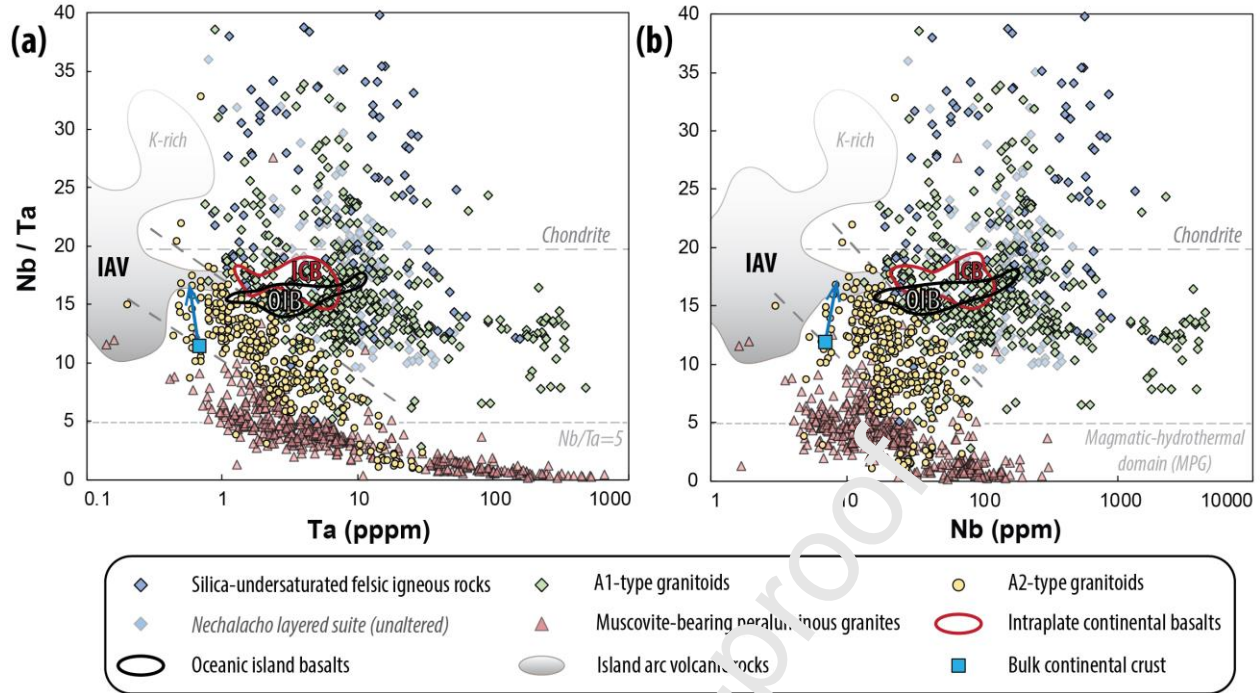


Fig. 3. Nb/Ta versus **a** Ta and **b** Nb content diagrams showing the whole-rock composition of MPG, A-type granitoids and silica-undersaturated felsic igneous rocks. The whole-rock compositional fields of OIB (Pfänder et al., 2007), intraplate continental basalts from Central Germany (ICB: Pfänder et al., 2012) and IAV (König and Schuth, 2011; Münker et al., 2004), including potassic (K-rich) arc magmas (Stolz et al., 1996), are indicated. The chondritic Nb/Ta value is from Münker et al. (2003) and the average composition of the bulk continental crust is from Rudnick and Gao (2003). The blue arrow points toward the composition of the bulk crust (Rudnick and Gao, 2003) and indicates the theoretical internal differentiation trend of a continental crust that underwent incipient partial melting by muscovite- to biotite-breakdown conditions followed by melt extraction (i.e. enrichment in residual biotite and ilmenite in the lower-middle crust; see text for detail). Oblique dashed lines delimit the common fields of silica-undersaturated + A1-type igneous rocks and A2-type igneous rocks (**a** $x = 0.3, 20; y = 20, 6.5$; **b** $x = 8, 100; y = 22, 8$) as well as A2-type igneous rocks and MPG (**a** $x = 0.2, 9; y = 15.5, 3$; **b** $x = 3, 40; y = 16, 3$). Unaltered nepheline syenites from the Nechalacho layered suite (Möller and Williams-Jones, 2016) are

shown separately to compensate the effect of oversampling ($n = 132$). The value of $Nb/Ta = 5$ delimits the magmatic-hydrothermal domain defined for MPG by Ballouard et al. (2016a).

Journal Pre-proof

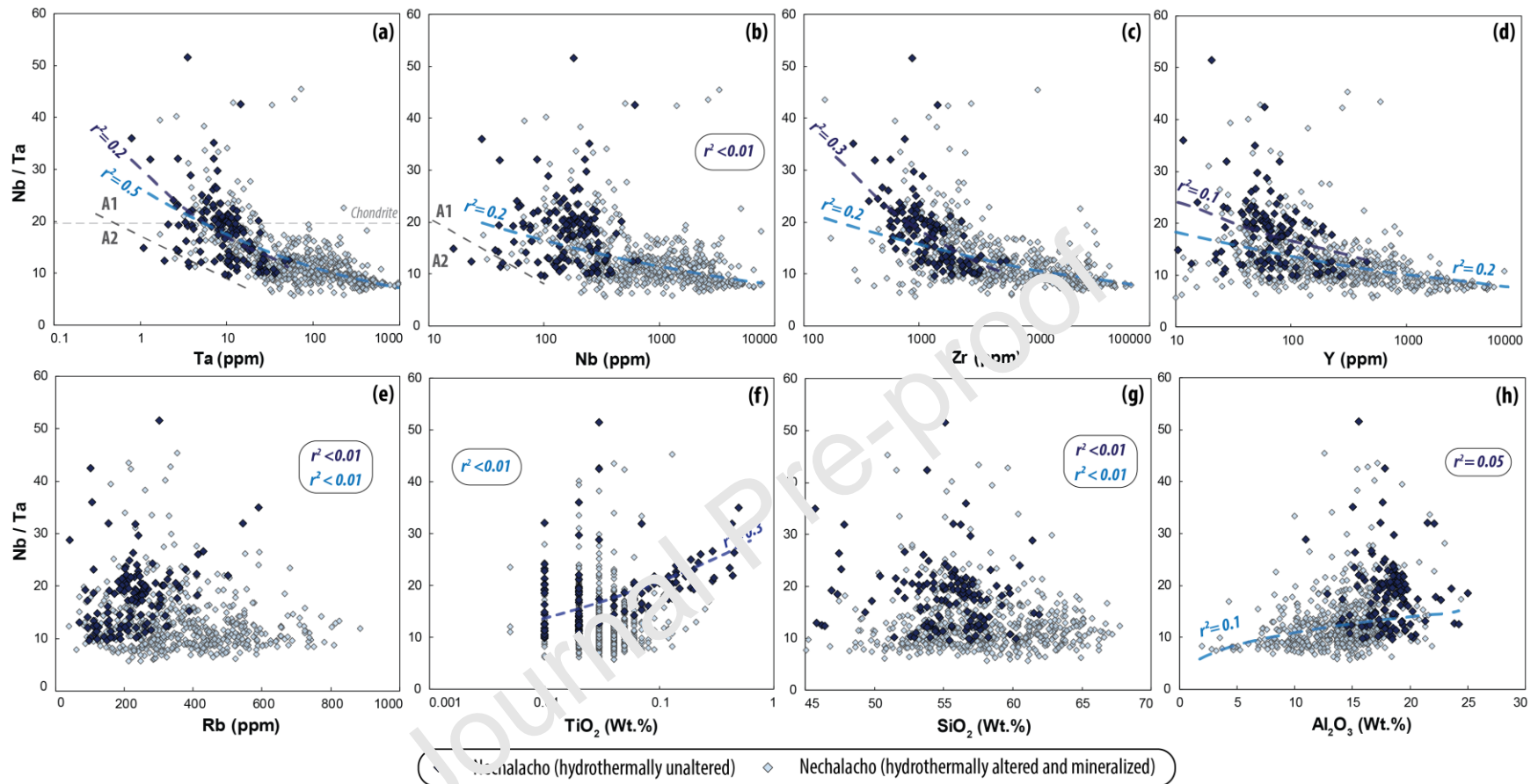


Fig. 4. Evolution of the Nb/Ta ratio as a function of **a** Ta, **b** Nb, **c** Zr, **d** Y, **e** Rb, **f** TiO₂, **g** SiO₂ and **h** Al₂O₃ contents for unaltered and altered/mineralized nepheline syenites from the Nechalacho layered suite (Canada). See Supplementary Table 1 for information about the intrusions. The determination coefficients r^2 and trendlines are indicated in dark blue for unaltered samples and in light blue for hydrothermally altered and mineralized samples. Trend lines were calculated using a power law ($y = a \cdot x^b$).

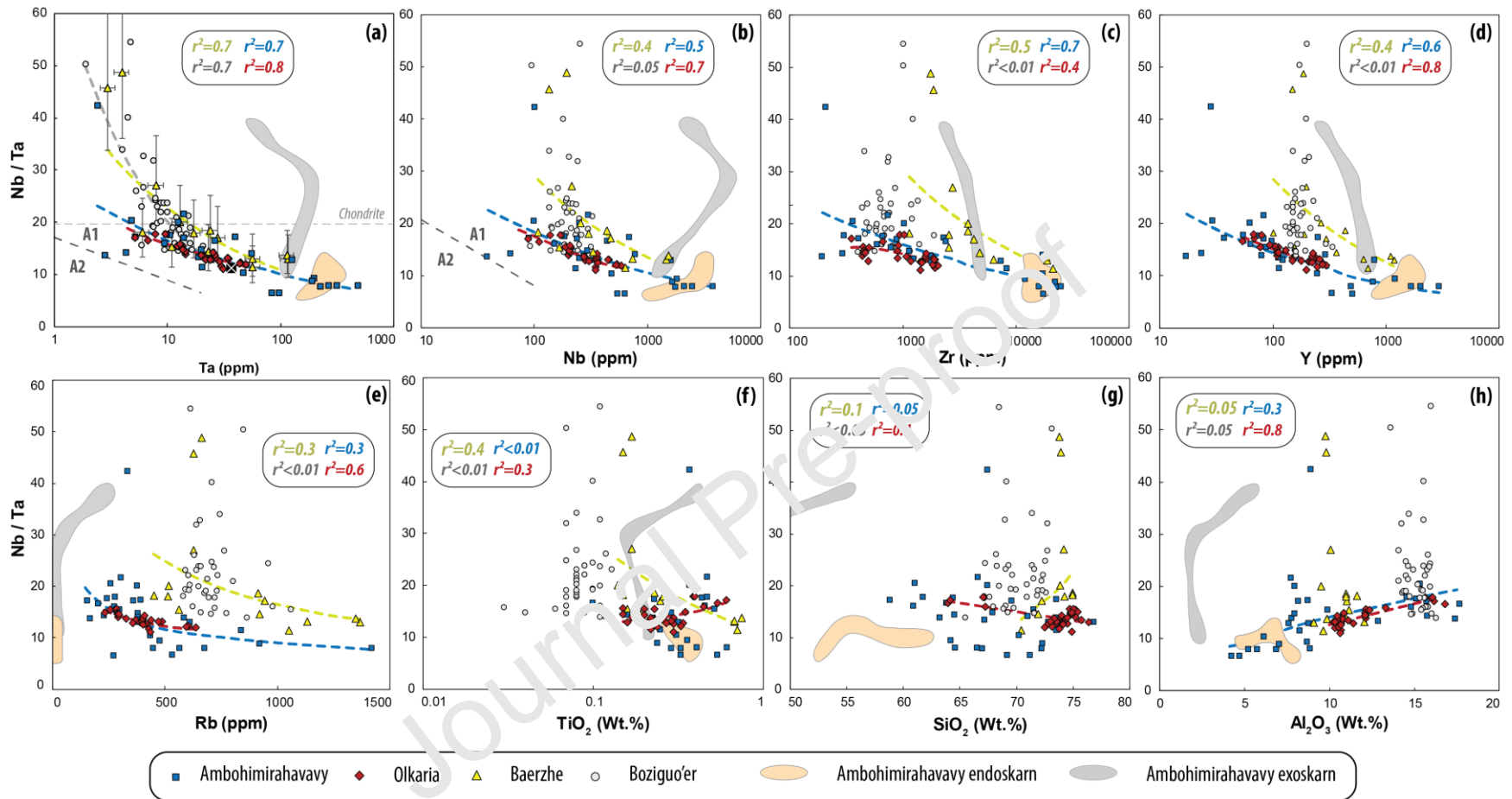


Fig. 5. Evolution of the Nb/Ta ratio as a function of **a** Ta, **b** Nb, **c** Zr, **d** Y, **e** Rb, **f** TiO₂, **g** SiO₂ and **h** Al₂O₃ contents for selected A1-type granitoid suites. These suites include granites (\pm pegmatites), syenites and trachytes from the Ambohimirahavavy complex (Madagascar), rhyolites and trachytes from the Olkaria volcanic complex (Kenya), granites from the Baerzhe pluton (NE China) and granites from Boziguo'er pluton (NW China). Fields in color represent the composition of endoskarns and exoskarns from the Ambohimirahavavy complex. See Supplementary Table 1

for information about the different suites. The determination coefficients r^2 and trendlines of each suite are indicated with the same color as the corresponding symbols. The trends were calculated using a power law ($y = a \cdot x^b$) except in **f** for the Olkaria volcanic complex where a linear law ($y = ax + b$) is used. In **a**, the error bars take into account the maximum analytical uncertainty of 15% estimated for the measurement of the trace element composition of samples from the Baerzhe pluton (Jahn et al., 2001).

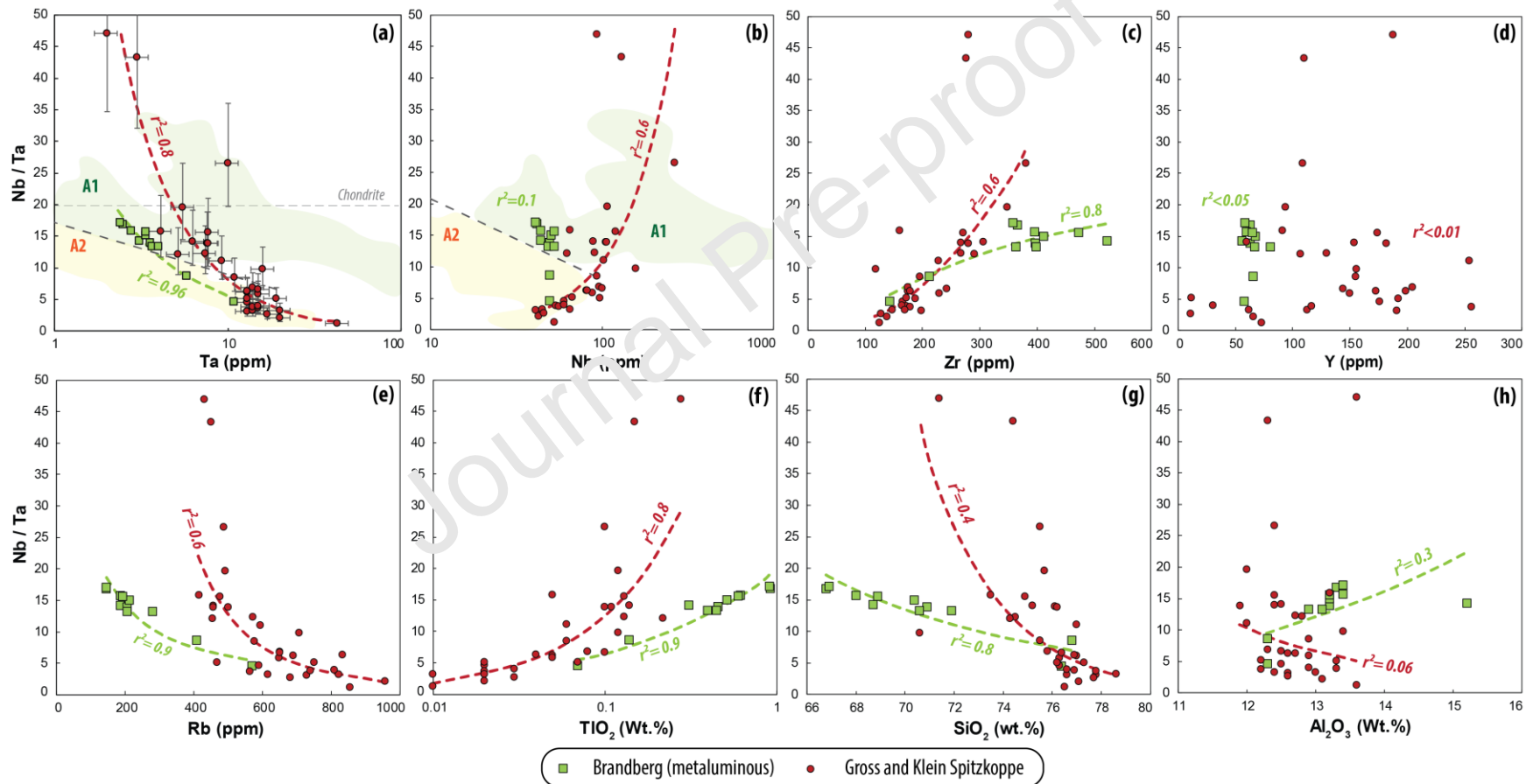


Fig. 6. Evolution of the Nb/Ta ratio as a function of **a** Ta, **b** Nb, **c** Zr, **d** Y, **e** Rb, **f** TiO₂, **g** SiO₂ and **h** Al₂O₃ contents for selected transitional A-type (A1-A2) granitoid suites from Namibia. These suites include the metaluminous granites and rhyodacites from the Brandberg complex and granites (\pm aplites) and rhyolites from Gross and Klein Spitzkoppe stocks. See Supplementary Table 1 for information about the different suites. The common fields of A1-type and A2-type granitoids are indicated for comparison along with coefficients r^2 and trendlines calculated using a power law ($y = a \cdot x^b$). Errors bars taking into account an analytical uncertainty of 15% for the measurement of Ta and Nb contents are shown as an example in **a** for the Gross and Klein Spitzkoppe stocks.

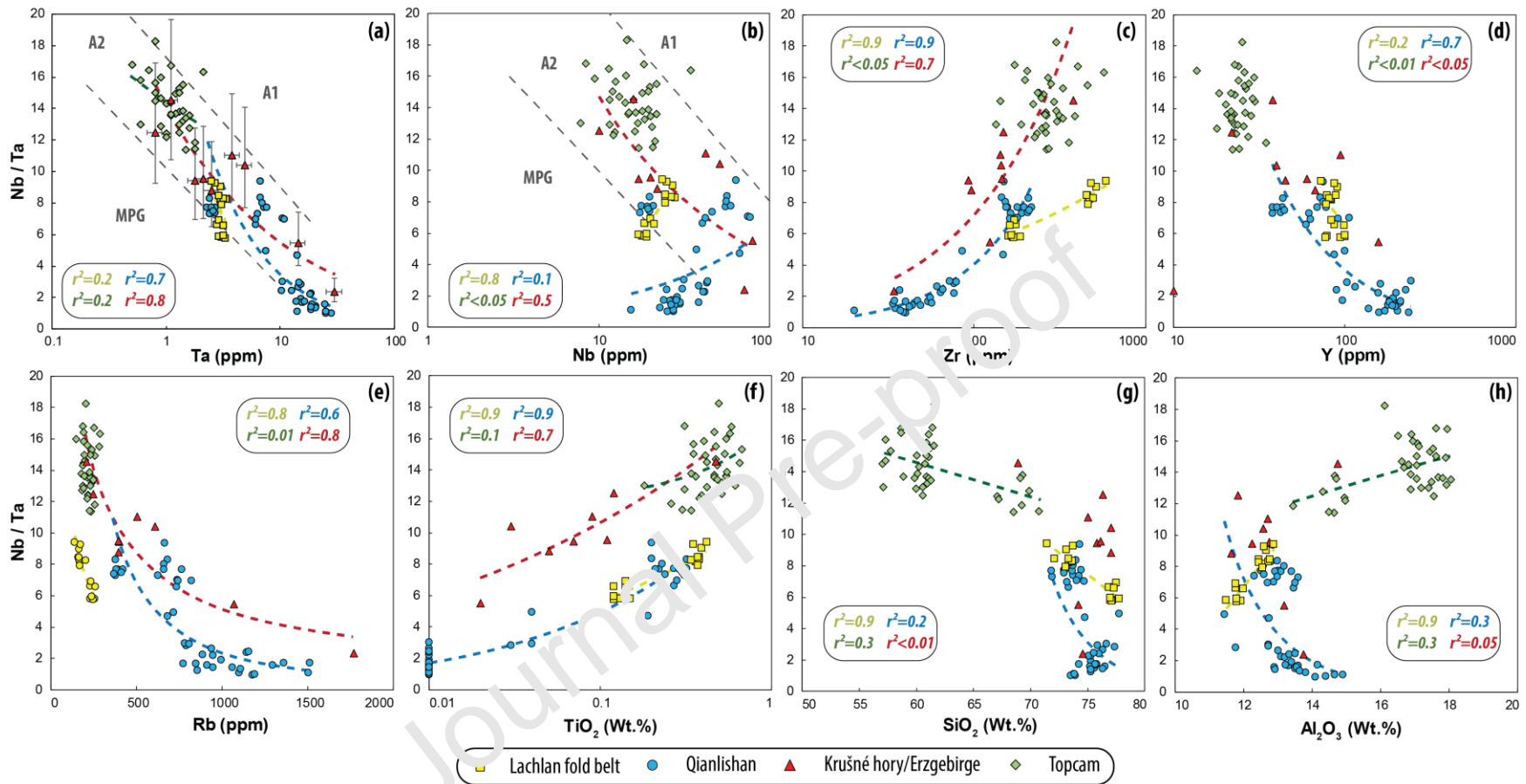


Fig. 7. Evolution of the Nb/Ta ratio as a function of **a** Ta, **b** Nb, **c** Zr, **d** Y, **e** Rb, **f** TiO₂, **g** SiO₂ and **h** Al₂O₃ contents for selected A2-type granitoid suites. These suites include granites from the Lachlan Fold Belt (SE Australia), granites from the Qianlishan complex (SE China), granites, tuffs and ignimbrites from the Krušné hory / Erzgebirge (Central Europe) and granites from the Topcam pluton (Turkey). See Supplementary Table 1 for information about the different suites. The determination coefficients r^2 and trendlines of each suite calculated using a power law ($y = a \cdot x^b$) are

indicated with the same color as the corresponding symbols. Errors bars taking into account an analytical uncertainty of 15% for the measurement of Ta and Nb contents are shown as an example in **a** for igneous rocks of the Krušné hory / Erzgebirge.

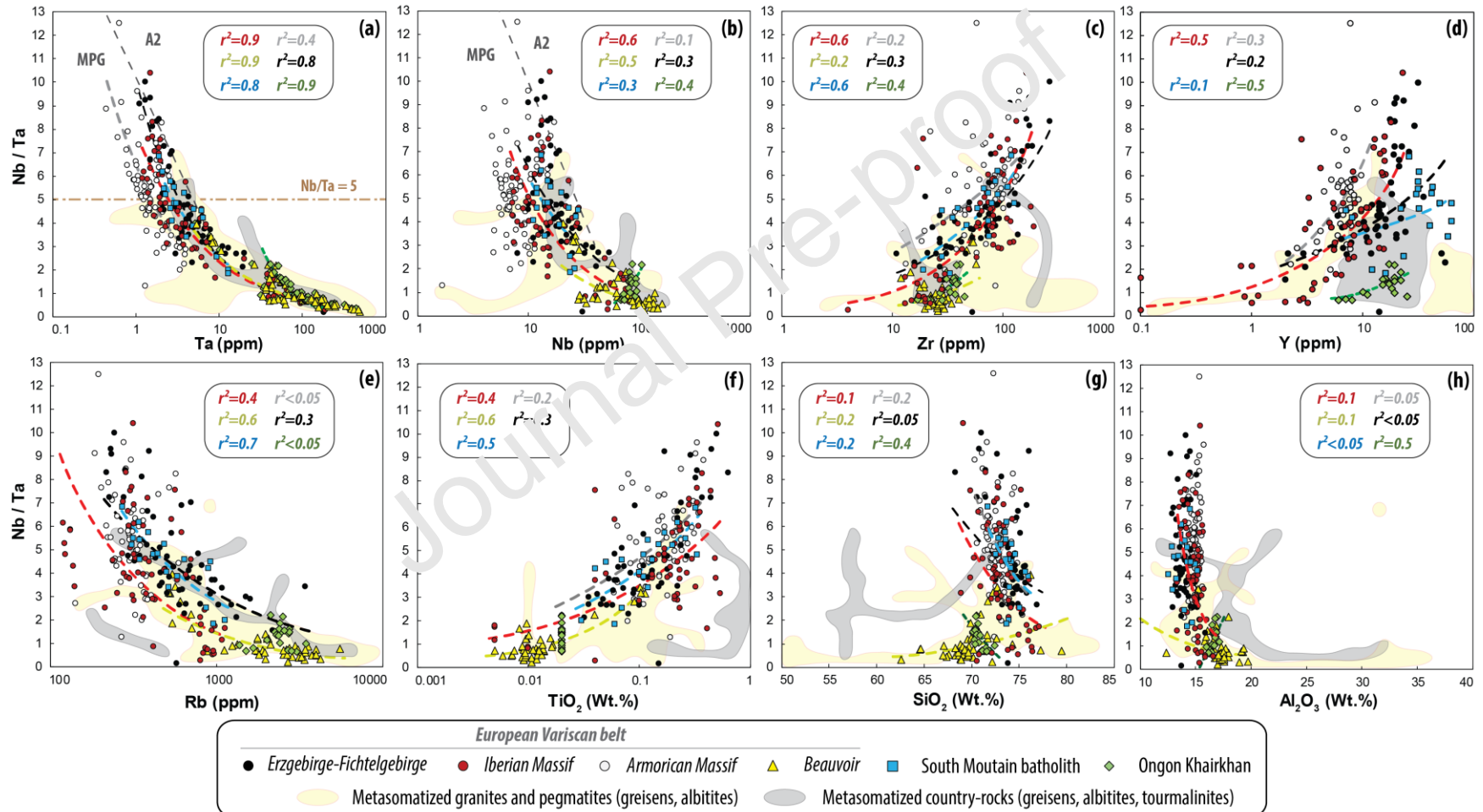


Fig. 8. Evolution of the Nb/Ta ratio as a function of **a** Ta, **b** Nb, **c** Zr, **d** Y, **e** Rb, **f** TiO₂, **g** SiO₂ and **h** Al₂O₃ contents for selected MPG suites. These suites include granites from the European Variscan belt (Erzgebirge-Fichtelgebirge, Iberian Massif, Armorican Massif, Massif Central-Beauvoir), South Mountain Batholith (Canada) as well as ongonites (microgranites) from Ongon Khairkhan (Mongolia). Fields in color represent the composition of metasomatized granites and pegmatites associated with MPG suites as well as the metasomatized country-rocks of LCT pegmatites from Cape Cross-Uis (Namibia) and the Orange River belt (South Africa). See Supplementary Table 1 for information and references of the different suites. The determination coefficients r^2 and trendlines of each suite calculated using a power law ($y = a \cdot x^b$) are indicated with the same color as the corresponding symbols.

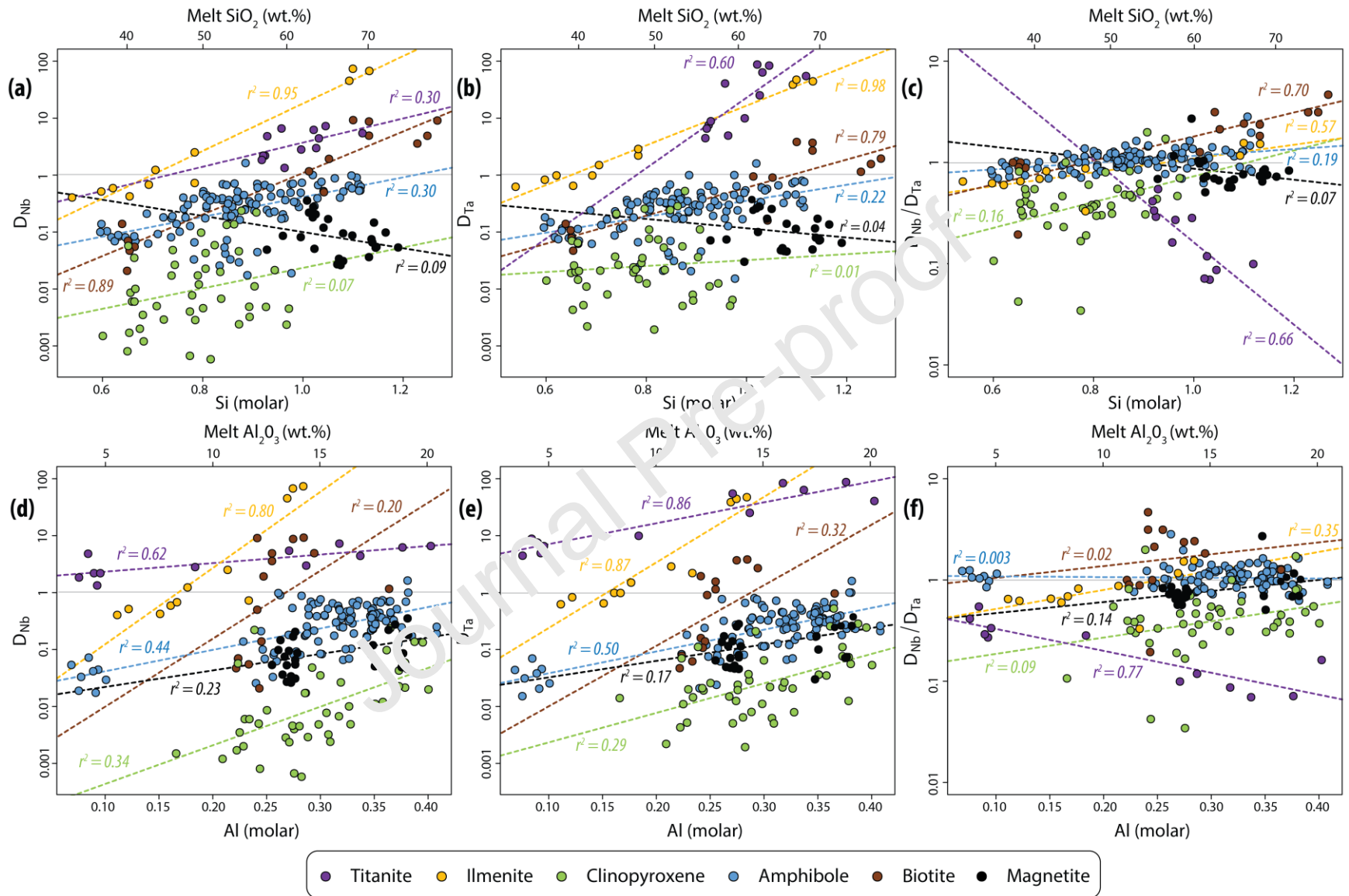


Fig. 9. Partition coefficients D_{Nb} , D_{Ta} and D_{Nb}/D_{Ta} as a function of the melt **a-c** Si and **c-d** Al contents (on a volatile-bearing basis) for different minerals typical for rare-metal-enriched felsic igneous rocks. The experimental database used in these diagrams is provided in Supplementary Material 4. The molar proportion of Si and Al is calculated using $Si_{\text{molar}} = SiO_2 \text{ wt.} \% / (\text{molecular weight of } SiO_2 = 60.084 \text{ g.mol}^{-1})$ and $Al_{\text{molar}} = 2 \cdot [Al_2O_3 \text{ wt.} \% / (\text{molecular weight of } Al_2O_3 = 101.961 \text{ g.mol}^{-1})]$.

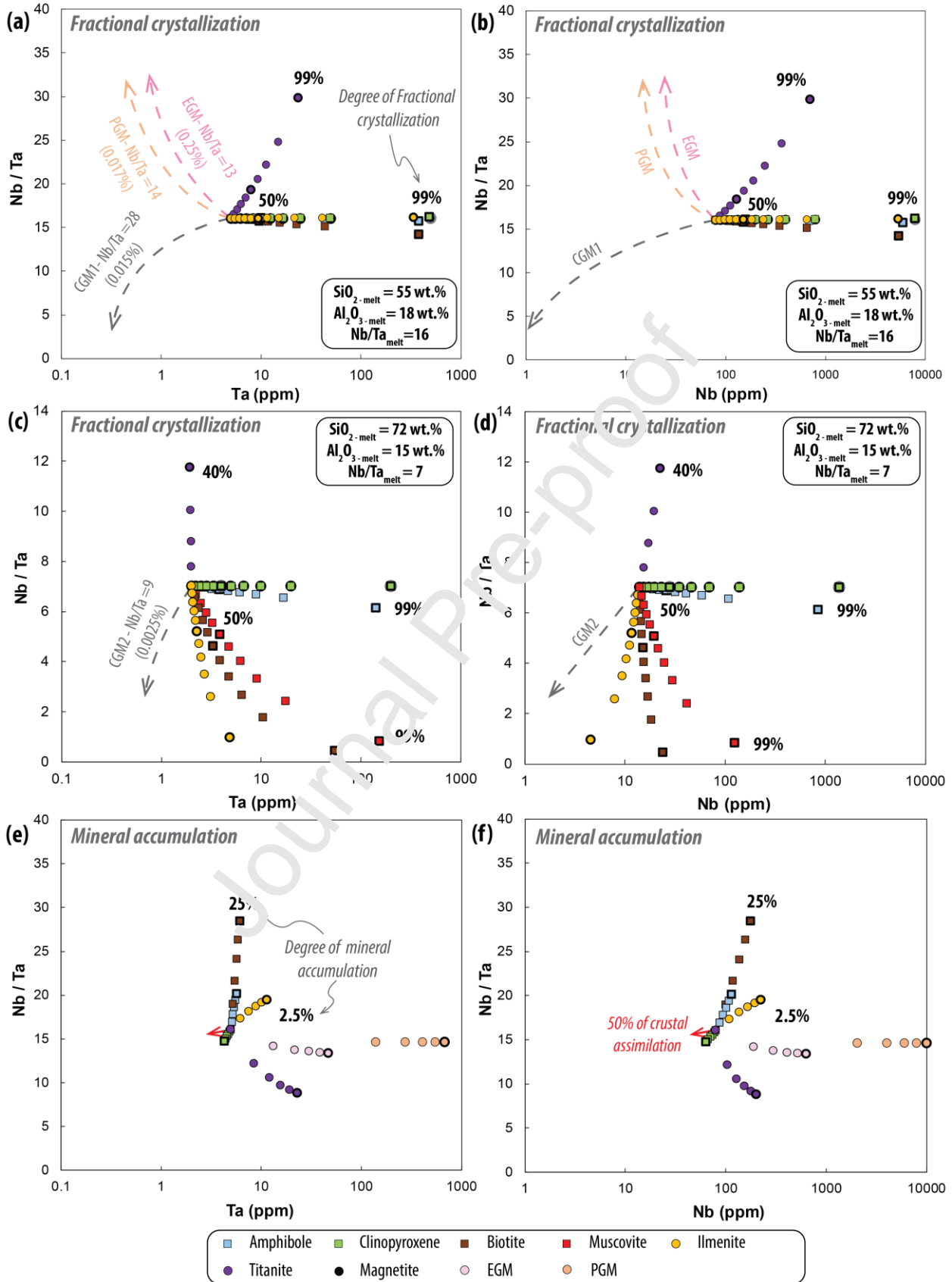


Fig. 10. Fractional crystallization and mineral accumulation modeling. **a-d** Nb/Ta versus Ta and Nb diagrams showing the compositional evolution of melts with **a-b** $\text{SiO}_2 = 55$ wt.% and $\text{Al}_2\text{O}_3 = 18$ wt.%, corresponding to the average whole-rock composition of silica-undersaturated felsic igneous rocks, and **c-d** $\text{SiO}_2 = 72$ wt.% and $\text{Al}_2\text{O}_3 = 18$ wt.%, corresponding to the average whole-rock composition of MPG, experiencing 10 to 99% of fractional crystallization of various minerals by increments of 10%. For each fractional crystallization model, the extracted mineral assemblage consists of mostly feldspar, to which a theoretical mineral/melt partition coefficient of 0 was attributed, along with a minor fraction of one specific Nb-Ta-bearing mineral phase. The mineral fraction used is 15% for major rock-forming minerals (squares: amphibole, pyroxene, biotite, muscovite) and 1% for titanite, magnetite and ilmenite (circles). Mineral/melt partition coefficients (D_{Nb} and D_{Ta}) are calculated based on the equations given in Table 4 except for muscovite ($D_{\text{Nb}} = 3.5$, $D_{\text{Ta}} = 0.4$, Table 1) and magnetite ($D_{\text{Nb}} = 0.11$, $D_{\text{Ta}} = 0.13$, mean value from Supplementary Material 5). The dashed arrows in **a-d** show the evolution of a melt experiencing a variable degree of crystallization of CGM (green), LGM (orange) and EGM (pink, see Table 5 for mineral compositions). **e-f** Nb/Ta versus Ta and Nb diagrams showing the compositional evolution of a melt experiencing 5 to 25% biotite, amphibole and clinopyroxene accumulation, in increments of 5% (squares), as well as 0.5 to 2.5% ilmenite, titanite, EGM and PGM accumulation in increments of 0.5% (circles); see Table 5 for mineral compositions. The red arrow indicates the evolution of a melt experiencing 50% of bulk continental crust assimilation (Rudnick and Gao, 2003). The parental liquid compositions used for modeling are Nb = 80 ppm, Ta = 5 ppm in **a-b** and **e-f** and Nb = 14 ppm, Ta = 2 ppm in **c-d**.

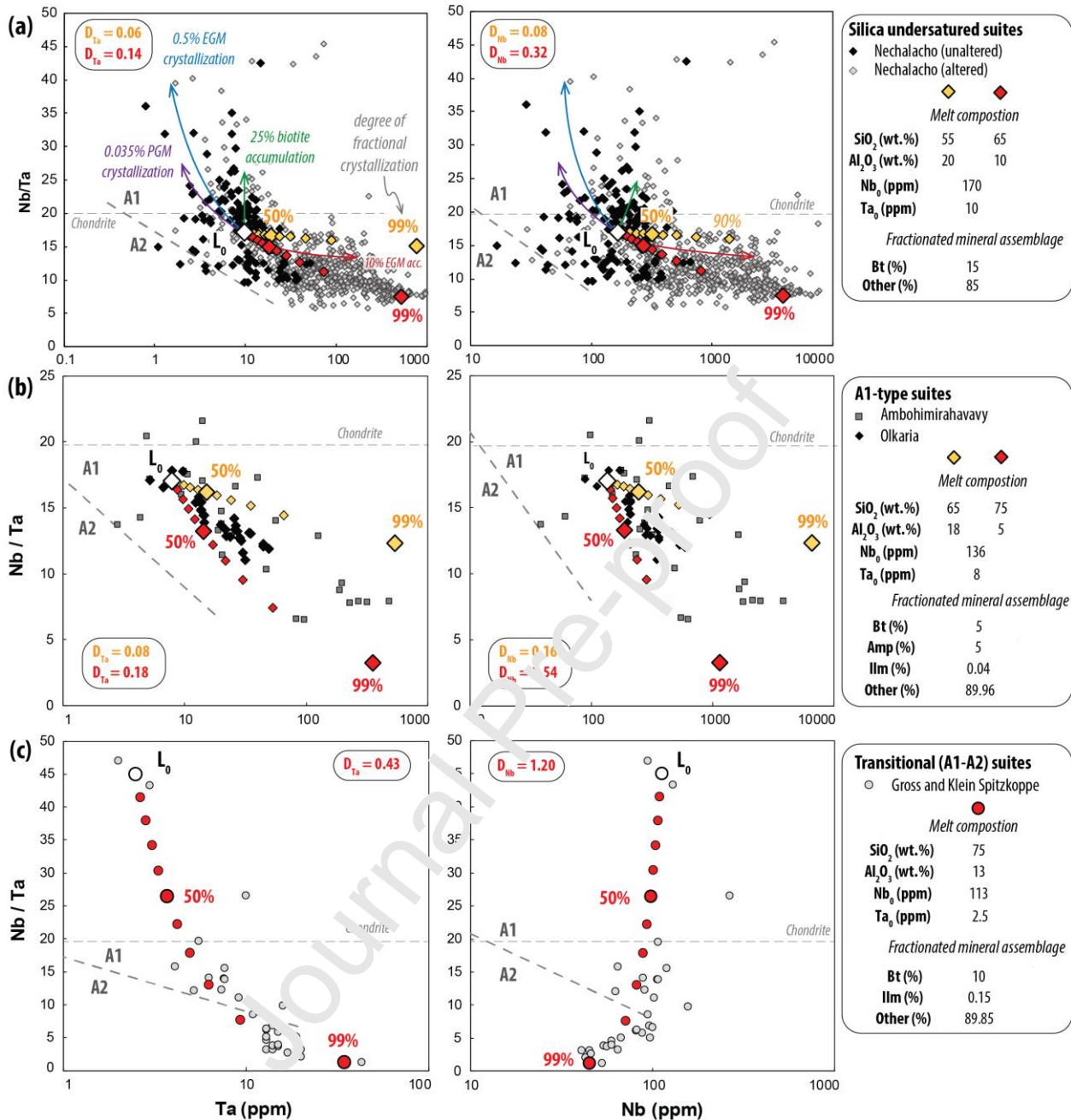


Fig. 11. Example of fractional crystallization modeling in Nb/Ta versus Ta and Nb diagrams for **a** silica-undersaturated, **b** A1-type, **c** transitional A-type, **d** A2-type and **e** MPG suites. The colored symbols represent the evolution of several theoretical melts (L_0) experiencing 10 to 99% of fractional crystallization in 10% increments and by considering variable melt SiO₂ and Al₂O₃ contents. The respective proportions of the fractionated mineral assemblages are listed in the figure legend together with the Nb and Ta contents of the parental melts (Ta₀ and Nb₀) that were fixed to match the composition of the

primitive samples of each magmatic suite (i.e. characterized by low Ta concentrations). The D_{Nb} and D_{Ta} of the segregated mineral assemblages are indicated in the diagrams with the same color as the corresponding symbols. The mineral/melt partition coefficients (D) of Nb and Ta for biotite (Bt), amphibole (Amp) and ilmenite (Ilm) are calculated at variable melt SiO_2 and Al_2O_3 contents based on the equations in Table 4 and muscovite (Ms)-melt partition coefficients ($D_{\text{Nb}} = 3.5$, $D_{\text{Ta}} = 0.4$) are from Raimbault and Burnol (1998). For simplification, the D_{Nb} and D_{Ta} of other minerals that cannot incorporate a significant amount of Nb and Ta including feldspar, feldspathoid, clinopyroxene or magnetite are fixed at 0. In **a-b**, the blue and purple arrows represent the chemical evolution of a melt L_0 experiencing the crystallization of 0.5% of EGM and 0.035% of IGM, whereas the green and red arrows show the evolution of a magma experiencing 25% of biotite and 10% of EGM accumulation (acc.). See Table 5 for the composition of respective minerals used for modeling.

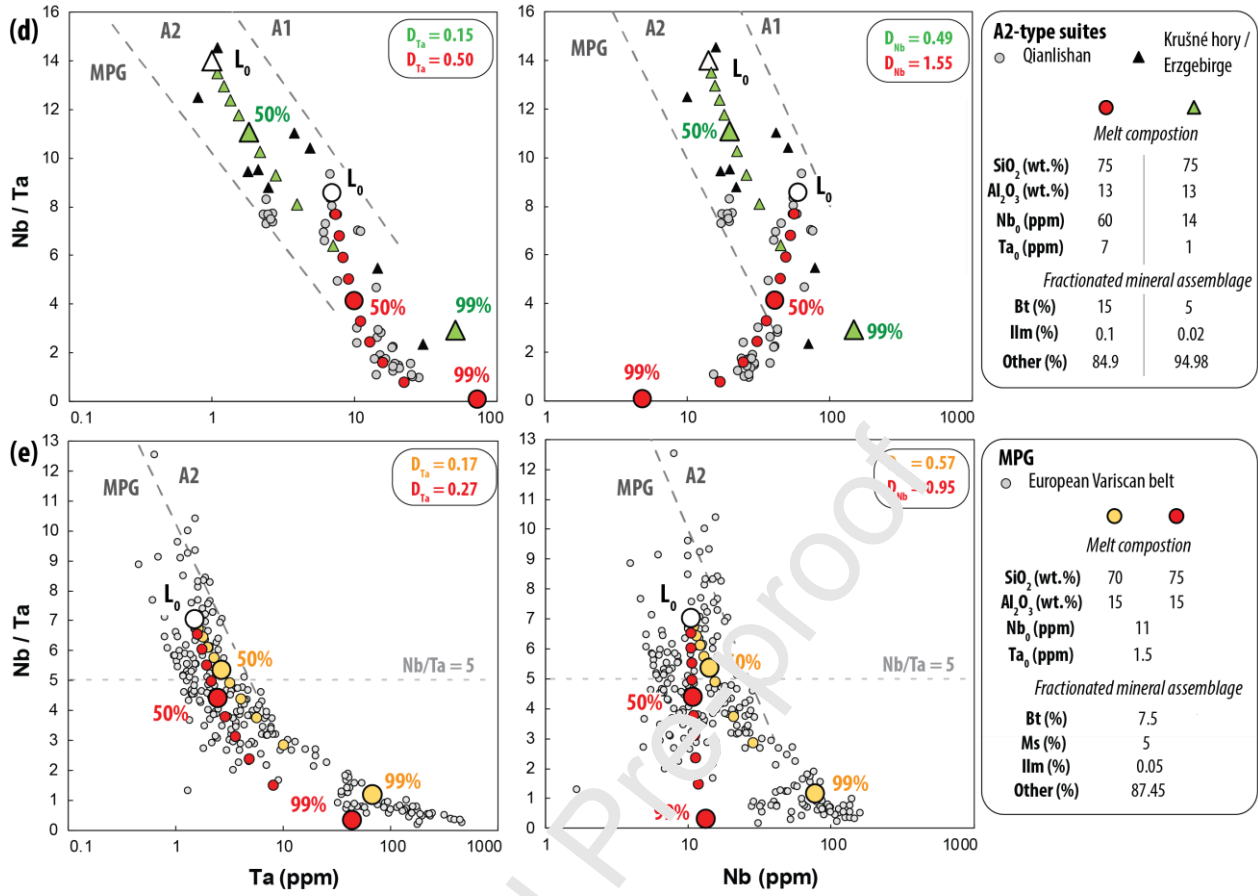


Fig. 11. (ctd.)

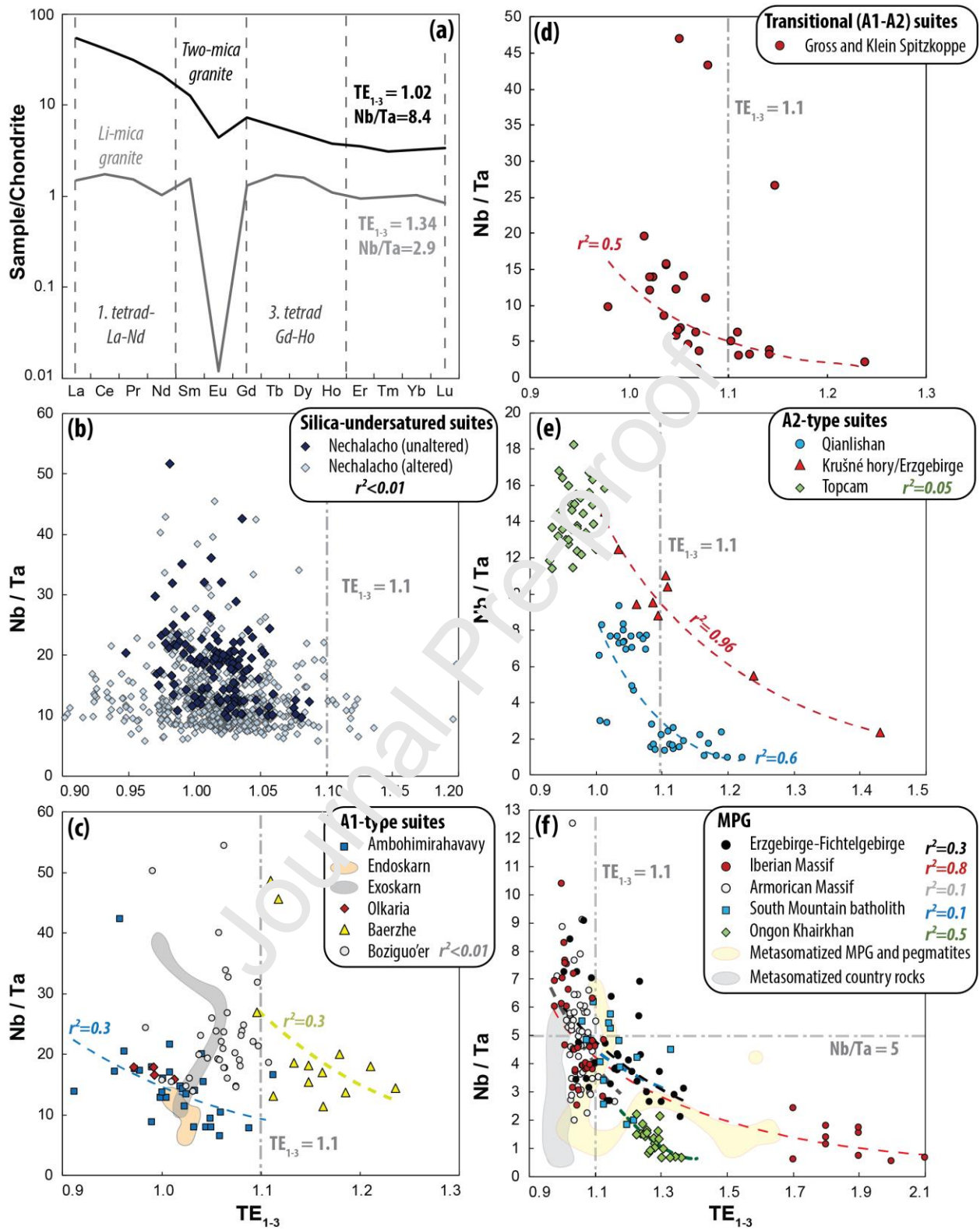


Fig. 12. Relationship between whole-rock Nb/Ta ratios and the tetrad effect in rare-metal-enriched felsic igneous suites and related metasomatic rocks **a** Comparison between chondrite-normalized REE patterns

of two MPG from the European Variscan belt (Erzgebirge, Förster et al., 1999). Normalization values from Palme and O'Neill (2014). The poorly evolved two-mica granite is characterized by an insignificant tetrad effect ($TE_{1-3} = 1.02$) and high Nb/Ta values of 8.4 whereas the highly evolved Li-mica MPG shows an important tetrad effect ($TE_{1-3} = 1.34$) and low Nb/Ta values of 2.9. The degree of the tetrad effect (TE_{1-3}) is significant only above 1.1 and was calculated following Irber (1999) with: $TE_{1-3} = (t1 \times t3)^{0.5}$; $t1 = (Ce/Ce^t \times Pr/Pr^t)^{0.5}$; $t3 = (Tb/Tb^t \times Dy/Dy^t)^{0.5}$; $Ce/Ce^t = Ce_{cn}/(La_{cn}^{2/3} \times Nd_{cn}^{2/3})$; $Pr/Pr^t = Pr_{cn}/(La_{cn}^{1/3} \times Nd_{cn}^{2/3})$; $Tb/Tb^t = Tb_{cn}/(Gd_{cn}^{2/3} \times Ho_{cn}^{1/3})$; $Dy/Dy^t = Dy_{cn}/(Gd_{cn}^{1/3} \times Ho_{cn}^{2/3})$; Ln_{cn} : chondrite-normalized lanthanide concentration. **b-f** Nb/Ta versus TE_{1-3} for selected **b** silica-undersaturated rocks, **c** A1-type igneous rocks, **d** transitional A-type (A1-A2) igneous rocks, **e** A2-type igneous rocks and **f** MPG. The trendlines and determination coefficient r^2 of each suite calculated using a power law ($y = a \cdot xb$) are indicated with the same color as the corresponding symbols. Note that in **d**, the three samples with Nb/Ta >25 were not taken into account for the calculation of the trendline.

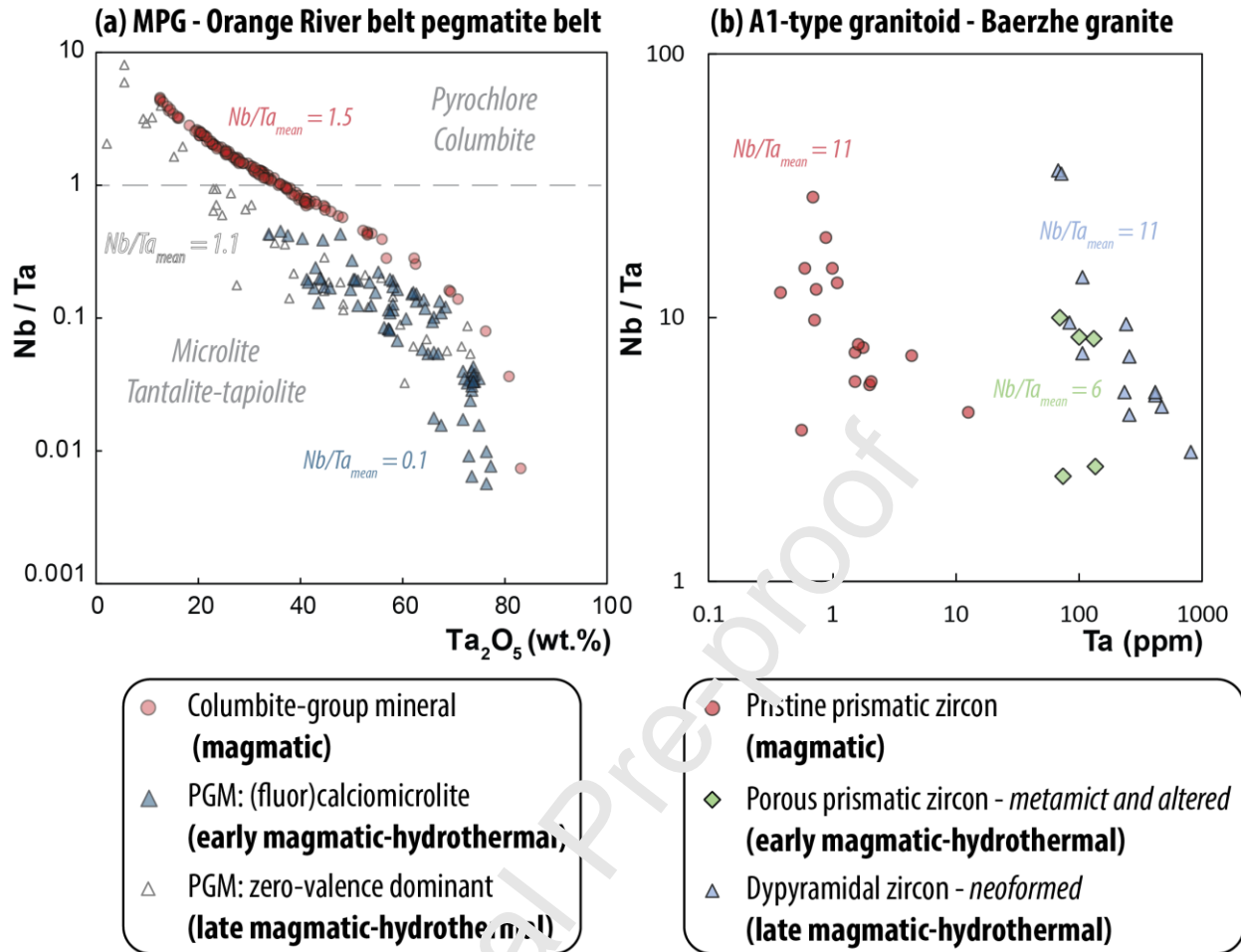


Fig. 13. Nb/Ta versus Ta content diagrams comparing the composition of magmatic to hydrothermal a Nb-Ta oxide minerals from (Li) Ta-Nb-Be mineralized LCT pegmatites from the Orange River pegmatite belt, South Africa (Ballouard et al., 2020) and b zircon crystals from the Zr-REE-Nb mineralized A1-type Baerzhe granite, China (Yang et al., 2014). Pyrochlore-group mineral (PGM) classification from Atencio et al. (2010).

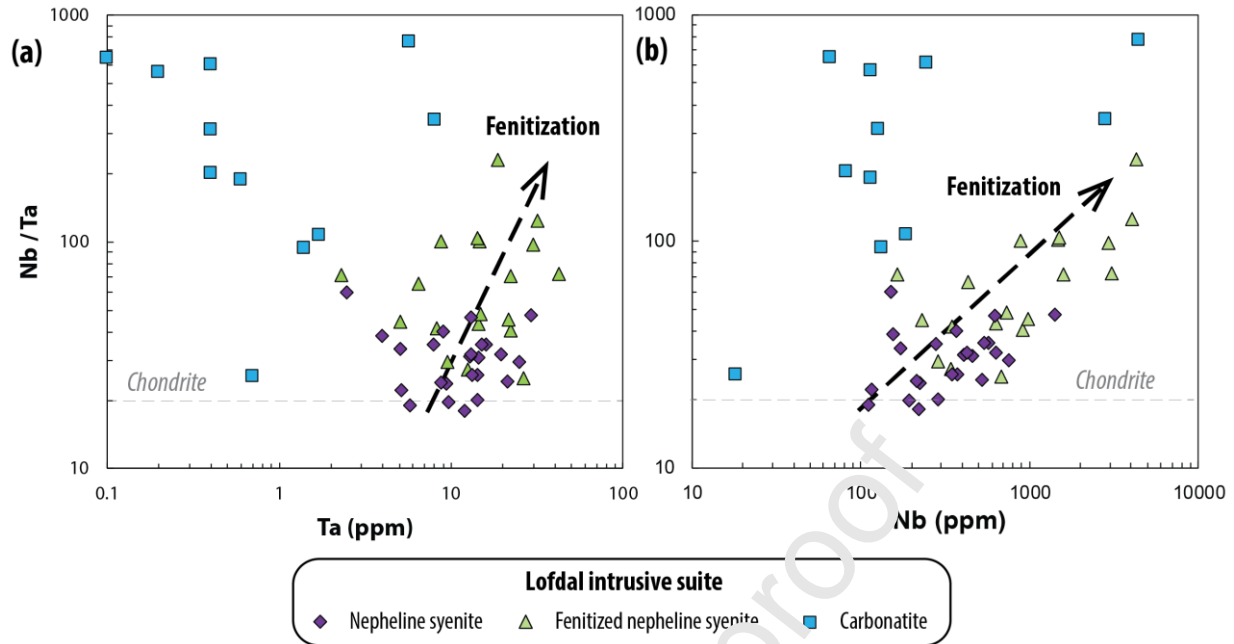


Fig. 14. Nb/Ta versus **a** Ta and **b** Nb content diagrams showing the whole-rock compositions of carbonatites, “unaltered” nepheline syenites and nepheline syenites fenitized at the contact with carbonatites in the Lofdal intrusive suite, Namibia (data from Bodeving et al., 2017).

Minerals		MPG	A2-type granitoids	A1-type granitoids	Nepheline syenites
Quartz		XXX	XX	XX	0
Feldspar		XXX	XXX	XXX	XXX
Feldspathoid		0	0	0	XXX
Biotite		XX	XXX	XX	XX
Muscovite		XXX	X	0	0
Cordierite		X	0	0	0
Garnet		XX	0	0	0
Tourmaline		XX	XX	X	X
Ca pyroxene		0	X	XX	XX
Na pyroxene		0	X	X, X	XXX
Ca amphibole		0	XX	X, X	XX
Na amphibole		0	X	XXX	XXX
Orthopyroxene		0	X	0	0
Olivine		0	0	0	X
Ilmenite		X	X	X	X
Magnetite		0	X	X	X
Titanite		0	X	X	X
Zircon		X	XX	XX	XX
Monazite		X	X	X	0
Xenotime		0	X	X	X
Allanite		0	XX	X	X
Apatite		X, X	XX	XX	XX
Fluorite		X	XX	XX	XX
Rare-metal - mineralized igneous rocks	Topaz	XX	XX	0	0
	Li-mica/spodumene	XX	X	X	0
	CGM	XXX	XXX (Nb>Ta)	XX (Nb>Ta)	X (Nb>Ta)
	PGM	XX (Ta>Nb)	X	XXX (Nb>Ta)	XXX (Nb>Ta)
	EGM	0	0	X	XXX
	Wodginite	XX	0	0	0
	Cassiterite	XX	XX	0	0

Table 1. Principal mineral assemblage of rare-metal-enriched felsic igneous rocks including rare-metal-mineralized equivalents. 0: absent; X: rare; XX: common (i.e. can be absent); XXX: abundant. CGM: columbite-group mineral, PGM: pyrochlore-group mineral, EGM: eudialyte-group mineral.

Chemistry	MPG	A2-type granitoids	A1-type granitoids	Nepheline syenites
Alumina saturation index	Highly peraluminous (A/CNK > 1.1)	Metaluminous to peraluminous (<i>rarely peralkaline</i>)	Peralkaline to metaluminous (<i>rarely peraluminous</i>)	Peralkaline to metaluminous
Agpaite index - (Na + K)/Al	0.6-0.9	0.6-1.1	0.9-1.5	
MALI vs. SiO₂ <i>Frost et al. (2001)</i>	Alkali-calcic to calc-alkalic	Alkalic, alkalic-calcic to calc-alkalic		Alkalic
FeO* / (FeO* + MgO) vs. SiO₂ <i>Frost and Frost (2008)</i>	Magnesian to ferroan		Ferroan	
Nb vs. Y (ppm) <i>Pearce et al. (1984)</i>	Syn-collisional	Syn-collisional to within plate	Within plate	
Ga/Al <i>Whalen et al. (1987)</i>	> 2.6	< 2.6 to > 2.6	> 2.6	< 2.6 to > 2.6
Zr + Ce + Nb + Y (ppm) <i>Whalen et al. (1987)</i>	< 350	350-1000	350-10000	
Y/Nb <i>(Eby, 1990, 1992)</i>	< 1.2 to > 1.2	> 1.2	< 1.2	
Rb/Nb <i>(Eby, 1990, 1992)</i>	10-60	4-60	< 10	
Nb/Ta	0.1-10	1-18	10-50	
Associated rare-metal mineralization	Li-Cs-Ta-(Nb)-Sn-W	Sn-W-Nb-REE	Nb-REE-Zr	

Table 2. Principal geochemical characteristics of rare-metal-enriched felsic igneous rocks.

	SiO ₂ range (wt.%)	D _{Nb}			D _{Ta}			D _{Nb} /D _{Ta}			References
		Min	Max	Mean	Min	Max	Mean	Min	Max	Mean	
Quartz (n=4)	72 - 75				0.007	0.008	0.008				1
K-feldspar (n=3)	61 - 68							0.01	0.13	0.07	2-3
K-feldspar (n=14)	61 - 76	0.001	0.14	0.03							2-4, 49
K-feldspar (n=7)	61 - 76				0.001	0.16	0.04				1-3
Plagioclase (n=4)	61 - 68	0.001	0.04	0.03	0.01	0.08	0.04	0.1	1.69	0.73	2-3
Clinopyroxene (n=44)*	36 - 58	0.002	0.009	0.03	0.005	0.18	0.06	0.29	0.81	0.49	4-19
Orthopyroxene (n=16)	39 - 59	0.001	0.03	0.003	0.001	0.03	0.004	0.22	1.9	0.88	5, 8, 18-22
Amphibole (n=110)*	36 - 67	0.07	0.69	0.35	0.07	0.64	0.37	0.77	1.38	1.08	8, 17, 21, 23-31
Garnet (n=48)*	32 - 68	0.001	0.06	0.03	0.001	0.11	0.05	0.25	1.20	0.70	2, 4-8, 10, 12, 14, 32-36
Biotite (n=14)	38 - 76	0.02	9.2	3.2	0.05	3.8	1.1	0.19	4.67	2.0	1, 2-3, 5, 8, 16, 37
Muscovite (n=1)	70		3.5			0.4			8.8		38
Olivine (n=1)	48		0.0001			0.0002			0.17		19
Olivine (n=4)	45 - 48	0.0001	0.004	0.001							19, 51-52
Olivine (n=2)	43 - 48				0.006	0.0006	0.005				8, 19
Magnetite (n=25)	56 - 72	0.03	0.37	0.17	0.03	0.37	0.13	0.51	2.71	0.83	3, 39-40
Rutile (n=47)*	48 - 72	28.1	193.5	60.9	42.1	212.8	121	0.52	0.97	0.71	41-44
Ilmenite (n=11)	32 - 68	0.40	73.6	17.6	0.62	47.3	12.8	0.33	1.56	0.86	2, 22, 40, 45
Titanite (n=12)	55 - 67	1.34	7.2	4.01	4.45	87.4	33.1	0.07	0.55	0.23	46-47
Zircon (n=1)	68		0.46			0.64			0.72		2
Monazite (n=1)	66		0.03			0.06			0.50		2
Apatite (n=1)	66		<0.01			0.01			0.45		2
Fluorine-bearing aqueous fluid (n=19)	65-71		0.002-0.08			0.005-0.08			0.6-4.7		48

Table 3. Summary of mineral/melt and fluid/melt partition coefficients available in the literature for Nb and Ta. 1: Nash and Crecraft (1985); 2: Acosta-Vigil et al. (2010); 3: Fedele et al. (2015); 4: Sweeney et al. (1995); 5: Green et al. (2000); 6: Klemme et al. (2002); 7: Bennett et al. (2004); 8: Adam and Green (2006); 9: Skulski et al. (1994); 10: Pertermann et al. (2004); 11: Wood and Trigila (2001); 12: Green et al. (1989); 13:

Elkins et al. (2008); 14: Spandler et al. (2017); 15: Blundy et al. (1998); 16: Adam et al. (1993); 17: Adam and Green (1994); 18: McDade et al. (2003a); 19: McDade et al. (2003b); 20: Frei et al. (2009); 21: Qian and Hermann (2013); 22: van Kan Parker et al. (2011); 23: Brenan et al. (1995); 24: Tiepolo et al. (2000); 25: Dalpé and Baker (2000); 26: Adam et al. (1993); 27: Hilyard et al. (2000); 28: Li et al. (2017); 29: Nandedkar et al. (2016); 30: Tiepolo et al. (2003); 31: Adam et al. (2007); 32: Corgne et al. (2012); 33: Qian and Hermann (2013); 34: Van Westrenen et al. (1999); 35: Van Westrenen et al. (2000); 36: Fulmer et al. (2010); 37: Stepanov and Hermann (2013); 38: Raimbault and Burnol (1998); 39: Nielsen and Beard (2000); 40: Sievwright et al. (2017); 41: Xiong et al. (2011); 42: Xiong et al. (2006); 43: Schmidt et al. (2004); 44: Klimm et al. (2008); 45: Dygert et al. (2013); 46: Prowatke and Klemme (2005); 47: Tiepolo et al. (2002); 48: Chevychelov et al. (2005); 49: White et al. (2003); 50: Mallmann and O'Neill (2009); 51: Salters et al. (2002). Note that expect for quartz, K-feldspar and olivine, only mineral/melt partition coefficient data where both Nb and Ta were provided are reported. *For the minerals with an important dataset (>40) including amphibole, clinopyroxene, garnet and rutile, the min and max value corresponds to the 10th and 90th percentiles.

$D_i = 10^{(a \cdot \text{Si molar} + b \cdot \text{Al molar} + c)}$							
	a	b	c	r ²	n	Experimental data range	
						SiO ₂ (wt.%)	Al ₂ O ₃ (wt.%)
D_{Nb}							
Amphibole	1.46 ± 0.18***	3.37 ± 0.33***	-2.91 ± 0.18***	0.648	110	36 - 68	4-21
Clinopyroxene	-0.91 ± 1.07	7.7 ± 1.81***	-3.6 ± 0.68***	0.354	44	36 - 58	9-20
Titanite	0.25 ± 1.05	1.43 ± 0.52*	-0.0093 ± 0.97	0.617	12	55 - 67	4-21
Biotite	3.65 ± 0.39***	-	-3.58 ± 0.38***	0.891	14	38 - 76	-
Ilmenite	4.17 ± 0.33***	-	-2.91 ± 0.27***	0.978	11	32 - 68	-
D_{Ta}							
Amphibole	1.11 ± 0.18***	3.54 ± 0.32***	-2.68 ± 0.17***	0.637	110	36 - 68	4-21
Clinopyroxene	-2 ± 0.89*	7.18 ± 1.5***	-2.18 ± 0.57***	0.365	44	36 - 58	9-20
Titanite	2.37 ± 1.03*	2.91 ± 0.51***	-1.69 ± 0.5	0.913	12	55 - 67	4-21
Biotite	2.47 ± 0.39***	-	-2.67 ± 0.56***	0.773	14	38 - 76	-
Ilmenite	3.48 ± 0.19***	-	-2.27 ± 0.15***	0.975	11	32 - 68	-

Table 4. Equations and respective coefficients a, b and c used in the calculation of mineral/melt partition coefficient for Nb (D_{Nb}) and Ta (D_{Ta}). Experimental melt SiO₂ and Al₂O₃ contents for which the equations were calibrated indicate their best accuracy and thus the compositional range for preferred application to natural rock suites. The determination coefficient r² is indicated along with the strength of calculated probability (p.value): * 0.01 < p.value < 0.05, ** 0.001 < p.value < 0.01, *** p.value < 0.001. The lower the p.value, the higher is the statistical link between log(D_i) and the terms Si, Al or intercept “c”. The method used to calculate the coefficients is described in Supplementary Material 7. The molar proportion of Si and Al is calculated using $\text{Si}_{\text{molar}} = \text{SiO}_2 \text{ wt.} \% / (\text{molecular weight of SiO}_2 = 60.084 \text{ g.mol}^{-1})$ and $\text{Al}_{\text{molar}} = 2 \cdot [\text{Al}_2\text{O}_3 \text{ wt.} \% / (\text{molecular weight of Al}_2\text{O}_3 = 101.961 \text{ g.mol}^{-1})]$.

Mineral	Nb (ppm)	Ta (ppm)	Nb/Ta
Biotite	462	10	46
Amphibole	200	8	25
Clinopyroxene	14	2	7
Ilmenite	5825	266	22
Titanite	4980	732	7
PGM	388840	26875	14
CGM1	526384	31203	17
CGM2	487936	52414	9
EGM	22147	1700	13

Table 5. composition of minerals used for the crystallization and accumulation modeling shown in Figures 10 and 11. The composition corresponds to the average contents of minerals from the Nechalacho layered suite (biotite, clinopyroxene, EGM, PGM, CGM1; Timofeev and Williams-Jones, 2015; Möller and Williams-Jones, 2016), Pilanesberg alkaline complex (amphibole, clinopyroxene, titanite; Giles, 2018), Ukrainian shield intrusions (ilmenite from foyite; Kryvdik, 2014) and Orange River pegmatite belt (CGM2, weakly mineralized LCT pegmatites; Bouchard et al., 2020).

Highlights

- Rare metal-enriched felsic igneous suites can be classified using Nb/Ta ratios
- The Nb/Ta ratio generally anticorrelates with Ta contents
- Equations are provided for the extrapolation of D_{Nb} and D_{Ta} in various minerals
- Decrease of the Nb/Ta ratio reflects magmatic and magmatic-hydrothermal evolution
- The Nb/Ta ratio fingerprints the nature and evolution of the source of igneous rocks

Journal Pre-proof

Declaration of interests

The authors declare that they have no known competing financial interests or personal relationships that could have appeared to influence the work reported in this paper.

The authors declare the following financial interests/personal relationships which may be considered as potential competing interests:

Journal Pre-proof